THE METABOLISM OF 4-(METHYLNITROSAMINO)-1-(3-PYRIDYL)-1-BUTANONE [NNK] AND THE ENANTIOMERS OF 4-(METHYLNITROSAMINO)-1-(3-PYRIDYL)-1-BUTANOL [NNAL] IN THE ISOLATED PERFUSED RAT LUNG SYSTEM

A DISSERTATION

SUBMITTED TO THE FACULTY OF THE GRADUATE SCHOOL

OF THE UNIVERSITY OF MINNESOTA

BY

LAURA A. MAERTENS

IN PARTIAL FULFILLMENT OF THE REQUIREMENTS

FOR THE DEGREE OF

DOCTOR OF PHILOSOPHY

CHERYL L. ZIMMERMAN, Ph.D., Advisor

August 2010

ACKNOWLEDGEMENTS

I would like to thank Dr. Cheryl Zimmerman for serving as my advisor and for allowing me the time and space to try and figure things out. I would also like to thank my co-advisor Dr. Stephen Hecht for his guidance and financial support. Furthermore I would like to thank Dr. Tim Tracy and Dr. William Elmquist for serving on my committee and for always making time to discuss my research.

None of this work would have been possible without the help of Dr. Douglas Wangansteen, Dr. Peter Byron, and Dr. Masahiro Sakagami, who all contributed to my learning the skills to successfully perform isolated lung perfusions.

I am grateful to Dr. Pramod Upadhyaya for providing standards and quantifying the formation of DNA adducts, Dr. Linda von Weymarn for her assistance with the S9 preparations, Adam Benoit and Andrew Davis for their assistance with the GC-TEA, Steve Carmella for his help with numerous equipment and procedural issues, and Dr. Ronald Sawchuk and Dr. Richard Brundage for their input and suggestions regarding the data modeling. Thanks to Dr. Swati Nagar, Dr. John Jalas, Dr. Hanson Wong, Dr. Shyeilla Dhuria, Sagar Agarwal, Dr. Belinda Chueng, Linda Cartier, Dr. Manthena Varma, and Sara Citrowske for all their help at various times throughout this process.

I would also like to acknowledge the 3M Science and Technology Fellowship, Edward Rippie Fellowship, Ted Rowell Graduate Fellowship, Schering-Plough Science and Innovation Award, PHS Grant CA-81301, and ACS Grant RP-00-138 for providing the financial support for this work.

ABSTRACT

4-(Methylnitrosamino)-1-(3-pyridyl)-1-butanone (NNK) is a potent carcinogen found specifically in tobacco products. It has been shown to be a lung-specific carcinogen in rodents, and may play a critical role in the formation of lung cancer in smokers. One of the enantiomers of 4-(methylnitrosamino)-1-(3-pyridyl)-1-butanol (NNAL), a metabolite of NNK, may be important to the selective pulmonary carcinogenicity of NNK. The objective of the current research was to better characterize the pulmonary metabolism of NNK, *(S)*-NNAL, and *(R)*-NNAL using the isolated perfused rat lung (IPRL) system to elucidate the mechanisms behind the lung-specific nature of NNK. This research examined metabolite formation, distribution of the metabolites between the perfusate and tissue, the formation of individual DNA adducts in the tissue, and the effects of concentration and the chemopreventive agent PEITC. The results showed that NNK was readily metabolized and DNA adducts were detected in the tissue at the end of the 180 min perfusions. Both an increase in NNK concentration and the co-administration of PEITC were shown to inhibit NNK metabolism. PEITC was also shown to significantly reduce the formation of DNA adducts. The results obtained for the NNK perfusions were in agreement with previously published results. *(S)*-NNAL and *(R)*-NNAL were not metabolized as extensively by the lung as NNK. The metabolism of the two enantiomers was similar, which was in contrast to previous *in vitro* and *in vivo* results. The only observed difference between the two enantiomers was the formation of low levels of a pyridyloxobutyl (POB)-DNA adduct in the *(S)*-NNAL perfusions, which indicated reoxidation to NNK. The unexpected results for the NNAL enantiomers may be a result

of diffusional barriers to the preformed metabolites that do not exist when the enantiomers are formed from NNK in the tissue. This work showed that the IPRL system was a valid system for examining the pulmonary metabolism of NNK and the formation of DNA adducts, but it may have some limitations for more polar compounds that cannot penetrate the diffusional barriers of the lung and the cells to gain access to the enzymatic sites responsible for metabolism.

TABLE OF CONTENTS

CHAPTER 3: NNK METABOLISM IN THE IPRL SYSTEM

LIST OF TABLES

LIST OF FIGURES

CHAPTER 1: INTRODUCTION

1.A – Lung Cancer and Smoking

Lung cancer has been the leading cause of cancer deaths in the United States for men for over the last 50 years, and women for over 20 years (Figure 1.1).

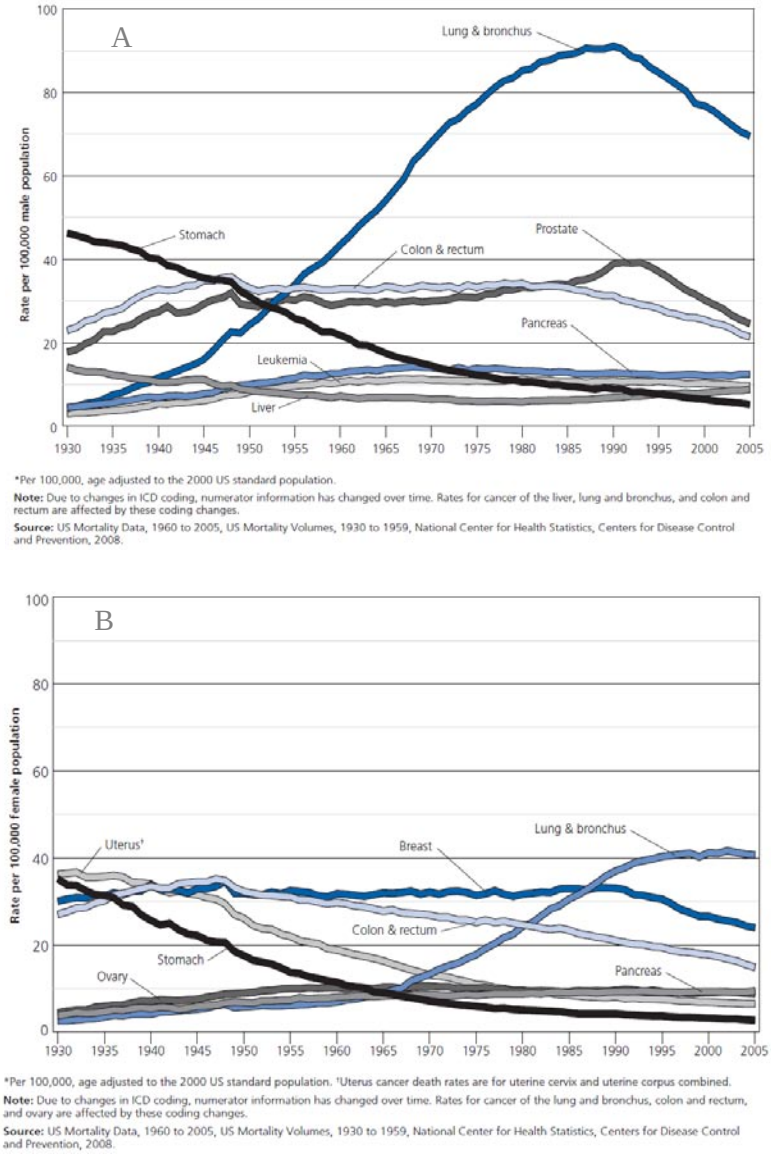

Figure 1.1 – *The age-adjusted cancer death rates for the most common forms of cancer in men (A) and women (B) in the United States from 1930 – 2005*[1]*. Reprinted with permission from the American Cancer Society. Cancer Facts and Figures 2009. Atlanta: American Cancer Society, Inc.*

Epidemiological data based on numerous case-control and cohort studies have shown a strong relationship between smoking and the development of lung cancer[2-4]. It is estimated that at least 80% of all lung cancer deaths are attributable to smoking (Figure 1.2), making lung cancer one of the most preventable diseases in our society[1]. Figure 1.3 illustrates that in the United States the lung cancer death rates in males have followed the smoking trends throughout the twentieth century[5]. As smoking became more popular in the mid-1900s, an increase in lung cancer followed.

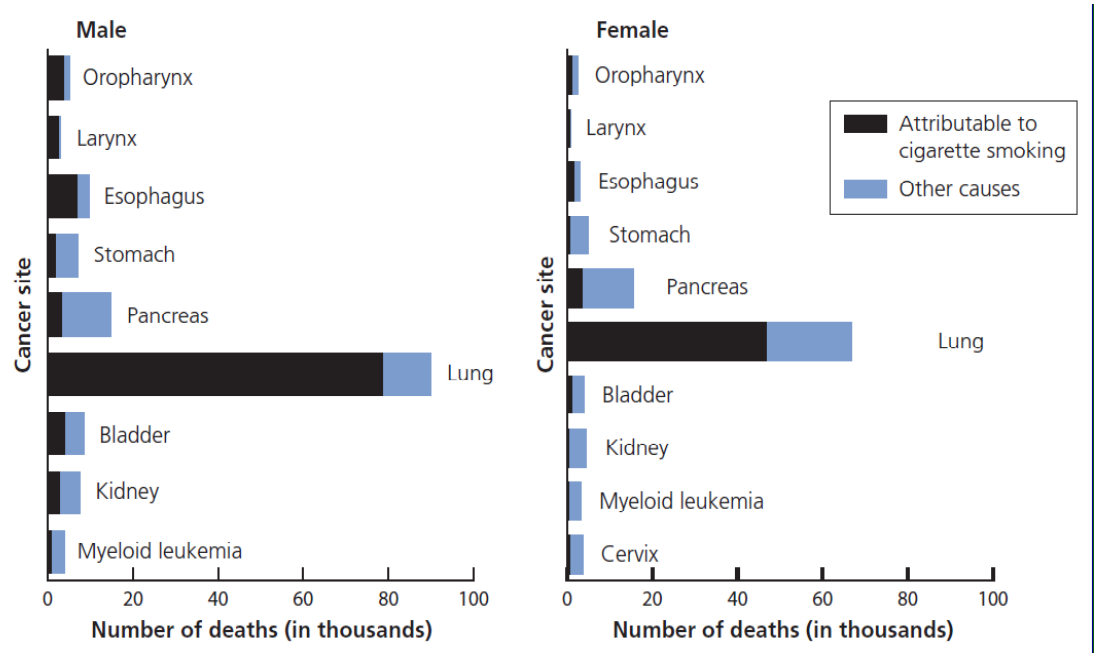

***Figure 1.2** – Annual number of cancer deaths attributable to smoking by sex and site in the United States, 2000 – 2004[1]. Reprinted with permission from the American Cancer Society. Cancer Facts and Figures 2009. Atlanta: American Cancer Society, Inc.*

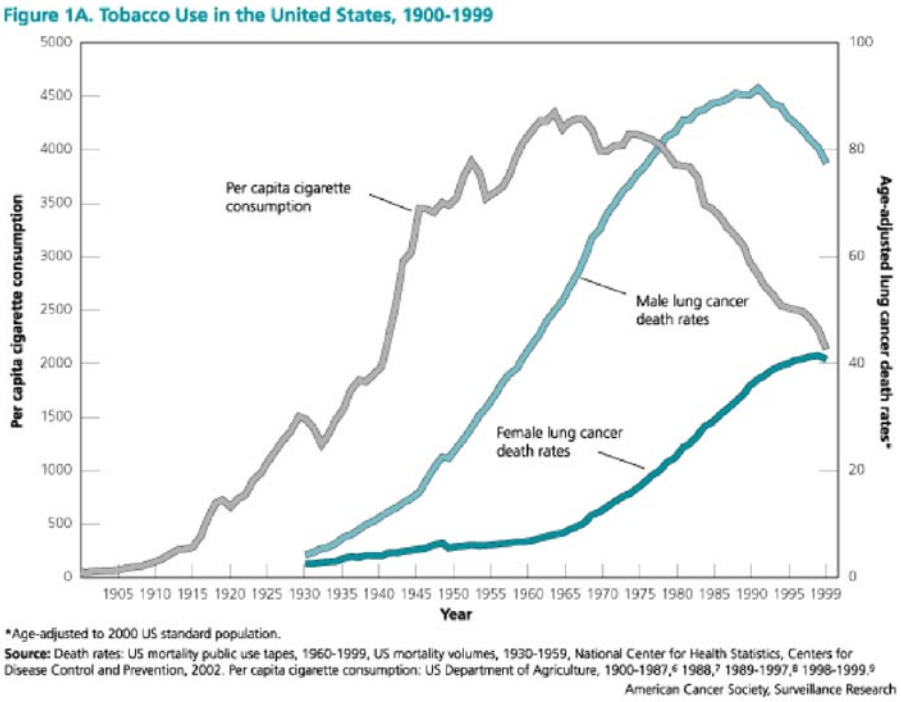

Figure 1.3 – *Tobacco use and cancer death rate trends in the United States, 1900-1999*[5]. *Reprinted with permission from the American Cancer Society. Cancer Prevention & Early Detection Facts and Figures 2009. Atlanta: American Cancer Society, Inc.*

1.B – NNK

Tobacco smoke is a complex mixture of toxicants, free radicals, and carcinogens[6,7]. So far, more than 60 known carcinogens have been identified in tobacco and of these a group of compounds referred to as the tobacco-specific nitrosamines (TSNA) are of great interest. Unlike other carcinogens and toxins found in smoke, TSNAs are only found in tobacco products[8,9]. 4-(Methylnitrosamino)-1-(3-pyridyl)-1-butanone (NNK) is one of the seven known TSNAs. NNK is formed from the nitrosation of nicotine or pseudo-oxynicotine during the curing, processing, and smoking of tobacco

and is present in larger quantities than many other known carcinogens in tobacco[10-15]. An intriguing characteristic of NNK is its ability to selectively induce pulmonary tumors in rodents[15]. This lung specificity, along with biochemical and epidemiologic data, implicates NNK as a plausible contributor to the development of lung cancer in smokers[6,16,17].

1.B.i – NNK Carcinogenicity

NNK is classified as a human carcinogen by the International Agency for Research on Cancer [IARC][16]. It is a strong and selective lung carcinogen in rodents, as shown by its ability to induce pulmonary tumors even when it is dosed outside of the lung[15,18-21]. Its carcinogenic effects are dose-dependent[20,22,23]. NNK can induce significantly more pulmonary tumors compared to controls at total doses as low as 6.0 mg/kg (0.029 mmol/kg), whereas it can take approximately 600 mg/kg (2.9 mmol/kg) to induce nasal tumors and 3000 mg/kg (14.5 mmol/kg) to induce liver tumors in F344 rats[22].

1.B.ii – NNK Metabolism

Metabolism is crucial to the elimination of NNK given its lipophilic nature. NNK is extensively metabolized in rodents and humans, which is illustrated by the low levels of NNK excreted unchanged in the urine[15]. While NNK can be metabolized through detoxification pathways that safely eliminate it from the body, it can also be bioactivated, resulting in the formation of unstable electrophiles that can covalently bind to DNA and

form adducts. If the adducts are not repaired, they can result in mutations that lead to tumor growth. The metabolic activation of NNK is considered to be primarily responsible for its carcinogenicity.

An important pathway in the metabolism of NNK is its carbonyl reduction to 4-(methylnitrosamino)-1-(3-pyridyl)-1-butanol (NNAL), a carcinogenic metabolite that undergoes subsequent metabolism through pathways parallel to those of NNK (Figure 1.4). Both NNK and NNAL are detoxified via *N*-oxidation to form 4-(methylnitrosamino)-1-(3-pyridyl-*N*-oxide)-1-butanone (NNK-*N*-oxide) or 4-(methylnitrosamino)-1-(3-pyridyl-*N*-oxide)-1-butanol (NNAL-*N*-oxide). NNAL can also be detoxified via glucuronidation *(not shown)*[24]. Both NNK and NNAL are bioactivated through α-hydroxylation pathways. α-Methylene hydroxylation of NNK and NNAL results in the formation of the reactive intermediate methanediazohydroxide, which can form methyl DNA adducts. This pathway also ultimately results in the formation of the metabolites 4-oxo-4-(3-pyridyl)butyric acid (keto acid) and 4-hydroxy-4-(3-pyridyl)butyric acid (hydroxy acid). When NNK undergoes α-methyl hydroxylation, the unstable intermediate 4-(3-pyridyl)-4-oxobutanediazohydroxide is formed, which can react with water to yield the metabolite 4-oxo-4-(3-pyridyl)butanol (keto alcohol) or bind to DNA to form pyridyloxobutyl (POB)-DNA adducts. Similarly, the α-methyl hydroxylation of NNAL can produce pyridylhydroxybutyl (PHB)-DNA adducts or the metabolite 4-hydroxy-4-(3-pyridyl)butanol (diol). Even though NNAL can be bioactivated through α-hydroxylation pathways, it has been suggested that it is the α-

hydroxylation of NNK that is crucial to the formation of pulmonary tumors due to its greater rate of metabolism by cytochrome P450 enzymes[25].

The cytochrome P450s are believed to be primarily responsible for the oxidative metabolism of NNK and NNAL[15]. Unfortunately, the exact isozymes responsible for each metabolic pathway are still largely unknown. Research has shown that rat cyp 2A3, mouse cyp 2A5, and human CYP 2A13 and 2B6 may play a significant role in the bioactivation of NNK and NNAL. Flavin monooxygenases (FMOs), another family of enzymes capable of catalyzing oxidative reactions, do not appear to contribute to the metabolism of NNK[26].

The carbonyl reduction of NNK to NNAL is believed to be primarily catalyzed by various carbonyl reductases rather than the CYP P450 enzymes. 11β-Hydroxysteroid dehydrogenase type 1 (11β-HSD 1), a microsomal protein, was the first enzyme identified to catalyze the reduction of NNK to NNAL[27,28]. However, the formation of NNAL was observed in red blood cells and cytosolic fractions as well as in microsomes, suggesting that other non-membrane-bound enzymes also contribute to the carbonyl reduction of NNK[29,30]. Further investigation has shown that carbonyl reductase (CR) and three isozymes of aldo-keto reductase (AKR), all cytosolic enzymes, can also metabolize NNK to NNAL[31-34].

The detoxification of NNAL through glucuronidation is catalyzed by the UDP-glucuronyl transferases (UGTs). NNAL glucuronidation can occur at either the carbinol group to form 4-(methylnitrosamino)-1-(3-pyridyl)-1-(*O*-*β*-D-glucopyranuronosyl)-

butane (NNAL-*O*-*G*luc), or on the nitrogen in the pyridine ring to form 4-(methylnitrosamino)-1-(3-pyridyl)-1-(*N*-*β*-D-glucopyranuronosyl)-butane (NNAL-*N*-Gluc). Human UGT1A9, UGT2B7, and UGT2B17 have been shown to catalyze the formation of NNAL-*O*-Gluc, while UGT1A4 and UGT2B10 catalyze the formation of NNAL-*N*-Gluc[24,35-37]. Evidence suggests that the major enzyme responsible for the glucuronidation of NNAL in rats is UGT2B1,[38] which catalyzes the formation of NNAL-*O*-Gluc. UGTs tend to be primarily expressed in the liver, as is the case with UGT2B1, but some UGTs have been found to be expressed in other extrahepatic tissues[39].

There is still a substantial amount of work that needs to be done before the specific enzymes contributing to the detoxification and bioactivation of NNK and NNAL are clearly identified.

1.B.iii – DNA Adducts

There are three major types of adducts that result from the bioactivation of NNK and NNAL: methyl, pyridyloxobutyl (POB), and pyridylhydroxybutyl (PHB) (Figure 1.5). As previously mentioned, methyl adducts are a result of the α-methylene hydroxylation of NNK and NNAL. However, these adducts can be produced by other methylating agents as well[40,41], so their formation cannot be directly correlated to exposure to NNK or NNAL in smokers. The more extensively researched methyl adducts are 7-methylguanine (7-methyl-Gua), O^6-methylguanine (O^6-methyl-Gua), and O^4-methylthymidine (O^4-methyl-Thd)[22,40,42-44]. Of these, special attention has been paid to O^6-methyl-Gua, due to its persistence in the lung tissue after exposure to NNK

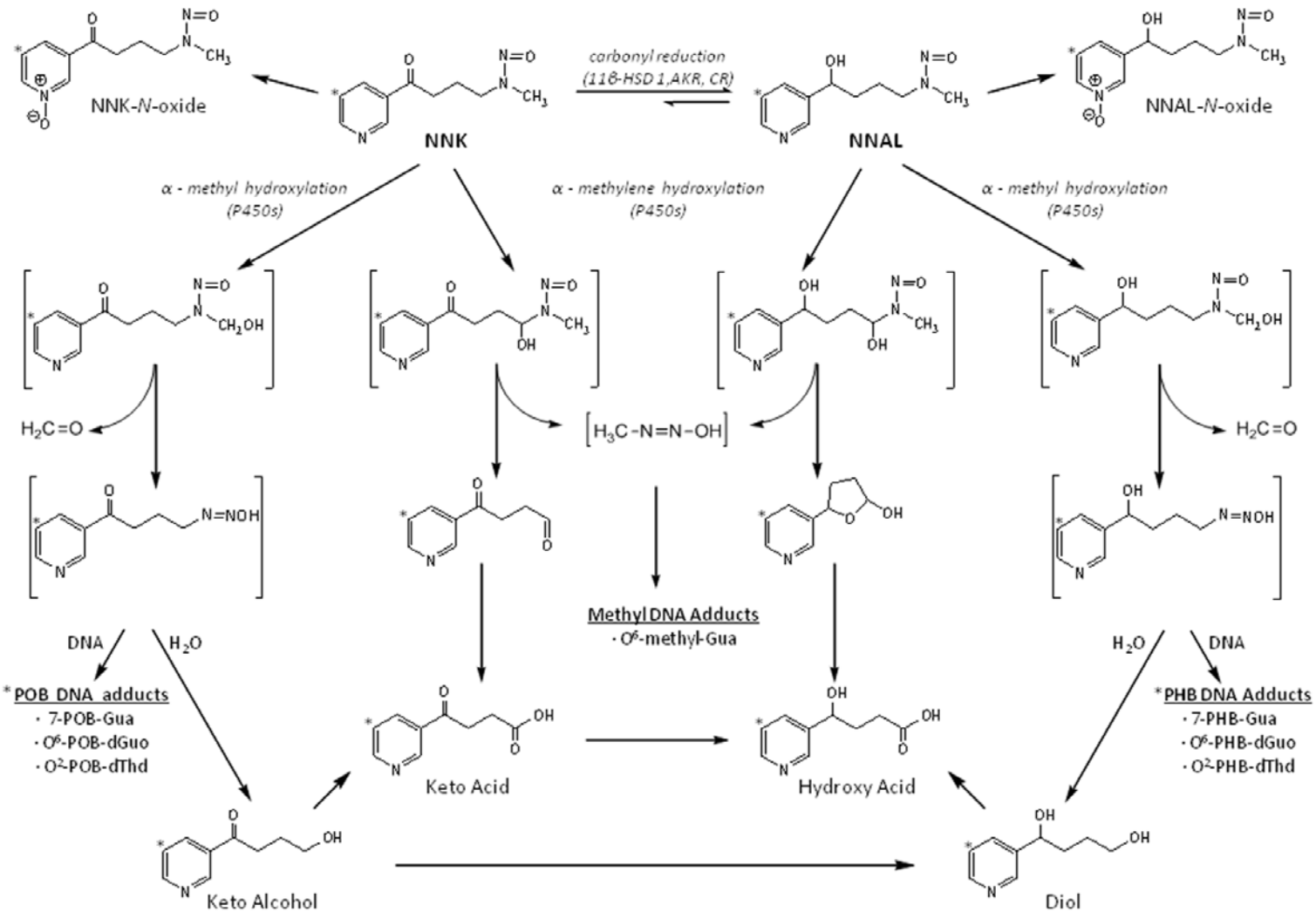

Figure 1.4 – *A general metabolic scheme of NNK*[45].

and its ability to result in miscoding and mutagenesis[42,46-49]. The persistence of O^6-methyl-Gua in the lung has been attributed to a decrease in activity of O^6-alkylguanine-DNA alkyltransferase (AGT), a DNA repair protein[42]. A correlation between O^6-methyl-Gua levels in Clara cells and tumor incidence has been observed. However, tumor formation appears to develop from alveolar type II cells and not Clara cells, so the significance of this correlation is unclear[22,50]

Pyridyloxobutyl (POB)-DNA adducts result from the α-methyl hydroxylation of NNK. Initial studies examined the formation of POB-DNA adducts by measuring the release of keto alcohol, or HPB, after acid or neutral thermal hydrolysis[51-53]. From this method it was observed that POB-DNA adducts formed and persisted in the lung along with methyl adducts, and likewise resulted in mutations[49,51,53-57]. A correlation between POB-DNA adducts and tumor incidence was observed in the alveolar type II cells, suggesting that they may be important to the carcinogenicity of NNK[52]. Furthermore, POB-DNA adducts were shown to inhibit AGT, which is responsible for the repair of O^6-methyl-Gua, and may provide an explanation for the persistence of the methyl adduct in the lung tissue[58]. More recently, methods and standards have been developed for the analysis of individual POB-DNA adducts, including O^6-[4-(3-pyridyl)-4-oxobut-1-yl]-2´-deoxyguanosine (O^6-POB-dGuo), O^2-[4-(3-pyridyl)-4-oxobut-1-yl]thymidine (O^2-POB-dThd), and 7-[4-(3-pyridyl)-4-oxobut-1-yl]guanine (7-POB-Gua) (Figure 1.5)[59].

The α-methyl hydroxylation of NNAL can lead to the formation of pyridylhydroxybutyl (PHB)-DNA adducts. Unlike the methyl and POB-DNA adducts, the PHB-DNA adducts have only recently been indentified and measured *in vivo*[60,61].

Some of the adducts quantified include O^6-[4-(3-pyridyl)-4-hydroxybut-1-yl]-2´-deoxyguanosine, (O^6-PHB-dGuo), O^2-[4-(3-pyridyl)-4-hydroxybut-1-yl]thymidine (O^2-PHB-dThd), and 7-[4-(3-pyridyl)-4-hydroxybut-1-yl]guanine (7-PHB-Gua)[59,62,63].

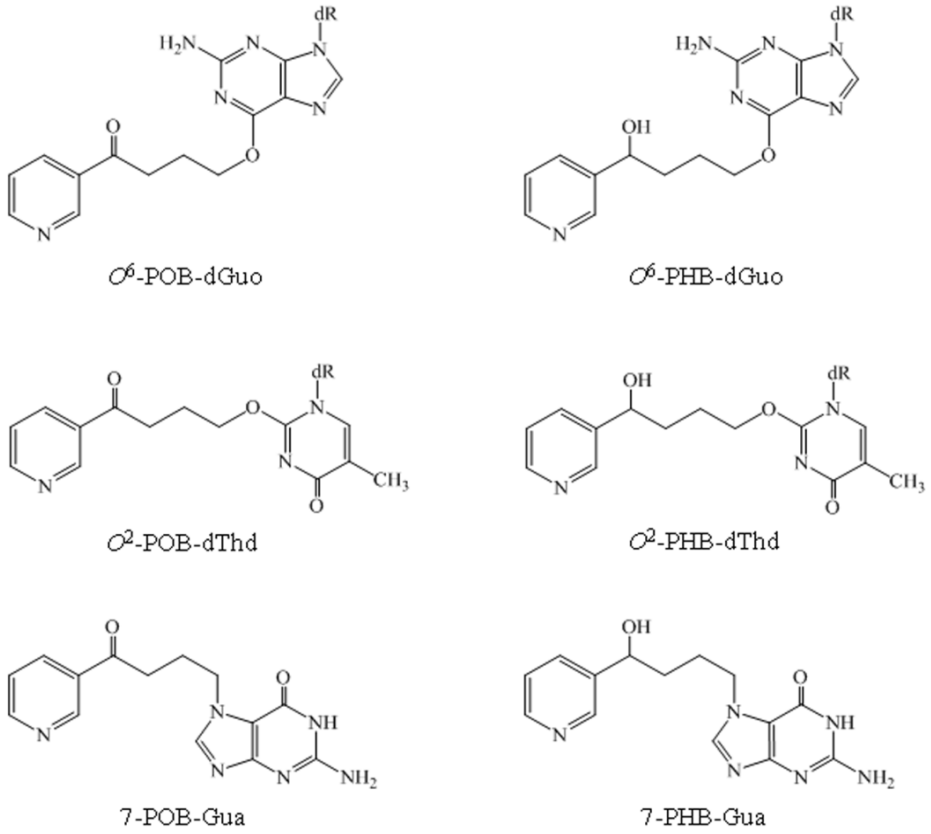

Figure 1.5 – *Structures of POB and PHB-DNA adducts, where dR represents 2'- deoxyribosyl.*

Recently the levels of methyl, POB, and PHB-DNA adducts were measured during the chronic administration of NNK in the drinking water of F344 rats. In the lung POB-DNA adducts were the most prevalent, while methyl and PHB-DNA adduct levels were lower[64]. In the liver, methyl DNA adducts were higher for the first two weeks and

then POB-DNA adducts were predominant until the end of the 20 week study. In fact, the methyl adduct levels decreased to the same level as the PHB-DNA adducts, which could be attributed to efficient DNA repair mechanisms of O^6-methyl-Gua in the liver[42]. In the lung O^2-POB-dThd was the major POB-DNA adduct throughout the 20 week bioassay ranging from 1080 ± 99 fmol/mg DNA at 1 week to 8260 ± 2730 fmol/mg DNA at 10 weeks. The level of 7-POB-Gua ranged from 750 ± 95 fmol/mg DNA at 1 week to 2200 ± 864 fmol/mg DNA at 10 weeks, while O^6-POB-dGuo levels were consistent around 20-40 fmol/mg DNA throughout. The high levels of POB-DNA adducts present in the lung further support their importance in the carcinogenicity of NNK.

For the PHB-DNA adducts, 7-PHB-Gua was the major adduct until week 5 and then O^2-PHB-dThd was the major adduct for the remainder of the bioassay. The level of O^6-PHB-dGuo was substantially lower than the other PHB-DNA adducts throughout the assay, and was detected in the lung and not the liver.

1.C – NNAL

1.C.i – Enantiomers

Enantiomers are pairs of compounds that are nonsuperimposable mirror images of one another. They have the same molecular formula and bonding order, but differ in their spatial orientation. Enantiomers have identical physical and chemical properties, but can differ in their interactions with chiral systems, such as the body[65]. As a result of the

possible differences in the pharmacokinetics and pharmacodynamics between enantiomers, the FDA set guidelines for the development of chiral drugs in 1992[66].

Warfarin, a commonly prescribed anticoagulant, provides an example of two enantiomers that react differently in the body. *(S)*-Warfarin is considered to be the more potent form, and is mainly metabolized by CYP2C9 to form 6-hydroxy and 7-hydroxy metabolites[65,67]. *(R)*-Warfarin, on the other hand, is less potent and is predominantly metabolized by CYP2C19 and CYP3A4 to form 8-hydroxy and 10-hydroxy metabolites. While both enantiomers appear to have a high affinity for binding to human serum albumin, differences in the mechanism of binding have been observed[68].

Nicotine, the precursor for NNK, also exists as two enantiomers and illustrates some of the difficulty in characterizing differences between enantiomers. *(S)*-Nicotine is the primary form in tobacco and is considered to be the more active enantiomer[69]. *(R)*-nicotine has often been observed to be less potent than *(S)*-nicotine, but further investigation has shown that the differences in activity and metabolism, or lack thereof, depends on the system and species used. Initial toxicity studies performed with the nicotine enantiomers by Pictet and Rotschy showed *(S)*-nicotine to be twice as toxic as *(R)*-nicotine, but later work in rats and guinea pigs showed similar toxicity between the two enantiomers[69-71]. In guinea pigs *(S)*-nicotine has been observed to be metabolized through only oxidative pathways, whereas *(R)*-nicotine formed oxidative and *N*-methylated metabolites[72-75]. However, *N*-methylated metabolites were not observed for either enantiomer in hamsters, rats, or rabbits[74]. In humans *(S)*-nicotine was found to activate the trigeminal sensory system to a greater extent than *(R)*-nicotine as measured

by the ability of the enantiomers to induce burning and stinging sensations. The stimulation of olfactory system, however, seemed to be comparable for the two enantiomers. These results indicate that stereoselective receptors may exist in the trigeminal system, but not the olfactory system[76].

Since NNK is a prochiral compound, its metabolism to NNAL results in the formation of two enantiomers, *(S)*-NNAL and *(R)*-NNAL. Although they are structurally similar, the carcinogenicity, metabolism, and pharmacokinetics of these two enantiomers have been showed to be vastly different.

1.C.ii – NNAL Carcinogenicity

The number of studies examining *(S)*-NNAL and *(R)*-NNAL are limited, but demonstrate the importance of characterizing the two enantiomers individually. In A/J mice, racemic NNAL formed about 50% fewer lung tumors than an equimolar dose of NNK after a single i.p. injection. However, when the enantiomers were dosed separately, *(S)*-NNAL generated the same number of pulmonary tumors as NNK. *(R)*-NNAL, on the other hand, induced only approximately 30% of the number of lung tumors as NNK and *(S)*-NNAL[21]. Both *in vitro* and *in vivo* work suggest that this disparity in the carcinogenicity of these two enantiomers could be due to differences in their metabolism and distribution[21,29,77,78]. In rats, when equimolar doses of NNK and racemic NNAL were chronically administered via drinking water, the same number of pulmonary tumors were induced[79]. However, the tumorgenicity of *(S)*-NNAL and *(R)*-NNAL has not been examined in rats.

1.C.iii – NNAL Metabolism and Distribution

NNAL is formed from the carbonyl reduction of NNK. However, evidence suggests that the formation of the two enantiomers from NNK is not equal, and that *(S)*-NNAL is preferentially formed over *(R)*-NNAL[29]. *In vitro* data in lung and liver microsomes for mice and rats have shown a difference in the formation rates of metabolites between the NNAL enantiomers[21,29]. In lung microsomes the formation of lactol, diol, and NNAL-*N*-oxide were all greater for *(S)*-NNAL than *(R)*-NNAL. Furthermore, *(S)*-NNAL was reoxidized to NNK to a greater extent than *(R)*-NNAL.

When the two enantiomers were dosed separately *in vivo* their metabolic profiles were substantially different. The profile of the metabolites in the urine of F344 rats shows that approximately 20% of *(S)*-NNAL was metabolized to either NNK or a subsequent metabolite of NNK, whereas roughly 5% of *(R)*-NNAL appeared to be reoxidized to NNK[77]. While *(S)*-NNAL was predominately metabolized through oxidative pathways, approximately 40% of *(R)*-NNAL was detoxified through the glucuronidation pathway and excreted in the bile[77,78]. Even after the administration of *(S)*-NNAL in rats, significantly more *(R)*-NNAL-Gluc was formed than *(S)*-NNAL-Gluc[77]. This indicates a possible preference by the glucuronidating enzymes for *(R)*-NNAL over *(S)*-NNAL. This preference may be accounted for by the role of UGT2B1 in the glucuronidation of NNAL[38] because it has been shown to stereoselectively metabolize ibuprofen[80].

A difference in pharmacokinetics may also contribute to the difference in carcinogenicity between *(S)*-NNAL and *(R)*-NNAL. One of the major differences

between these two enantiomers *in vivo* was their steady-state volumes of distribution[77]. Though both enantiomers have larger steady-state volumes than NNK, the volume of *(S)*-NNAL was almost three times greater than that of *(R)*-NNAL[77,78]. The difference in the volumes most likely explains the elimination half-life of *(S)*-NNAL being longer than that of *(R)*-NNAL because a statistically significant difference between the clearances of the enantiomers was not observed. These results suggest that *(S)*-NNAL distributes into the tissue more than *(R)*-NNAL and as a result it is eliminated from the body slower than *(R)*-NNAL. This is further supported by the observation that 90% of the total *(R)*-NNAL dose was recovered after 24 hrs, while only 65% of the *(S)*-NNAL dose was recovered[77].

The lower recovery of the *(S)*-NNAL dose may be a result of its greater persistence in the lung tissue compared to *(R)*-NNAL. Four hours after the administration of NNK, *(S)*-NNAL was observed to be the predominant enantiomer in the lung, which was not true for the liver or kidney[78]. Furthermore, after a dose of racemic NNAL, the ratio of *(S)*-NNAL to *(R)*-NNAL in the lung was substantially higher than that in the liver or kidney 24 hours post-dose. These results suggested that *(S)*-NNAL was being selectively retained in the lung tissue. Twenty-four hours after administration of *(S)*-NNAL, almost 80% of the radioactivity in the lung was attributed to NNAL, with the amount of *(S)*-NNAL being four times greater than that of *(R)*-NNAL[77]. In the liver and kidney the major metabolite after 24 hours was keto acid. When *(R)*-NNAL was dosed, NNAL was not detected in any of the tissues 24 hours post-dose, nor were any other metabolites present. This showed that *(R)*-NNAL was eliminated from the body and the

lung more readily than *(S)*-NNAL, possibly as a result of *(S)*-NNAL interacting with the lung in a way that prolongs its time in the pulmonary tissue.

1.C.iv – NNAL DNA Adducts

Chronic exposure of F344 rats to *(S)*-NNAL produces similar DNA adducts as chronic administration of NNK[62,63,81]. The levels of POB-DNA adducts were comparable after NNK and *(S)*-NNAL treatment, and were significantly greater than the levels in *(R)*-NNAL treated animals. However, the level of PHB-DNA adducts were significantly higher in the *(R)*-NNAL animals than in the NNK or *(S)*-NNAL treatment groups. This was observed in all of the tissues that were measured, which included the lung, liver, nasal respiratory mucosa, nasal olfactory mucosa, oral mucosa, and pancreas[62,63,81].

In the lung, O^2-POB-dThd was the major adduct followed by 7-POB-Gua for both *(S)*-NNAL and *(R)*-NNAL treatments. However, the levels of the adducts were approximately 10 times greater in the *(S)*-NNAL treated animals. O^6-POB-dGuo was present in the *(S)*-NNAL animals for the entire 20 week bioassay, but were only detected in the *(R)*-NNAL animals for the first 10 weeks[62]. Since POB-DNA adducts are believed to only be formed from NNK bioactivation[81], the DNA adduct results suggest that *(S)*-NNAL is reoxidized to NNK to a greater extent than *(R)*-NNAL, which is consistent with *in vivo* metabolism data.

The levels of all the individual PHB-DNA adducts were about 10 times greater in the *(R)*-NNAL group than the *(S)*-NNAL and NNK groups. For all three treatment groups

7-PHB-Gua was the major adduct until week 5, then O^2-PHB-dThd was the major PHB-DNA adduct for the remainder of the 20 weeks[63]. These results suggest that there may be a repair mechanism for 7-PHB-Gua. The level of O^6-PHB-dGuo was much lower than that of O^2-PHB-dThd or 7-PHB-Gua, and was only detected in the lung of rats treated with NNK or *(S)*-NNAL. O^6-PHB-dGuo was detected in the liver of the *(R)*-NNAL group, but only for the first 5 weeks.

Based on the data available, it has been hypothesized that the persistence of *(S)*-NNAL in the lung tissue coupled with its apparent ability to reoxidize to NNK, may be important to the lung-specific carcinogenicity of NNK. The general mechanism is believed to involve NNK being inhaled via smoking and preferentially metabolized to *(S)*-NNAL, which is retained in the lung tissue. *(S)*-NNAL can then be reoxidized back to NNK and be bioactivated to form POB-DNA adducts. Thus, *(S)*-NNAL may be prolonging the exposure of the lung to NNK, which may be critical to the lung carcinogenicity of NNK.

1.D – PEITC

The ultimate goal of cancer research is to better understand the mechanisms responsible the formation of cancer so that it is possible to identify ways to reduce and prevent its development. One way to intervene in the cancer progression process is through chemoprevention. Chemoprevention is the use of natural, synthetic, or biological compounds to prevent, suppress, or reverse cancer progression.

Phenethyl isothiocyanate (PEITC) is a chemopreventive agent that exists as the glucosinolate conjugate, gluconasturtiin, in certain cruciferous vegetables, such as watercress. When the leaves of the plant are damaged, from cutting or chewing, the enzyme myrosinase is released and gluconasturtiin is hydrolyzed to form PEITC (Figure 1.6). PEITC has been shown to inhibit the tumorgenicity of NNK in mice and rats when given prior to or along with NNK[53,82-84]. When given after NNK administration in A/J mice, a reduction in tumor formation was not observed[85]. Research suggests that the ability of PEITC to reduce the formation of pulmonary tumors as a result of NNK exposure is primarily due to its ability to inhibit the oxidative metabolism of NNK and decrease the formation of certain DNA adducts[52,53,83,84,86-88]. PEITC has been shown to be a competive inhibitor for some CYP P450 enzymes and a possible mechanism-based inhibitor for others[89-92].

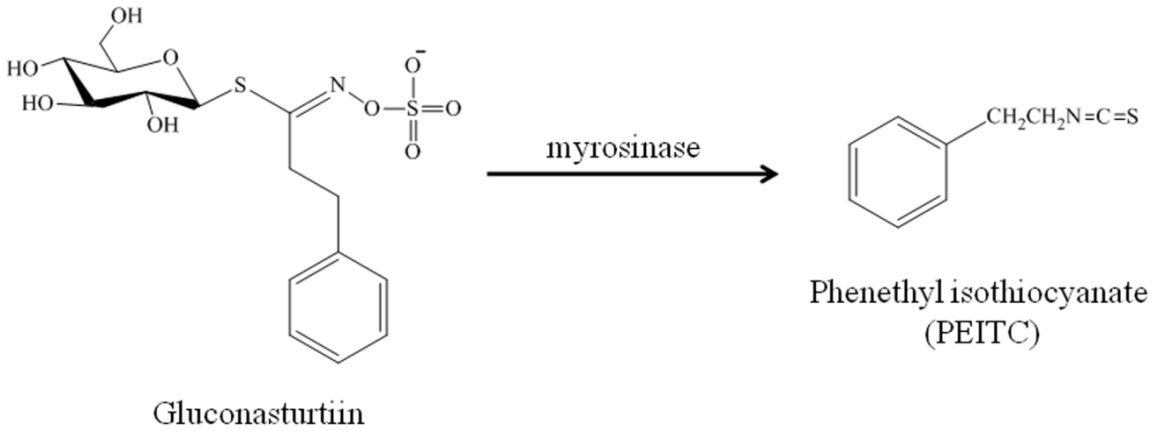

Figure 1.6 – *Structures of gluconasturtiin and PEITC.*

1.E – Objectives

The objectives of the current research were to:

1) To evaluate the metabolism and distribution of NNK, *(S)*-NNAL, and *(R)*-NNAL in the isolated perfused rat lung (IPRL) system, and to measure the formation of DNA-adducts.
2) To evaluate the effects of PEITC and carcinogen concentration on the metabolism, distribution, and formation of DNA-adducts in the IPRL system.
3) To assess the stereospecific and stereoselective binding of *(S)*-NNAL and *(R)*-NNAL in the lung tissue using the IPRL system.

The ultimate goal of this research was to better understand the mechanisms responsible for the lung-specific carcinogenicity of NNK in rodents, so that the role that NNK plays in the formation of lung cancer in smokers could be elucidated. By determining the mechanisms responsible for its carcinogenicity, we may be able to identify ways to intervene in the process to prevent the development of lung cancer. Furthermore, it is possible that the knowledge gained from determining the mechanisms responsible for the carcinogenicity of NNK could be useful in understanding the mechanisms of other carcinogens and the formation of other cancers and diseases.

CHAPTER 2 – METHODS DEVELOPMENT

2.A – Isolated Lung Perfusion System

The isolated perfused lung system can be a useful tool for examining a variety of pulmonary functions, but the setup of the system can be challenging. Several system criteria have to be set because a universally accepted procedure has not been established. Some aspects of the experimental design that have to be determined include the type of perfusate, the system setup, the surgical procedure, whether to perfuse at a constant flow or constant pressure, whether to use a single-pass or recirculating perfusion, how the lungs will be ventilated, and how viability will be determined[93,94]. Determining the viability of the lung is perhaps the most difficult aspect of the perfusion system. If edema (swelling due to fluid retention) occurs, the system is not considered viable. The following chapter discusses some of the steps that were taken to develop a system that produced successful lung perfusions.

2.A.i – 200 mL Single Reservoir System

Initial perfusion attempts were performed using a MX Amber perfuser TWO/TEN (MX International, Aurora, CO) perfusion system. This system had been previously used in our laboratory for liver perfusion studies[95,96]. The Amber perfuser was self-contained with two reservoirs, a peristaltic pump, an internal oxygenation system, and an internal circulating water bath that maintained the reservoirs at 37˚C. Given the size of the perfusion system it was not feasible to use a small perfusate volume. Therefore, initial

NNK perfusion studies used a reservoir volume of 200 mL. One reservoir chamber contained blank buffer for rinsing the lung, and the other chamber contained perfusate spiked with [5-^{3}H]NNK. Once the lung was rinsed and the flow rate was set (8 mL/min), the perfusate was switched from blank to spiked perfusate. The lungs were suspended above the chamber containing the spiked perfusate to establish a recirculating perfusion, and were gently wrapped in plastic wrap to hold in the warmth and moisture of the lung.

The results from these initial perfusions showed limited metabolism of NNK (Figure 2.1). In the first perfusion, the lung was perfused for 100 min, at the end of which 80% of the initial concentration of NNK remained unmetabolized and metabolites were not detected. In the second perfusion, a higher concentration of NNK was used and the duration of the perfusion was extended to 150 min to increase metabolite formation. At the end of the perfusion 75% of the initial concentration of NNK remained unmetabolized. Furthermore, the concentrations of the metabolites were very low, and close to the limit of detection for the HPLC assay. It was concluded that the large reservoir volume resulted in an increase in the metabolic half-life of NNK and that the metabolites were too dilute to measure their formation accurately. Therefore, a new system was constructed that would implement the use of a smaller reservoir volume.

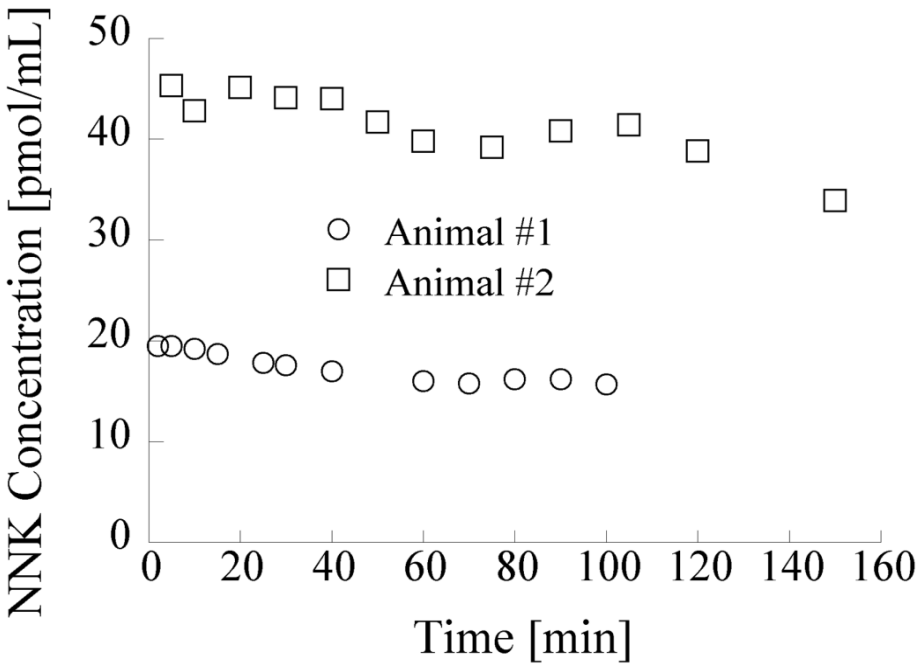

Figure 2.1 – *Concentration-time data of NNK (pmol/mL) in the 200 mL reservoir perfusion system*[97].

2.A.ii – 50 mL Two-reservoir System

In order to perfuse the lung using a 50 mL perfusate reservoir, a new system had to be constructed of individual components. One of the main criteria for the system was to ensure that adequate oxygenation of the perfusate occurred. The new system contained two reservoirs, an oxygenating reservoir (B) and a secondary reservoir (H) (Figure 2.2). The oxygenating reservoir was a three-necked, jacketed, 25 mL European flask (Chemglass, Vineland, NJ) which was used to oxygenate the perfusate. A jacketed condenser (C) was attached through the center port of the flask and was used to increase the surface area of the perfusate to help facilitate oxygenation. A stream of 95% O_2 / 5% CO_2 gas entered through a side port in the flask after being passed through a gas washing

cylinder (A) containing distilled water to humidify the oxygen; this was intended to prevent evaporation of the perfusate. The other side port was used to pump perfusate from the oxygenating reservoir into the lung. All three of the ports of the oxygenating reservoir were sealed tightly, to force the flow of oxygen through the condenser in order to better oxygenate the perfusate. A Masterflex peristaltic pump (D) (Cole-Parmer, Vernon Hills, IL) was used to pump the perfusate from the oxygenating reservoir through a bubbletrap (E), a pressure transducer (F), and into the lung. The tubing leading to the lung was placed in a circulating water bath (G) to warm the perfusate before it entered the lung. The lung was suspended in the secondary reservoir (H), a jacketed beaker, to keep the lung warm. A Minipuls 3 peristaltic pump (I) (Gilson, Middleton, WI) was used to pump the perfusate from the secondary reservoir back into the condenser. Both of the reservoirs were placed on top of stir plates (J) to ensure that the perfusate was well mixed.

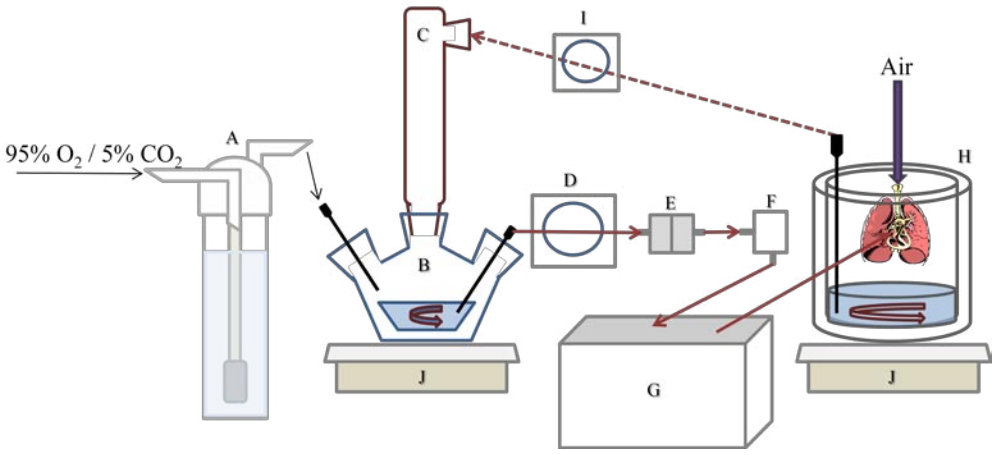

Figure 2.2 – *Schematic of the 50 mL two-reservoir perfusion system, which was comprised of a gas wash cylinder (A), a 25 mL European flask (B), a condenser (C), two peristaltic pumps (D & I), a bubbletrap (E), a pressure transducer (F), a circulating water bath (G), a 50 mL jacketed beaker (H), and two stir plates (J).*

At the start of the perfusion, 100 mL of perfusate was added to the secondary reservoir (H), which was then recirculated through the system for 20 – 30 min to oxygenate and warm the perfusate. The surgery was then performed and the lungs were rinsed of blood with approximately 50 mL of the perfusate, leaving roughly 50 mL of perfusate to perfuse the lung with. A recirculating perfusion was established by hanging the lungs in the secondary reservoir, and a bolus dose of [5-^{3}H]NNK (4.5 nmol) was administered to the oxygenating reservoir (B) and samples were taken from there as well.

The concentration-time data of NNK showed that significantly more metabolism occurred in the 50 mL, compared to the 200 mL system (Figure 2.3A). At the end of a 120 min perfusion less than 10% of NNK remained unmetabolized. The concentrations of the metabolites were high enough to monitor their formation throughout the course of the perfusion (Figure 1.3B & C). The final composition of the perfusate metabolites was similar to the results previously published by Schrader *et al.*[98]; thus it was concluded that the 50 mL system was a better system for monitoring the metabolism of NNK than the 200 mL system.

There were still several flaws with the two-reservoir perfusion system, and thus a simpler system was ultimately constructed. One of the main problems was coordinating the perfusate volumes between the two reservoirs. Since the oxygenation reservoir was only 25 mL, it could only hold half of the perfusate volume. It was necessary to keep a balance of perfusate between the reservoirs, but inconsistency with the flow from the Minipuls 3 and impaired flow from the condenser into the oxygenation reservoir made it difficult. Furthermore, the bolus dose administered to the oxygenation reservoir was only

diluted in part of the perfusate. As a result the initial sharp decrease in the NNK concentration was the result of dilution, and not due to metabolism or distribution into the tissue (Figure 2.3A). This was further complicated by inconsistent perfusate volumes. The initial system volume was 100 mL, and approximately 50 mL was used to rinse the lungs prior to the perfusion. However, while the wash volume was measured, it was difficult to obtain the same perfusate volume for each perfusion. Inconsistent reservoir volumes most likely attributed to the large variability in the concentration at the first time point. At this time the rate of success for a perfusion was less than 50% due to the formation of edema in the lung. Edema resulted in the swelling of the tissue, which impaired the metabolism of the lung. The cause of the edema formation was unknown, but it was suspected that inadequate oxygenation due to impaired flow between the condenser and the oxygenating reservoir, and the presence of endotoxins due to unsatisfactory cleaning of the complex system might be potential reasons. As a result, the system was simplified.

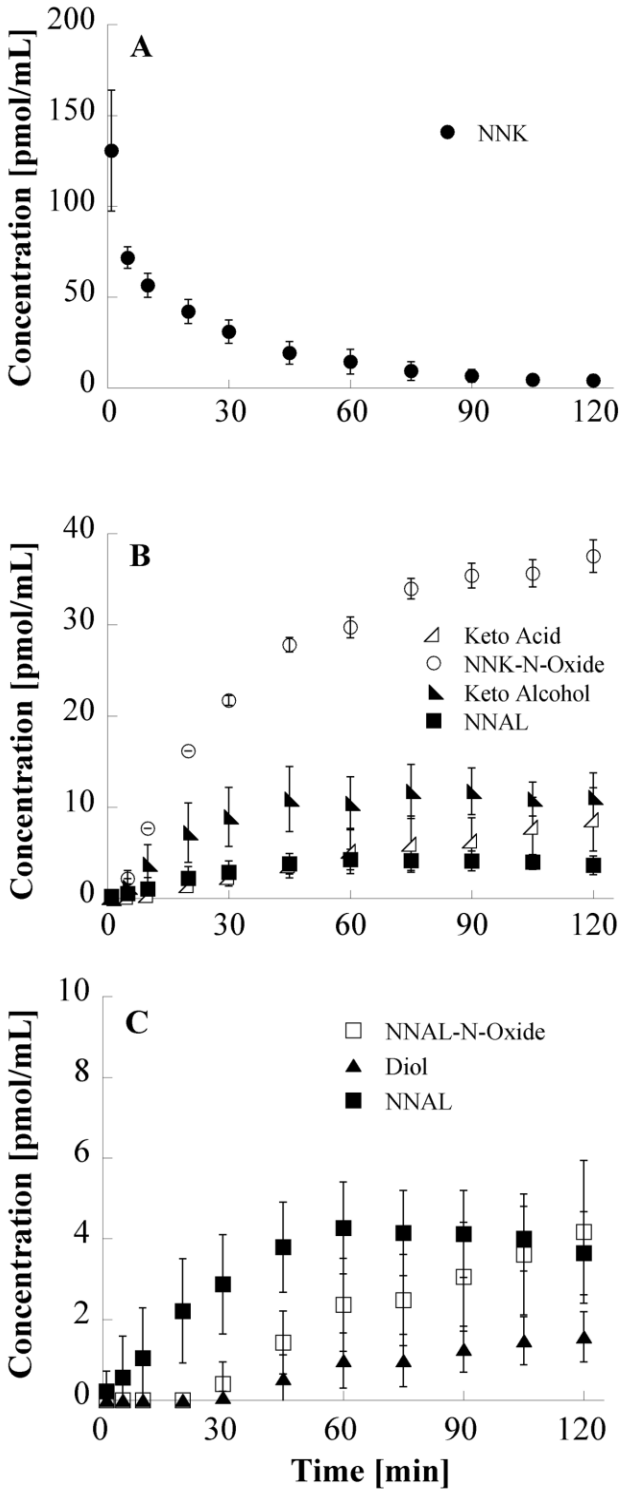

Figure 2.3 – *Average concentration-time (pmol/mL) data of NNK (A), NNK metabolites (B), and NNAL metabolites (C) in the perfusate of the 50 mL two-reservoir system (n=5)*[97].

2.A.iii – 50 mL Single Reservoir System

A schematic of the final perfusion system that was used for examining the pulmonary metabolism of NNK, *(S)*-NNAL, and *(R)*-NNAL is shown in Figure 2.4. A 200 mL jacketed beaker (B) served as the reservoir and the chamber in which the lungs were hung. The reservoir was placed atop a stir plate (F) to ensure that the perfusate was well mixed. A circulating water bath (G) was used to maintain the temperature of the system at 37 °C. The perfusate was pumped from the reservoir and through the system using a Masterflex peristaltic pump (C) (Cole-Parmer, Vernon Hills, IL). Masterflex Tygon tubing (solid line, L/S 14, Cole-Parmer) and 1/16" ID Tygon tubing (dashed line, C-06408-62, Cole-Parmer) were used to connect the components in the system. The perfusate was pumped from the reservoir through a bubble trap (D) and pressure transducer (E). The perfusate then returned to the lungs. The tubing connecting the pressure transducer and the lung was passed through the circulating water bath (G) to rewarm the perfusate before reaching the lung. The perfusate was oxygenated throughout the perfusion with 95% O_2 / 5% CO_2 that was passed through a gas washing cylinder (A) to humidify it. The lungs were inflated with air at a pressure of 4 cm H_2O. Probes for temperature and pH were placed in the reservoir to monitor these parameters throughout the perfusion *(not shown)*.

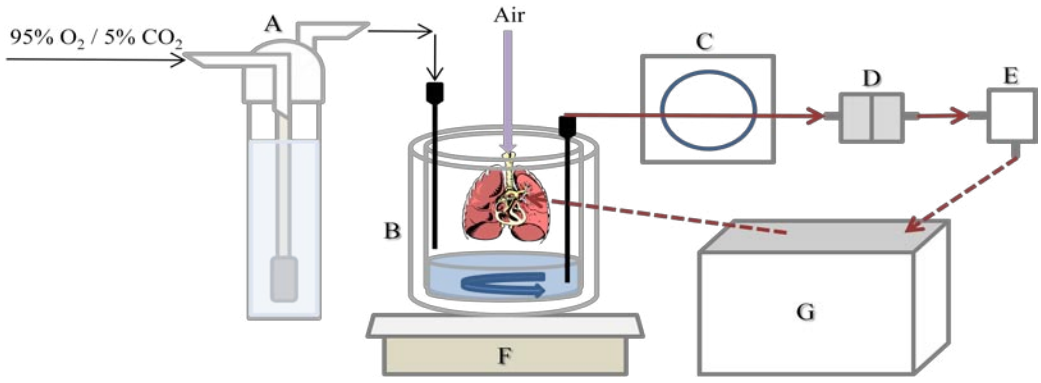

Figure 2.4 – *Schematic of the final perfusion system. The system used for all subsequent perfusions was comprised of a gas wash cylinder (A), a 50 mL jacketed beaker (B), a peristaltic pump (C), a bubbletrap (D), a pressure transducer (E), a circulating water bath (G), and a stir plate (F).*

The metabolism results using the simplified system are reported in Chapters 3 and 4.

2.B – Potential Sources of Edema

Although the perfusion system was simplified in an effort to reduce the formation of edema, problems persisted. As a result, each part of the perfusion setup was examined to determine what could potentially be contributing to development of edema in the lungs.

2.B.i – Perfusate

The lungs were perfused with a Ringers solution comprised of 2.68 mM KCl, 1.25 mM $MgSO_4 \cdot 7H_2O$, 1.82 mM $CaCl_2$, 5.55 mM D-glucose, 12 mM HEPES, 137 mM NaCl, 1% dextran 70, and 0.5% albumin. The choice of perfusate was based on the perfusion

setup used by Dr. Douglas Wangensteen[99,100]. Initially the perfusate was made fresh by weighing out each component. However, when the reservoir volume decreased it was not feasible to weigh out the small quantities required for some of the compounds. Therefore, a series of bulk solutions were tried. The initial bulk solution contained all of the compounds excluding albumin, which was added immediately before each perfusion. When edema problems continued to persist, the bulk solution was changed to include all the compounds except glucose, dextran 70, and albumin, which were added fresh before each perfusion. To ensure that the chemicals used in the perfusate were pure and fresh, all new perfusate chemicals were purchased. When that did not help, the source of albumin was switched from 25% albumin in Tyrode's buffer to powdered albumin. Changes to the perfusate, along with different filtration methods, and duration of oxygenation did not resolve the problem.

Ultimately, solutions of KCl (11.2 mM), $CaCl_2$ (7.7 mM), and $MgSO_4 \cdot 7H_2O$ (5.3 mM) were made in advance in 500 mL aliquots and stored at 4 ºC. The perfusate was made fresh by combining 60 mL of each of the pre-made solutions, with 0.25 g glucose, 2.0 g NaCl, 0.71 g HEPES, and 2.5 g dextran 70. The solution was stirred until all of the dextran was incorporated. A separate solution of albumin was made by adding 70 mL dH_2O to 1.25 g albumin (A7906-500G, Sigma). The albumin solution was not stirred; it was simply allowed to sit until the albumin dissolved. After the dextran was incorporated into the salt solution, it and the albumin solution were warmed to approximately 37 ºC. The salt solution was adjusted to a pH of 7.4 with 1M NaOH, and was then oxygenated by bubbling humidified 95% O_2 / 5% CO_2 into the solution for 20 min. The solution was

oxygenated in the absence of albumin to avoid bubbling. After oxygenation the albumin solution was added to the salt solution, and the pH was readjusted to 7.4. The perfusate was then filtered by gravity filtration through coarse 25 µm cellulose filter paper (09-790-12F, Fisher Scientific). Fifty mL of perfusate was filtered into the reservoir and the remainder was filtered into a bottle. The bottle was placed in the circulating water bath to maintain the temperature at 37 ºC to keep the perfusate warm for the initial and final rinses. The tubing was filled with perfusate and air was removed from the system. The perfusate was then allowed to recirculate through the system. Once the lung were excised from the chest cavity and rinsed of blood, the perfusate flow was switched to the reservoir and the lungs were hung inside the beaker to establish a recirculating perfusion.

2.B.ii – Animal Source

The source of the F344 rats was examined as a possible cause for edema. All rats were initially purchased from Harlan Laboratories (Madison, WI), but in some animals dark spots were observed on the lung tissue when the chest cavity was opened. Dr. Roland Gunther, a Research Animal Resources (RAR) clinical specialist at the University of Minnesota, believed the small lesions could have been a result of interstitial pneumonia caused by the Rat Respiratory Virus. This was never confirmed, but the animal source was switched to Charles River Laboratories (Portage, MI) to ensure that the edema that developed during the perfusions was not a result of a preexisting pulmonary condition in the rats. Even though the rats from Charles River did not appear to have lung lesions, the formation of edema during the perfusions still persisted.

2.B.iii – Surgical Procedure

The surgical procedure is described in detail in Chapter 3, and is only briefly outlined here to provide context for the development of the procedure. Rats were anesthetized and a tracheotomy was performed. The chest cavity was opened and the pulmonary artery was cannulated. The lungs were removed from the chest cavity and the heart was cut to allow for perfusate flow out of the lungs. The lungs were suspended by the trachea from a ring stand, where they were rinsed of blood with perfusate. The lungs were inflated and deflated two to three times, following which they were inflated at a constant pressure of 4 cm H_2O. The flow rate was set to 8 mL/min, and once the lungs were rinsed, they were placed in the reservoir to establish a recirculating perfusion.

Some laboratories had reported using heparin in their surgical procedure. Heparin is an anticoagulant and it was used to allow the blood in the pulmonary vasculature to be removed more easily and reduce the risk of tissue damage[99,101-103]. However, heparin had not been used in our perfusions. To test if the absence of heparin resulted in edema, 100 units of heparin was injected into the pulmonary artery immediately before it was cannulated to help facilitate the removal of blood from the tissue. Unfortunately, the use of heparin in the surgical procedure did not have a noticeable effect on preventing edema.

The time at which the heart was cut was also examined as a potential cause of edema. In initial perfusions the heart was not cut until the lungs were excised from the chest cavity and suspended. The perfusate flow was turned off before the cannula was inserted into the pulmonary artery, and was not resumed until immediately before the

heart was cut. The perfusate flow was turned off to prevent a buildup of fluid and pressure in the lung while they were being removed from the chest cavity, which could result in tissue damage. At the time it was taking approximately 5 – 10 min to remove the lungs from the body and start the flow of perfusate through the lungs. It was thought that perhaps a lack of oxygen to the tissue during this non-perfusing time could possibly be leading to tissue damage. Therefore the heart was cut immediately after the insertion of the pulmonary artery cannula and a low flow rate was used to perfuse the lung until it was removed from the body. The immediate cutting of the heart to allow for perfusate flow through the lungs did not curtail the formation of edema.

Finally, after conversing with Dr. Masahiro Sakagami at Virginia Commonwealth University and observing his isolated lung perfusion procedure, he proposed that the formation of edema in the lungs may be due to the restriction of perfusate flow from the heart. An increase in pressure was observed before the formation of edema, but it was taken as a sign that edema was forming. Dr. Sakagami, however, suggested that the increase in pressure indicated restricted flow, and it was this obstruction of perfusate flow from the heart that was causing the lungs to swell and retain fluid. If the obstruction of flow was eliminated and the pressure was decreased, then perhaps edema would not form. He demonstrated that the heart had to be extensively cut to ensure that perfusate could flow freely from the heart. The heart was cut off as high up as possible and then was cut up the sides to ensure that the valves between the atrium and the ventricles were not inhibiting flow, being careful not to cut too close to the pulmonary artery. When the heart was extensively cut the edema problems appeared to be eliminated.

2.C – Impaired Metabolism

When the edema issue was remedied, a substantial decrease in NNK metabolism was noticed. Limited NNK metabolism had been observed previously, but was attributed to the formation of edema in the lungs. Since a number of things had been changed in the system to try to resolve the problem with edema formation, it was unclear what was causing the reduced metabolism of NNK. Thus, the system had to be systematically checked for all potential causes of the reduced metabolism. Some of the components that were checked included the source of dextran 70, the type of albumin (powdered vs 25% albumin in Tyrode's buffer), the source of F344 rats (Harlan vs Charles River), potential changes in the food or bedding of the animals, the use of heparin in the surgical procedure, the time at which the heart was cut, the oxygenation and pH of the perfusate, and the temperature. None of these had a visible effect on the metabolism of NNK.

The radiopurity of the [5-^{3}H]NNK was also checked via HPLC and appeared to be pure. It was proposed to check the overall purity of the [5-^{3}H]NNK solution via NMR, but because the solution had a high specific activity, almost all of the remaining stock solution would have been required for NMR analysis. When a new batch of [5-^{3}H]NNK was purchased from Moravek, the metabolism was similar to that observed in the initial perfusions and from Schrader *et al*[98]. After conversing with Moravek, it appeared that the batch of [5-^{3}H]NNK that had resulted in decreased metabolism, was synthesized with a precursor that had impurities in it that affected the production yield of NNK. Once the impurity was eliminated from the starting compound, the yield of [5-^{3}H]NNK synthesis increased and the metabolism of NNK in the IPRL system was similar to previous results.

In another batch of [5-^{3}H]NNK, a peak eluting near the solvent front was observed in the perfusate within a minute of the administration of NNK. Since that was not enough time for NNK to pass through the system and into the lung, it was unlikely that the peak was a quick forming metabolite. The peak was identified to be [^{3}H]H_2O and was also observed when [5-^{3}H]NNK was placed in a $NaHCO_3$ solution with a basic pH. Eventually it was discovered that Moravek had switched their tritium labeling process from catalytic dehalogenation with tritium gas to exchange with tritiated water. Catalytic dehalogenation uses [5'-pyridine] brominated NNK as a precursor for [5-^{3}H]NNK synthesis and is a selective method for labeling at the 5' position of the NNK pyridine ring, which is a stable location for the tritium label. When Moravek ran out of the precursor they switched to the less selective tritiated water exchange method. As a result the tritium label was not selectively located at the 5' position of the pyridine ring. Some of the label was exchanged onto the carbons adjacent to the nitroso group, where the tritium label can exchange to water under acidic or basic conditions. When Moravek did a quality control test on some of their batches of [5-^{3}H]NNK using the water exchange method they found a significant decrease in specific activity with time. Therefore they had to synthesize [5'-pyridine] brominated NNK as previously reported[104], so that the more selective catalytic dehalogenation labeling method could be used. For all subsequent tritiated compounds purchased from Moravek, the stability of the label was tested by incubating 1 μCi of the compound in 25 mM $NaHCO_3$ for 60 min and 24 hrs at 60 °C and then analyzing the solution on HPLC to see if tritiated water was formed.

2.D – Determination of PEITC Concentration

In vitro and *in vivo* studies have shown PEITC to inhibit the metabolism of NNK and to reduce the formation of certain DNA adducts. However, a majority of the *in vitro* work dosed PEITC to the whole animal[52,87-89,91,105], so the tissue concentration of PEITC necessary to see metabolic inhibition was not well defined. One *in vitro* study examined the inhibition of specific human CYP P450 isozymes using PEITC concentrations ranging from 2.5 μM to 50 μM[90]. Since PEITC was thought to be a potent inhibitor, metabolic inhibition of NNK was expected to be seen at low concentrations of PEITC. To test the potency of PEITC it was first given at the same initial concentration as NNK, 0.1 μM (Figure 2.6 D, E, & F). When no noticeable effects on NNK metabolism were observed, the concentration of PEITC was increased to 0.2 μM (Figure 2.6 G, H, & I). Since low concentrations of PEITC did not appear to effect NNK metabolism, a much larger dose of PEITC was used to ensure that inhibition would occur. Complete inhibition of NNK induced pulmonary tumors was observed *in vivo* when the daily dose of PEITC was roughly 200 times greater than the daily NNK dose[84]. Therefore, the initial reservoir concentration of PEITC was increased to 20 μM (Figure 2.7 G, H, & I). The higher concentration of PEITC resulted in a decrease in NNK oxidative metabolism.

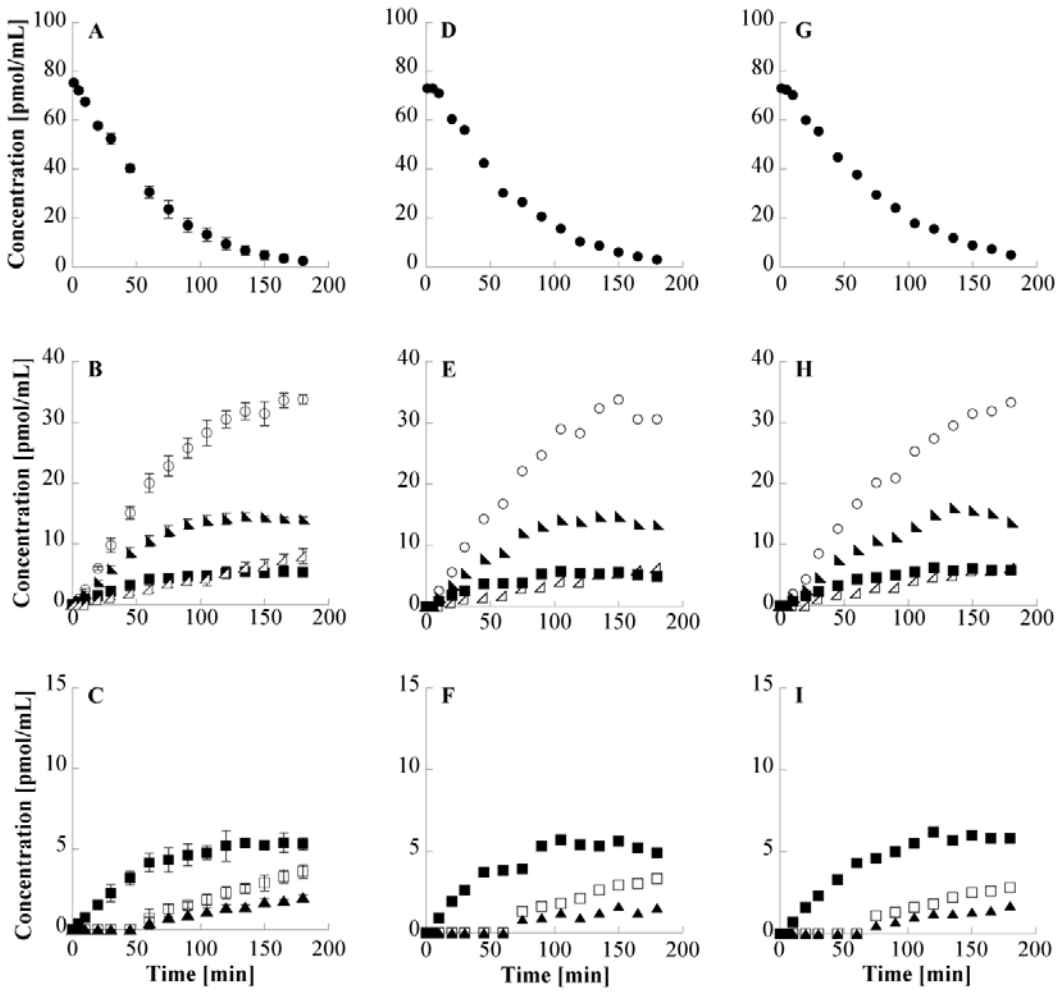

Figure 2.5 – *Concentration (pmol/mL) vs time (min) profiles of NNK and metabolites in the perfusate of 0.1 µM NNK plus either 0 µM PEITC (A, B, C), 0.1 µM PEITC (D, E, F), or 0.2 µM PEITC (G, H, I). Symbol designations are as follows: NNK, ●; NNK-N-oxide, ❍; NNAL, ■; NNAL- N-oxide, ❑; keto alchol, ◣; keto acid, ◅; diol, ▲. The profile of NNAL is replotted in figures C, F, and I for comparison purposes. The perfusions containing 0.1 and 0.2 µM PEITC were single perfusions. For perfusions with 0 µM PEITC, n = 3.*

The effect of 10 µM PEITC was also examined (Figure 2.7 D, E, & F). Both the 10 µM and 20 µM PEITC concentrations resulted in similar metabolic profiles for NNK. At both

concentrations the oxidative metabolism of NNK was decreased and the formation of NNAL appeared to increase. The 20 µM PEITC concentration was chosen for the inhibition perfusions to be performed with NNK and PEITC.

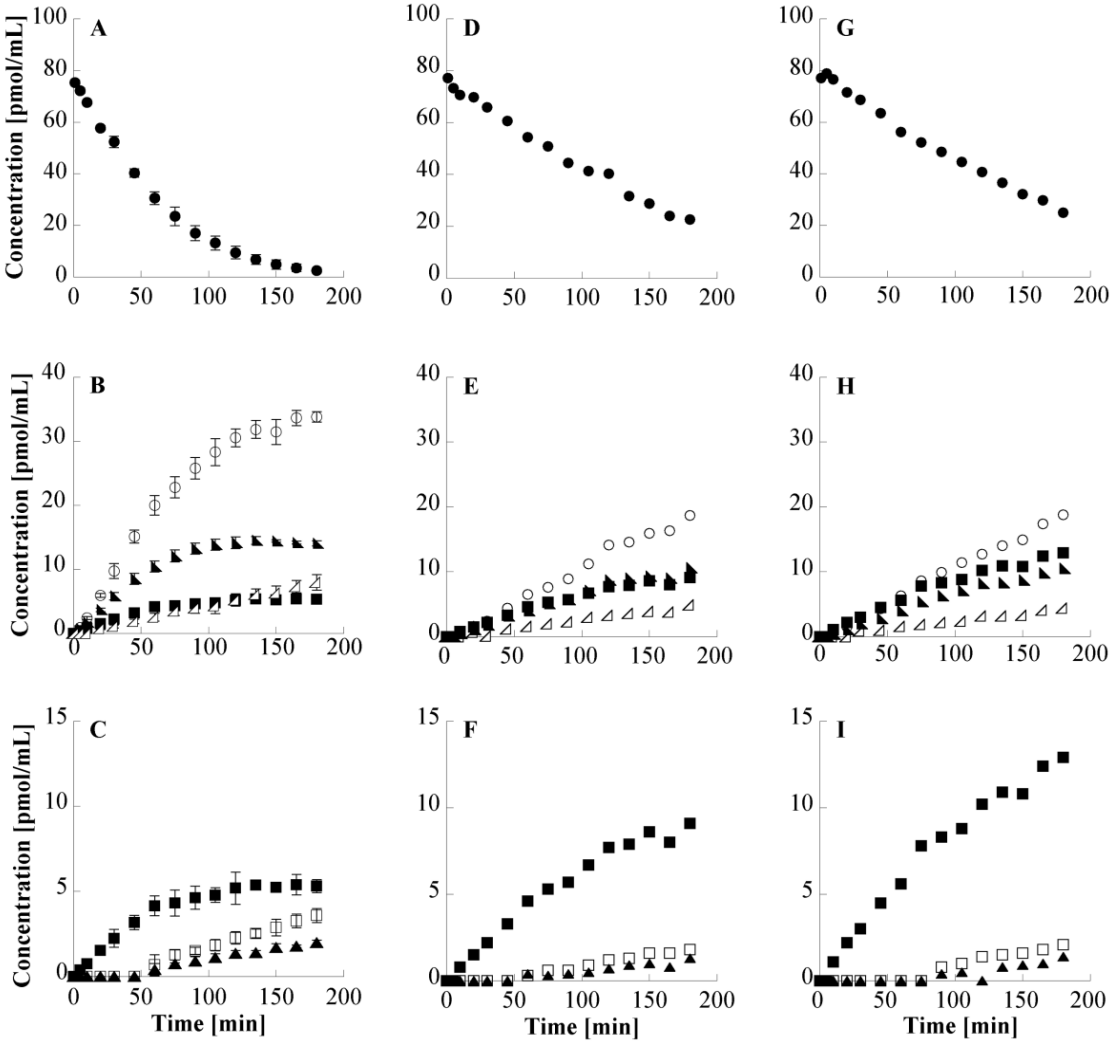

Figure 2.6 – *Concentration (pmol/mL) vs time (min) profiles of NNK and metabolites in the perfusate of 0.1 µM NNK plus either 0 µM PEITC (A, B, C), 10 µM PEITC (D, E, F), or 20 µM PEITC (G, H, I). Symbol designations are as follows: NNK, ●; NNK-N-oxide, ❍; NNAL, ■; NNAL- N-oxide, ❑; keto alchol, ◣; keto acid, ◅; diol, ▲. The profile of NNAL is replotted in figures C, F, and I for comparison purposes. The perfusions containing 10 and 20 µM PEITC were single perfusions. For perfusions with 0 µM PEITC, n = 3.*

It should be noted that PEITC was not soluble in water, so all of the PEITC solutions were made in 100% ethanol (EtOH). For each PEITC perfusion (0.1, 0.2, 10, 20 μM) a bolus of 10 μL of the necessary PEITC solution was administered to the reservoir immediately before the bolus of NNK. It is unlikely that the addition of EtOH affected the metabolism or viability of the lung because the low concentrations of PEITC (0.1 and 0.2 μM) showed the same metabolism and metabolic profiles as the control NNK perfusions. If the addition of EtOH impaired the metabolism of NNK it should have been observed in the perfusions with the low concentration of PEITC, but it was not. Since the same volume of EtOH was added to the reservoir in the low concentration PEITC perfusions (0.1 and 0.2 μM) and in the higher concentration PEITC perfusions (10 and 20 μM), it can be concluded that the inhibition of NNK metabolism was a result of the presence of PEITC and not the presence of EtOH.

2.E – Preliminary *(S)*-NNAL and *(R)*-NNAL Perfusions

The initial plan was to repeat the same perfusion experiments that were conducted with NNK using *(S)*-NNAL and *(R)*-NNAL. However, when 0.1 μM *(S)*-NNAL was perfused for 180 min, limited metabolism was observed (Figure 2.8). At the end of the perfusion, unmetabolized NNAL (40 ± 4 pmol/mL) accounted for approximately 58% of the final perfusate concentration. The major perfusate metabolite was NNAL-*N*-oxide (20 ± 3 pmol/mL), which accounted for roughly 30% of the final concentration. Hydroxy acid (3.7 ± 0.5 pmol/mL) and diol (4.4 ± 0.3 pmol/mL) were also detected in the perfusate, but at much lower concentrations than NNAL-*N*-oxide and NNAL. Neither

NNK nor any of its subsequent metabolites were detected in the perfusate. The estimated apparent pharmacokinetic parameters for the pulmonary metabolism of *(S)*-NNAL are listed in Table 2.1.

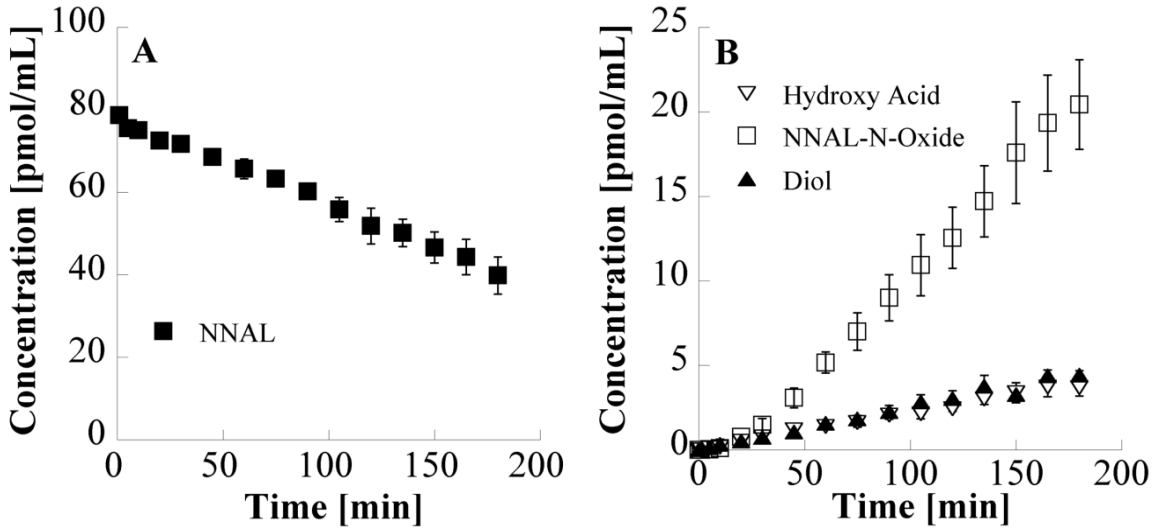

Figure 2.7 – *Average concentration (pmol/mL ± SD) vs time (min) profiles of NNAL (A) and metabolites (B) in the perfusate of 0.1 µM (S)-NNAL during a 180 min perfusion, (n=3). Where error bars are not visible, they are smaller than the symbol.*

Table 2.1 – *The apparent pharmacokinetic parameters (mean ± SD, n=3) for the pulmonary metabolism of 0.1 µM (S)-NNAL based on a 180 min perfusion. Estimates were obtained from non-compartmental analysis using WinNonlin.*

$t_{1/2,\,app}$ [min]	167 ± 48
V_z [mL]	60 ± 6
CL_{app} [mL/min]	0.26 ± 0.06
ER_{app}	0.033 ± 0.007

NNAL-*N*-oxide was the major metabolite in the tissue, accounting for approximately 70% of the total radioactivity. Hydroxy acid (11%), keto acid (3%), and NNAL (2%) were also detected in the tissue. Diol was not clearly observed in the tissue, but it is possible that it was formed. If diol was formed to a much lesser extent than NNAL-*N*-oxide, it may not be possible to see it separate from NNAL-*N*-oxide since it elutes on the tail end of the oxide peak. NNK was not detected in the tissue, neither were any DNA adducts.

Since the formation of NNK was expected in the *(S)*-NNAL perfusions but was not observed, a single perfusion with each enantiomer was performed using 50 µCi of only the labeled compound to ensure that the compounds were not misidentified. The specific activity of [5-^{3}H]*(S)*-NNAL (21.2 Ci/mol) was lower than [5-^{3}H]*(R)*-NNAL (25.8 Ci/mol), so the initial reservoir concentration in the two perfusions were not the same. Neither NNK nor any of its metabolites were observed in either of the perfusions. The metabolism of *(R)*-NNAL and *(S)*-NNAL appeared to be similar, with perhaps *(R)*-NNAL being metabolized to a slightly greater extent (Figures 2.9 & 2.10). At the end of the 180 min perfusion the concentration of *(R)*-NNAL accounted for 50% of the total concentration, while *(S)*-NNAL accounted for approximately 60%.

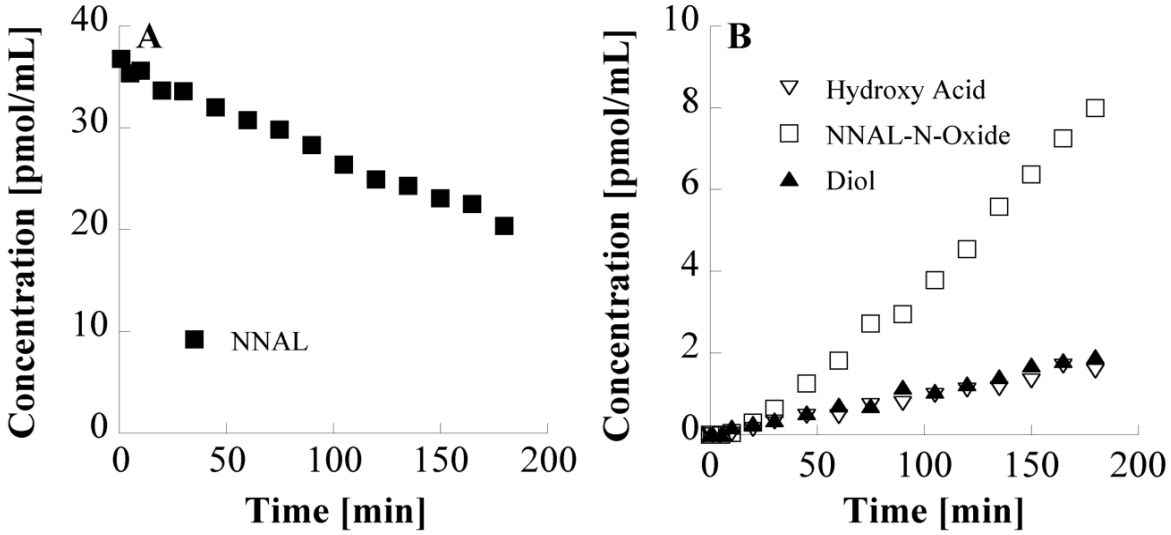

Figure 2.8 *– Concentration (pmol/mL) vs time (min) profiles of NNAL (A) and metabolites (B) in the perfusate after a 50 µL bolus dose of [5-* ^{3}*H](S)-NNAL during a 180 min perfusion (n=1).*

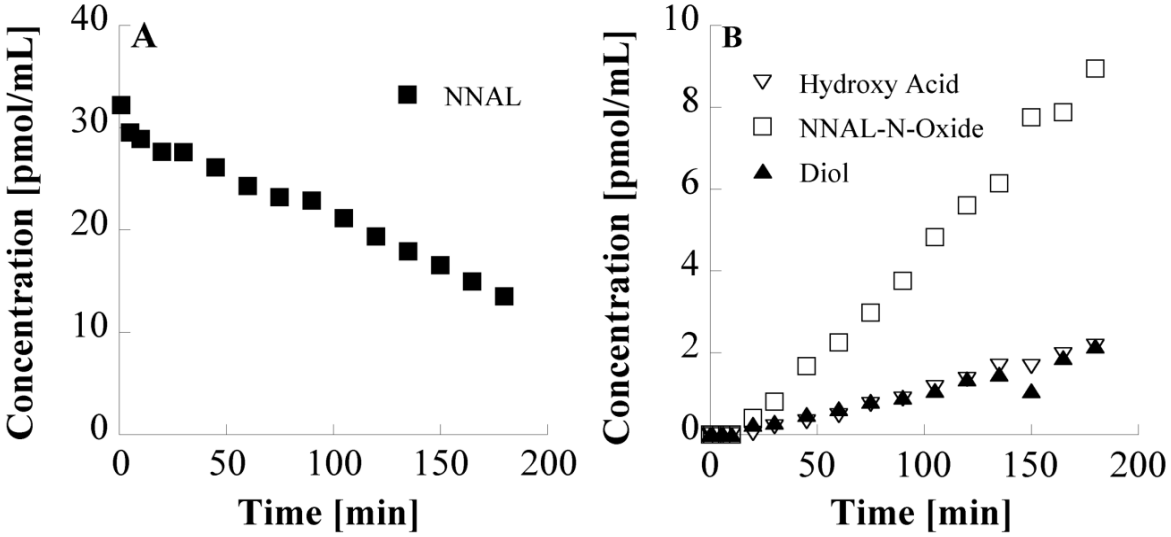

Figure 2.9 – *Concentration (pmol/mL) vs time (min) profiles of NNAL (A) and metabolites (B) in the perfusate after a 50 µL bolus dose of [5-* ^{3}*H](R)-NNAL during a 180 min perfusion (n=1).*

NNAL-*N*-oxide, hydroxy acid, and diol composition of the final perfusate concentration were similar for both *(R)*-NNAL (33%, 8%, and 8%) and *(S)*-NNAL (25%, 5%, and 6%). The composition of metabolites in the tissue was also similar for both enantiomers *(data not shown)*.

Since previous *in vitro* and *in vivo* data reported a difference in the metabolism of the NNAL enantiomers, both labeled and unlabeled *(S)*-NNAL and *(R)*-NNAL solutions were analyzed via GC-TEA to ensure that each enantiomer was pure and properly identified. GC analysis confirmed that all four solutions were primarily one enantiomer and were properly identified.

With approximately half of the final perfusate concentration attributed to unmetabolized NNAL, it was hypothesized that more NNAL needed to be metabolized before NNK and its metabolites could be detected. Thus the duration of the perfusions were extended from 180 min to 360 min. Both enantiomers were perfused at 0.1 μM for 360 min to see if NNK formation could be detected. Neither NNK nor its metabolites were detected in the perfusate or tissue.

One final test perfusion was performed with *(S)*-NNAL at an initial reservoir concentration of 1.2 μM for 360 min. It was thought that perhaps a higher concentration of NNAL was needed to see the formation of NNK or that a higher concentration was needed to force the reaction towards NNK. Once again NNK and its metabolites were not formed in the perfusate or the tissue.

At this point there was not enough [5-^{3}H]*(S)*-NNAL remaining to carry out all the proposed experiments, so the 1.2 µM initial concentration was chosen. Since there did not appear to be a difference in metabolite formation or the pharmacokinetic parameters between the 0.1 µM and 1.2 µM *(S)*-NNAL 360 min perfusions, the higher concentration was used for both enantiomers so that the metabolism results could be compared to the perfusions in which DNA adduct formation was determined. In the NNK perfusions only one adduct was detected at the 0.1 µM concentration, whereas several more adducts were detected at the 1.2 µM concentration. Therefore, the metabolism perfusions involving *(S)*-NNAL and *(R)*-NNAL used an initial reservoir concentration of 1.2 µM and were carried out for 360 min. Since limited metabolism was observed and limited *(S)*-NNAL remained, perfusions with PEITC were not carried out.

2.F – Conclusions

The keys to a successful isolated lung perfusion include: 1) have a simple system that is clean and free of endotoxins; 2) select a perfusate that has an osmolality similar to plasma, is well oxygenated, and is maintained at a temperature of 37 °C and a pH of 7.4; 3) cut the heart extremely well. Failure to cut the heart adequately will result in restricted perfusate flow out of the lung, which in turn will increase the pressure in the pulmonary vasculature and lead to the formation of edema in the lungs.

PEITC did not appear to have inhibitory effects on the metabolism of NNK at concentrations of 0.1 µM and 0.2 µM. However, the higher PEITC concentrations of 10

μM and 20 μM both appeared to have inhibitory effects on the oxidative metabolism of NNK. Since previous *in vivo* experiments showed complete inhibition of NNK tumor formation with PEITC doses that were 200 times greater than the NNK dose, the 20 μM concentration of PEITC was used in subsequent perfusions.

Preliminary perfusions with *(S)*-NNAL and *(R)*-NNAL showed that the enantiomers were not metabolized by the lung as efficiently as NNK. As a result, the duration of the NNAL perfusions had to be increased from 180 min to 360 min to allow more time for the enantiomers to be metabolized by the lung.

CHAPTER 3: NNK METABOLISM IN THE IPRL SYSTEM

All data presented in this chapter was previously published in:

Laura A. Maertens, Pramod Upadhyaya, Stephen S. Hecht, and Cheryl L. Zimmerman. Formation and Distribution of NNK Metabolites in an Isolated Perfused Rat Lung. *Drug Metab Dipos* May 2010 38:752-760

3.A - Introduction

The objective of this chapter was to better understand the carcinogenicity of NNK in the lung by examining the effects of PEITC and NNK concentration on perfusate and tissue metabolites, the formation and distribution of *(S)*-NNAL and *(R)*-NNAL in the perfusate and tissue, as well as DNA adduct formation in the IPRL system. The present lung perfusions expand on previous studies by quantitating metabolites and the individual NNAL enantiomers in the tissue as well as in the perfusate, allowing for a better understanding of the distribution of metabolites between the perfusate and the tissue. Furthermore, the characterization of individual DNA adducts shows that metabolic bioactivation in lung leads directly to DNA damage, in the absence of the liver. This is the first study to examine the formation of DNA adducts and the effect of PEITC on NNK metabolism in the lung using the IPRL system.

3.B – Material and Methods

3.B.i - Chemicals

Unlabeled NNK, racemic NNAL, NNK-*N*-oxide, NNAL-*N*-oxide, keto alcohol, keto acid, and diol were purchased from Toronto Research Chemicals (North York, Ontario). Hydroxy acid, *(S)*-NNAL, and *(R)*-NNAL were synthesized and generously provided by Dr. Pramod Upadhyaya [106-108]. [5-^{3}H]NNK (21.7 Ci/mmol) was purchased from Moravek Biochemicals (Brea, CA). HPLC grade ACN and isopropanol were obtained from Fisher Scientific (Hampton, NH). Dextran 70 was acquired from Pharmacosmos (Holbaek, Denmark). The Puregene® DNA isolation kit was purchased from Qiagen (Germantown, MD). PEITC, bovine serum albumin (A7906-500G), and all other chemicals were obtained from Sigma-Aldrich (St. Louis, MO).

3.B.ii - Animals

Male Fisher 344 rats were purchased from Charles River Laboratories (Portage, MI). They were housed two to three per cage containing corn cob bedding, and were maintained under standard conditions (20 ± 2 ºC, 12 h light-dark cycle). Animals were given food (Teklad 2018, Harlan, Madison, WI) and water *ad libitum.* After arrival, they were allowed to acclimate in the housing facility for at least 1 week before use. The animal protocol for these experiments was approved by the University of Minnesota Institutional Animal Care and Use Committee (IACUC).

3.B.iii - Isolated Lung Perfusion

The general principles of the isolated lung perfusion procedure used were adopted from the laboratory of Dr. Douglas Wangensteen (University of Minnesota) and have been previously described [99,100]. To remove the lungs from the chest cavity, rats were anesthetized with a 60 mg/kg intraperitoneal dose of pentobarbital sodium (Ovation Pharmaceuticals, Deerfield, IL). A tracheotomy was performed and a 0.75 - 1 in piece of PE 240 tubing (Becton Dickinson, Sparks, MD) was inserted into the trachea and tied securely into place with suture (Deknatel, Mansfield, MA). Next, an incision was made into the abdomen and the chest cavity was opened by cutting up the midline of the rib cage. The chest cavity was held open with a retractor, and 100 units of heparin sodium (APP Pharmaceuticals, Schaumburg, IL) were slowly injected into the right heart immediately below the pulmonary artery. A small incision was then made at the site of the heparin injection and a polyethylene cannula (PE 190) connected to the perfusate supply was inserted into the pulmonary artery and tied into place. The heart was cut thoroughly to allow for unrestricted flow of perfusate out of the lung. The lungs were then excised from the chest cavity and suspended by the trachea from a ring stand, where they were rinsed of blood with perfusate. The lungs were inflated and deflated two to three times to help facilitate the removal of the blood from the vessels, following which they were inflated at a constant pressure of 4 cm H_2O. The flow rate was set to 8 mL/min, and once the lungs were adequately rinsed, as determined by visual inspection, they were placed in the jacketed beaker that served as the reservoir.

The lungs were perfused in a 50 mL recirculating system with a Ringers solution (pH 7.4) that was comprised of 2.68 mM KCl, 1.25 mM $MgSO_4 \cdot 7H_2O$, 1.82 mM $CaCl_2$, 5.55 mM D-glucose, 137 mM NaCl, 12 mM HEPES, 1% dextran 70, and 0.5% albumin. The perfusate was oxygenated with 95% O_2 and 5% CO_2, and the system was maintained at 37 °C. The pressure, temperature, and pH were monitored with transducers throughout the perfusion. A lung was discarded if excessive swelling and water retention were observed throughout the course of the perfusion.

3.B.iii.a - Metabolism Studies

The metabolism of NNK in the lung was examined using two initial concentrations of NNK with and without PEITC. Three animals were used for each of four treatments: 1) 0.1 μM NNK; 2) 0.1 μM NNK + 20 μM PEITC; 3) 1.2 μM NNK; and 4) 1.2 μM NNK + 20 μM PEITC. Once the lungs were rinsed of blood and a recirculating perfusion was established, a bolus dose of each of the appropriate compounds was injected into the perfusate reservoir. To detect the formation of metabolites, a 50 μL bolus (~50 μCi) of [5-^{3}H]NNK was administered to each perfusion. To achieve the desired initial reservoir concentration of NNK an aliquot of unlabeled NNK solution (0.29 nmol/μL in EtOH:H_2O (50:50)) was simultaneously administered. In the 0.1 μM perfusions 10 μL of the unlabeled NNK solution was added along with the [5-^{3}H]NNK, while the 1.2 μM concentration was achieved by adding 200 μL of the unlabeled NNK solution with the [5-^{3}H]NNK. PEITC was dissolved in 100% ethanol to produce a dosing

solution with a concentration of 100 nmol/μL; thus 10 μL of the PEITC solution was administered to achieve an initial reservoir concentration of 20 μM PEITC.

Perfusate samples of 250 μL were taken from the reservoir at 0, 1, 5, 10, 20, 30, 45, 60, 75, 90, 105, 120, 135, 150, 165 and 180 min post dose. Immediately following the collection of the 180 min perfuate sample, an additional 5 mL perfusate sample was collected and stored at -4 °C, and was used to determine the ratio of *(S)*-NNAL to *(R)*-NNAL in the final perfusate. Then the lungs were perfused with 50 mL of blank perfusate. The tissue was then minced, weighed, flash-frozen in liquid nitrogen, and stored at -80 °C until further analysis.

3.B.iii.b - DNA Adduct Studies

The perfusions for studying DNA adducts were carried out in the same manner as those conducted for metabolism, except that only unlabeled NNK was used and perfusate samples were not collected. For the 0.1 μM perfusions 17 μL of the unlabeled NNK (0.29 nmol/μL) solution was added to the reservoir, and 206 μL was added for the 1.2 μM perfusions. After the 180 min perfusion the lungs were perfused with 50 mL of blank perfusate; the tissue was then minced, weighed, flash-frozen in liquid nitrogen, and stored at -80 °C until analysis for individual DNA adduct formation was performed.

3.B.iv - Perfusate Analysis

The amount of total radioactivity in each perfusate sample was determined by analyzing a 50 µL aliquot by LSC. The remaining 200 µL of each sample was used to quantitate metabolite formation. Protein was precipitated from the perfusate samples by adding 500 µL of ACN, vortexing, then centrifuging at 13,000 x g (235B, Fisher Scientific) for three min. The supernatant was then concentrated to dryness with a stream of nitrogen while heating in a 37 ºC water bath. The samples were reconstituted with 220 µL of 20 mM $NaHPO_4$ buffer containing 1 mM EDTA, and centrifuged at 13,000 x g for 1 min. The metabolites were analyzed by injecting 100 µL of the final supernatant onto HPLC with UV and radioflow detectors.

The 5 mL perfusate sample taken at the end of each perfusion was used to analyze the ratio of the NNAL enantiomers in the perfusate at the end of the perfusion. The extra perfusate sample was taken to ensure that NNAL could be detectable by the GC-TEA assay. The samples were stored at -4 °C until GC analysis could be carried out. At that time the samples were thawed and the protein was precipitated from the perfusate sample by adding 5 mL of ACN, vortexing, and then centrifuging at 1228 x g (IEC Medispin) for 15 min. The supernatant was evaporated to dryness in a 37 ºC water bath with a gentle stream of nitrogen. The concentrated sample was then reconstituted with 300 µL of distilled water. The sample was vortexed and centrifuged at 1228 x g for 15 min, then transferred to HPLC vials containing UV standards of keto alcohol and NNK. To ensure that degradation of the sample did not occur during storage, 100 µL of the sample was

analyzed on HPLC with UV and radioflow detectors. The metabolite profile was compared to the profile from the previously analyzed 180 min perfusion sample.

3.B.v - Tissue Analysis

Tissue samples from the metabolism perfusions were used to quantitate the metabolites and to estimate the total covalent binding in the tissue. The lung samples were homogenized with a PowerGen 125 homogenizer (Fisher Scientific). A small aliquot of homogenate was solubilized with 6 mL of 1M NaOH and analyzed by LSC to estimate the total radioactivity in the tissue. The remaining homogenate was used to quantitate the metabolites and covalent binding in the lung.

3.B.v.a- Metabolites

To the remaining homogenized lung tissue, 6 mL of 0.1M HCl was added and the tissue was further homogenized. The sample was then centrifuged at 2950 x g (Sorvall Legend RT, Fisher Scientific) for 30 min. The resulting tissue pellet was used for total covalent binding analysis. The resulting cloudy supernatant was used to determine tissue metabolites and was transferred to a clean test tube and neutralized. To buffer the solution, 1 mL of 0.1 M $NaPO_4$ was added to the supernatant before neutralizing with 1M NaOH. The neutralized supernatant was then centrifuged at 1228 x g for 20 min. The resulting clear supernatant was transferred and concentrated to dryness in a 37 ºC water bath with a gentle stream of nitrogen. Once dried, the sample was reconstituted with 400

μL of distilled H_2O. Tissue metabolites were determined by injecting 100 μL of the reconstituted sample onto HPLC with UV and radioflow detectors.

3.B.v.b - Total Covalent Binding

The tissue pellet that remained after the initial metabolite extraction was used to estimate the total covalent binding in the lung tissue. The pellet was homogenized with 6 mL aliquots of 0.1M HCl and then centrifuged at 1228 x g for 15 min until the counts in the wash solution were not more than twice the level of background, approximately nine washes. The tissue pellet was then solubilized with 10 mL of 1M NaOH, and analyzed by LSC. The protein concentration of the solubilized tissue pellet was determined using the BCA Protein Assay Kit (Fisher Scientific) with an albumin standard.

3.B.vi - HPLC Analysis

HPLC analysis was performed on a system that consisted of a Waters 600 system controller, two Waters 501 pumps, a Waters 440 absorbance detector (254 nm) (Waters Corp., Milford, CA), a Hewlett Packard 1100 series autosampler (Agilent Technologies, Santa Clara, CA), and a β-ram radioflow detector (IN/US Systems, Tampa, FL). A Luna C_{18}(2) reversed-phase column (250 x 4.6 mm, 5 μm; Phenomenex, Torrance, CA) was used for the separation. The metabolites were eluted using a linear gradient from 92 % A (20 mM $NaHPO_4$ and 1 mM EDTA, pH 6.0) to 80% A over 30 min, and then to 50% A in 5 min; B was acetonitrile [109]. The flow rate was 0.5 mL/min, which was mixed with 1.5 mL/min of Monoflow® (National Diagnostics, Atlanta, GA).

3.B.vii - Collection of NNAL Peaks

The NNAL peak from each perfusate and tissue sample was collected via HPLC. Perfusate and tissue samples could not be analyzed directly by GC-TEA because NNAL co-eluted with NNAL-*N*-oxide and the samples contained salts that interfered with the analysis. The HPLC system and the column used for separation were the same as that used for determining metabolite formation, only the aqueous mobile phase and gradient profile changed. NNAL was eluted with 10 mM ammonium acetate buffer (A) and ACN (B) at a flow rate of 0.5 mL/min using the linear gradient program listed in Table 3.1. Fraction collections were based on the elution time of the keto alcohol UV standard. Monoflow® was not used since the radioactivity in the samples was not monitored.

Table 3.1 – *HPLC gradient used to collect NNAL peaks.*

Time Interval [min]	**%A** (10 mM ammonium acetate buffer)	**%B** (ACN)
0 – 14	85	15
14 – 14.5	85 - 55	15 – 45
14.5 - 26	55	45
26 - 27	55 - 85	45 – 15

For perfusate samples, 150 µL was injected onto the column, whereas all of the remaining tissue sample was injected due to the low concentration in the tissue. One minute after keto alcohol had finished eluting (~15-16 min), three 10 sec fractions were collected. Then the eluate was collected for 3 mins, followed by another three 10 sec fractions. The radioactivity in each fraction was estimated by LSC and the appropriate fractions were then dried with nitrogen in a 37 ºC water bath. The samples were reconstituted with 300 µL ACN and transferred to a GC vial, where the samples were then concentrated to dryness with nitrogen.

3.B.viii - GC-TEA Analysis

Concentrated tissue samples were derivatized with 4 µL of bis(trimethylsilyl) triflouro-acetamide containing 1% trimethylchlorosilane (BSTFA) (Regis Technologies, Morton Grove, IL) containing the injection standard *N*'-nitrosopentyl-(3-picolyl)amine (NPPA) (Toronto Research Chemicals). The perfusate samples were derivatized with a volume of BSTFA that resulted in a concentration of approximately 1-3 ng/µL. Derivatization of the samples was completed by heating the samples at 60 ºC for 60 min. For each sample, 4 µL was injected onto a HP 6890 GC (Agilent Technologies) coupled with a Model 543 TEA (Orion Research). The enantiomers were separated on a Cyclosil-B chiral column (30 m x 0.25 mm, Agilent Technologies) with helium as the carrier gas. The oven temperature was programmed to start at 60 ºC and was held there for 2 min. The temperature was then increased at a rate of 12 ºC/min to 166 ºC and held for 85 min before being ramped up to 220 ºC at a rate of 12 ºC/min, where it was held for 10 min.

The pressure gradient started at 9.3 psi and was increased to 15.9 at a rate of 0.72 psi/min. The injection was pulse splitless at a pressure of 14.0 psi and temperature of 225 ºC. PeakSimple 3.54 software (SRI, Menlo Park, CA) was used to collect and analyze the GC chromatographs. The total run time was 120 min with *(S)*-NNAL eluting at 95.9 min and *(R)*-NNAL at 97.4 min. The limit of detection was approximately 0.5 ng on column.

3.B.ix - DNA Isolation

DNA was isolated using a slightly modified version of the Gentra Puregene® Tissue Kit protocol. The lung was weighed and divided into approximately two 500 mg aliquots. The samples were kept frozen on dry ice and minced with a razor blade. The aliquots were transferred to a 15 mL glass homogenizer containing 5 mL of Cell Lysis Solution and then homogenized on ice. The homogenate was transferred to a 50 mL centrifuge tube into which the remaining 13 mL of Cell Lysis Solution was added. Then 75 µL of Puregene Proteinase K were added and the tubes were inverted 25 times before being placed in an orbital shaker (Maxq 4450, Fisher Scientific) and shaken at 80 rpm overnight at 55˚C. Once the tissue was completely lysed, 90 µL of RNase A Solution were added. The tubes were inverted 25 times and then replaced in the orbital shaker for 60 min at 80 rpm and 37˚C. The solution was then put on ice for 3-5 min. Six mL of Protein Precipitation Solution were added and the samples were vortexed on high for approximately 20 sec. The samples were then centrifuged at 2000 x g (Sorvall Legend RT) for 10 min. The resulting supernatant was carefully poured into a clean 50 mL tube

containing 18 mL of ice cold 100% isopropanol. The tube was slowly inverted 50 times resulting in the formation of a clump of DNA strands. The DNA was rinsed three times with 6 mL aliquots of 70% cold EtOH, and then three more times with 6 mL aliquots of 100% cold EtOH. The DNA was then dried with a gentle stream of nitrogen. Samples were stored at -4 ºC until further analysis.

3.B.x - Quantification of DNA Adducts

DNA adduct formation was analyzed by Dr. Pramod Upadhyaya using the LC/ESI-MS/MS-SRM method previously described for POB or PHB DNA adducts [59,62,63]. Briefly, deuterated POB or PHB internal standards were added to 0.5 - 2 mg of isolated DNA and neutral thermal hydrolysis was carried out at 100 ºC for 30 min. Then, enzymatic hydrolysis was carried out with micrococcal nuclease, phosphodiesterase II (Worthington Biochemical Corp, Lake Wood, NJ), and alkaline phosphatase (Roche Molecular Biochemicals, Indianapolis, IN). The resulting hydroylsate was then purified by solid-phase extraction (Strata-X cartridge, Phenomenex, Torrance, CA), and injected into a Finnigan TSQ Quantum Discovery Max triple quadrupole mass spectrometer (Thermo Electron, San Jose, CA). The limit of detection for the POB and PHB adducts were: 7-POB-Gua (3 fmol/mg DNA), O^6-POB-dGuo (1 fmol/mg DNA), O^2-POB-dThd (100 amol/mg DNA), 7-PHB-Gua (18 fmol/mg DNA), O^6-PHB-dGuo (1.5 fmol/mg DNA), and O^2-PHB-dThd (1.5 fmol/mg DNA).

For O^6-methyl-Gua analysis, 0.05 - 1 mg of each DNA sample plus [CD_3]O^6-methyl-Gua internal standard was dissolved in 1 mL of HCl (0.1N) and heated at 80 ºC

for 30 min, cooled, and neutralized with 1N NaOH to pH 7.0. The resulting solution was applied to a solid-phase extraction cartridge (Strata-X) and analyzed by capillary LC/ESI-MS/MS-SRM as described previously [64]. The limit of detection for O^6-methyl-Gua was 3 fmol/mg DNA.

3.B.xi - Pharmacokinetic Analysis

The apparent pharmacokinetic parameters for the metabolism of NNK in the lung were estimated by non-compartmental analysis of the NNK concentration-time data in the perfusate using WinNonlin® version 5.2 (Pharsight, Mountain View, CA). The area under the curve from 0 to 180 min (AUC_0^{180}) was calculated by WinNonlin via the linear trapezoidal rule. The AUC_{180}^{∞} was extrapolated by dividing the concentration of NNK in the perfusate at 180 min (C_{last}) by the estimated elimination rate constant, λ_z. The concentration-time data from 45 min to 180 min were used to estimate λ_z, using uniform weighting. The combined value of AUCs yielded the AUC_0^{∞}, which was used to calculate the apparent clearance (CL_{app}). The apparent extraction ratio (ER_{app}) was calculated by dividing CL_{app} by the perfusate flow rate (8 ml/min).

3.B.xii - Statistical Analysis

Statistical analysis of the data was carried out using SigmaStat version 3.1 (Aspire Software International, Ashburn, VA). Unpaired t-tests were used to compare tissue metabolites, perfusate metabolite AUCs, ratio of *(S)*-NNAL and *(R)*-NNAL, total

covalent binding, and individual DNA adduct levels between the PEITC and non-PEITC groups at the two doses. A 2-way ANOVA was used to compare the apparent pharmacokinetic parameters between the PEITC and non-PEITC groups at each dose, and to compare the parameters between the two doses of NNK. The Holm-Sidak method was used for pairwise multiple comparisons. A *p*-value of < 0.05 was considered significant for all tests.

3.C – Results

3.C.i - 0.1 μM NNK Perfusions

The perfusate concentration-time profiles of NNK and its metabolites for the 0.1 μM NNK perfusions are shown in Figure 3.1 (A, C, E). Less than 5% of the radioactivity in the final perfusate was attributed to unmetabolized NNK after the 180 min perfusion. The apparent metabolic clearance of the lung (CL_{app}) was 1.07 ± 0.09 mL/min, the apparent extraction ratio (ER_{app}) was 0.133 ± 0.011, and the apparent half-life ($t_{1/2,app}$) was 34 ± 5 min (Table 3.2).

NNK-*N*-oxide (33.8 ± 0.8 pmol/mL) was the major perfusate metabolite and accounted for approximately 49% of the total radioactivity in the perfusate. The final concentration of keto alcohol (14.0 ± 0.4 pmol/mL) in the perfusate was greater than that of keto acid (8.0 ± 1.2 pmol/mL). NNAL (5.3 ± 0.4 pmol/mL) and its subsequent metabolites were formed to a lesser extent than the NNK metabolites. However, the subsequent metabolism of NNAL was analogous to that of NNK. NNAL-*N*-oxide (3.6 ±

0.4 pmol/mL) was the major NNAL metabolite, followed by diol (2.0 ± 0.2 pmol/mL). Hydroxy acid was not detected in the perfusate.

Table 3.2 – *Apparent pharmacokinetic parameters (mean ± SD, n=3) for the pulmonary metabolism of 0.1 µM and 1.2 µM NNK with and without 20 µM PEITC. Estimates were obtained from WinNonlin non-compartmental analysis.*

	0.1 µM NNK	**0.1 µM + PEITC**	**1.2 µM NNK**	**1.2 µM + PEITC**
$t_{1/2,\,app}$ [min]	34 ± 5	108 ± 8[a]	64 ± 16[a]	149 ± 11[b]
V_z [mL]	51 ± 3	60 ± 1	61 ± 11	76 ± 3[b]
CL_{app} [mL/min]	1.07 ± 0.09	0.39 ± 0.03[a]	0.66 ± 0.09[a]	0.36 ± 0.03[b]
ER_{app}	0.133 ± 0.011	0.048 ± 0.005[a]	0.083 ± 0.011[a]	0.044 ± 0.004[b]

A 2-way ANOVA with Holm-Sidak was used for determining significant differences.

[a] *p*-value < 0.05, when compared to 0.1 µM NNK

[b] *p*-value < 0.05, when compared to 1.2 µM NNK

Table 3.3 – *Levels of individual DNA adducts (fmol/mg DNA) (mean ± SD, n=3) in the lung tissue after 180 min perfusions of 0.1 µM and 1.2 µM NNK with and without PEITC.*

	0.1 µM		1.2 µM	
DNA Adducts	*NNK*	*NNK + PEITC*	*NNK*	*NNK + PEITC*
O^2-POB-dThd	36.0 ± 2.9	9.9 ± 2.0[a]	362 ± 11	89.2 ± 2.2[a]
O^6-POB-dGuo	-	-	43.7 ± 2.4	11.4 ± 2.1[a]
7-POB-Gua	-	-	32.1 ± 3.2	18.0 ± 10.0
O^6-methyl-Gua	-	-	284 ± 14	163 ± 3[a]

[a] *p*-value < 0.05; *PHB-DNA adducts were not detected in any of the lung tissue samples.*

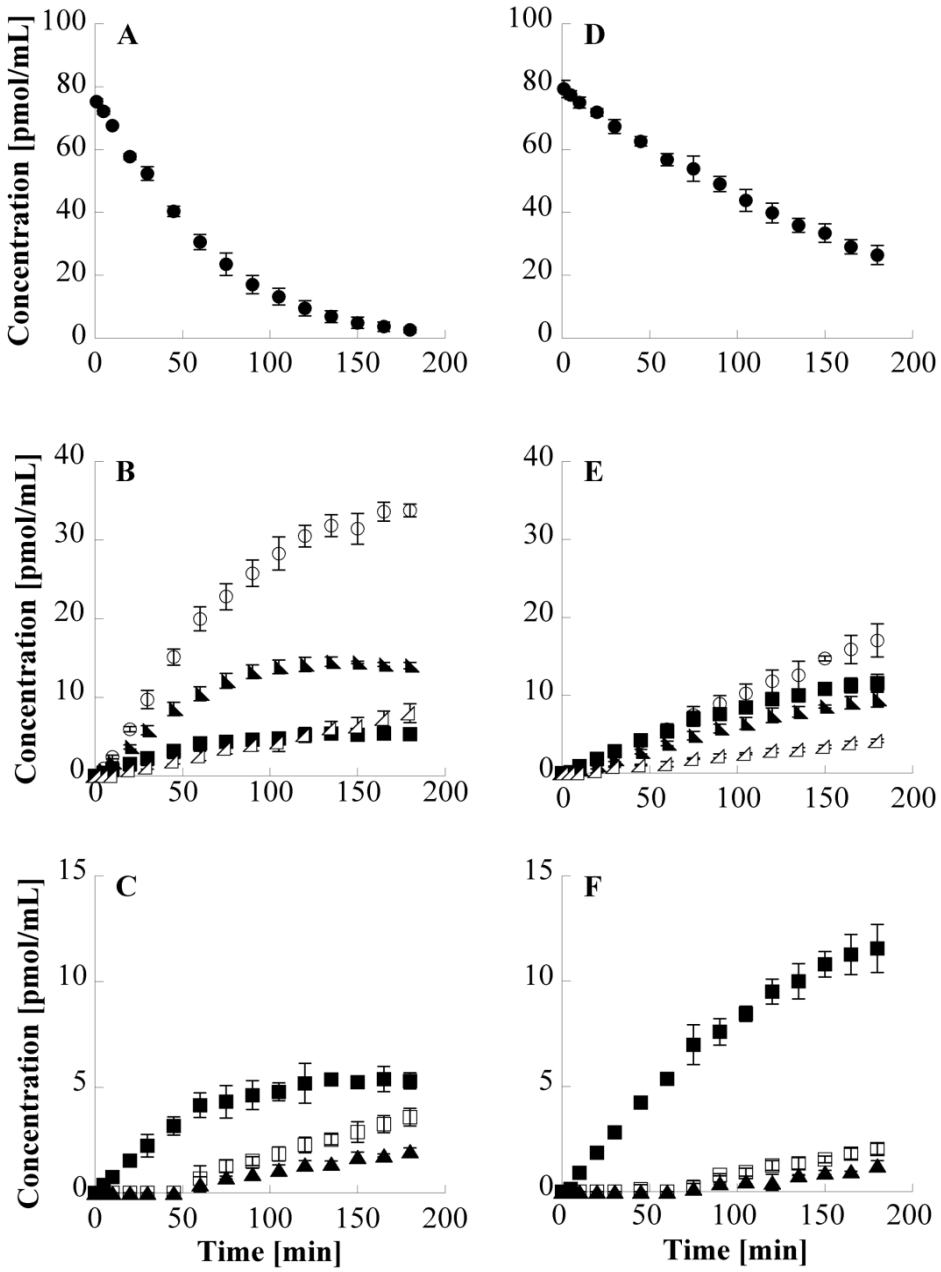

Figure 3.1 – *Average concentration (pmol/mL ± SD) vs time (min) profiles of NNK and metabolites in the perfusate of 0.1 µM NNK (A, B, C) and 0.1 µM NNK + PEITC (D, E, F), (n=3). Symbol designations are as follows: NNK, ●; NNK-N-oxide, ❍; NNAL, ■; NNAL- N-oxide, ❑; keto alchol, ◣; keto acid, ◅ ; diol, ▲. The profile of NNAL is replotted in figures E and F for comparison purposes. Where error bars are not apparent, they are smaller than the symbol.*

In the tissue, hydroxy acid (0.77 ± 0.37 pmol/mg protein) and NNAL-*N*-oxide (0.32 ± 0.06 pmol/mg protein) were the major metabolites, accounting for approximately 42% and 17% of the total tissue concentration (Figure 3.2). Overall, PEITC did not have a significant effect on the individual metabolite concentrations in the tissue. The only DNA adduct detected in the 0.1 μM NNK perfusions was O^2-POB-dThd (Table 3.3).

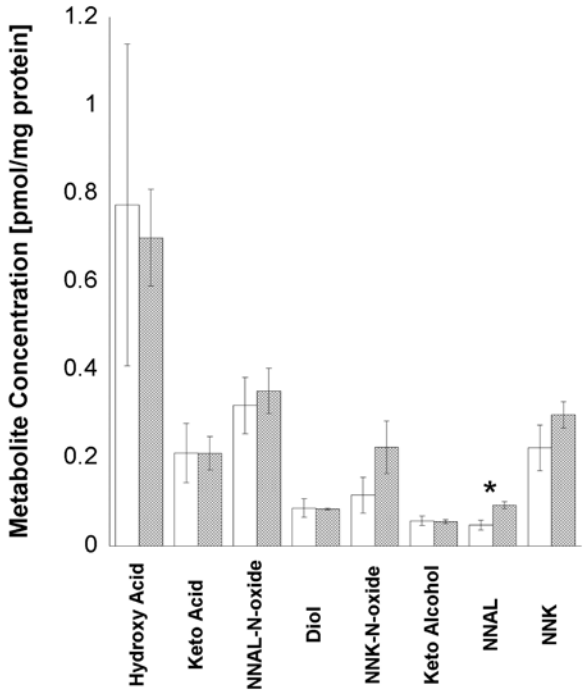

Figure 3.2 – *Average concentration of metabolites (pmol/mg tissue ± SD) in the tissue following a 180 min perfusion with 0.1 μM NNK (open bars) or 0.1 μM NNK + PEITC (shaded bars), (n=3). * p-value < 0.05.*

The average ratio of *(S)*-NNAL to *(R)*-NNAL in the perfusate was approximately 2.07 (Table 3.4). The ratio was based on two samples because there was not an adequate amount of the third sample for analysis. The ratio of NNAL in the tissue could not be determined due to the low level of NNAL in the tissue.

Table 3.4 – *Ratio of (S)-NNAL to (R)-NNAL (mean ± SD, n=3) in the perfusate and tissue of the 0.1 μM and 1.2 μM NNK perfusions with and without 20 μM PEITC.*

	0.1 μM NNK	**0.1 μM + PEITC**	**1.2 μM NNK**	**1.2 μM + PEITC**
Perfusate	2.07[+] *(1.87, 2.28)*	1.82 ± 0.04	2.16 ± 0.06	1.86 ± 0.05[*]
Tissue	ND	ND	1.59[£]	3.32[+] *(3.33, 3.31)*

[+] *average based on two samples (individual values)*

[£] *based on a single value*

[*] *p*-value < 0.05, when compared to 1.2 μM NNK

3.C.ii - 0.1 μM NNK + 20 μM PEITC Perfusions

Figure 3.1 (B, D, F) illustrates the concentration-time data for NNK and its metabolites in the perfusate of the 0.1 μM NNK + PEITC perfusions. Compared to the 0.1 μM NNK perfusions, the metabolism of NNK was reduced in the presence of PEITC. Unmetabolized NNK (26.4 ± 3.0 pmol/mL) accounted for approximately 30-40% of the metabolites at the end of the perfusion with PEITC, compared to less than 5% when NNK was perfused alone. The observed decrease in NNK metabolism corresponded to changes in its apparent pharmacokinetic parameters (Table 3.2). There was a significant decrease

in ER_{app} and CL_{app} from 0.133 ± 0.011 to 0.048 ± 0.005, and 1.07 ± 0.09 mL/min to 0.39 ± 0.03 mL/min, respectively. Meanwhile, the $t_{1/2,app}$ increased significantly from 34 ± 5 min to 108 ± 8 min in the presence of PEITC.

The formation of all metabolites, except NNAL, was decreased with the addition of PEITC. NNK-*N*-oxide (17.0 ± 2.1 pmol/mL) remained the major metabolite in the perfusate, but only accounted for approximately 24% of the total perfusate metabolites, instead of the 49% that was observed when NNK was administered alone. Keto alcohol (9.5 ± 1.0 pmol/mL) still formed to a greater extent than keto acid (4.2 ± 0.2 pmol/mL), but the overall formation of both bioactivation metabolites was decreased. The concentration of NNAL (11.6 ± 1.1 pmol/mL) increased, while the formation of its subsequent metabolites, NNAL-*N*-oxide (2.0 ± 0.3 pmol/mL) and diol (1.2 ± 0.2 pmol/mL) decreased along with the other oxidative metabolites. To determine the effect of PEITC on metabolite formation, the AUC from time 0 to 180 min was calculated for each perfusate metabolite (Table 3.5). There was a significant decrease (p-value < 0.05) in AUC for all oxidative metabolites and a significant increase in AUC for NNAL and NNK when PEITC was co-administered with NNK.

While the concentration of metabolites in the perfusate changed significantly with the addition of PEITC, overall there was not a significant change in metabolite concentrations in the tissue (Figure 3.2). Hydroxy acid (0.70 ± 0.12 pmol/mg protein) remained the major tissue metabolite, followed by NNAL-*N*-oxide (0.35 ± 0.05 pmol/mg protein). While tissue metabolite concentrations seemed unaffected, covalent binding in the tissue decreased significantly with the presence of PEITC. The level of O^2-POB-dThd

was significantly decreased from 36.0 ± 2.9 fmol/mg DNA when NNK was perfused alone, to 9.9 ± 2.0 fmol/mg DNA when PEITC was co-administered (Table 3.3). The total covalent binding also decreased significantly from 0.25 ± 0.01 pmol/mg protein to 0.17 ± 0.02 pmol/mg protein.

The ratio of *(S)*-NNAL to *(R)*-NNAL in the perfusate did not change significantly with the addition of PEITC (Table 3.4). The level of NNAL in the tissue was not detectable, thus the ratio of NNAL in the tissue could not be determined.

3.C.iii - 1.2 μM NNK Perfusions

The perfusate concentration-time profiles of NNK and its metabolites in the 1.2 μM NNK perfusions are depicted in Figure 3.3 (A, C, E). Unmetabolized NNK (138 ± 45 pmol/mL) constituted approximately 16% of the compounds in the perfusate at the end of the perfusion, which was greater than the 5% in the 0.1 μM NNK perfusions. The major perfusate metabolites were NNK-*N*-oxide (338 ± 64 pmol/mL) and keto alcohol (167 ± 29 pmol/mL). Overall, the metabolic profile in the perfusate was similar in the 1.2 μM and 0.1 μM NNK treatments. However, the higher dose of NNK appeared to have an inhibitory effect on the overall metabolism, resulting in a CL_{app} of 0.66 ± 0.09 mL/min, an ER_{app} of 0.083 ± 0.011, and a $t_{1/2,app}$ of 64 ± 16 min (Table 3.2).

Table 3.5 – *The mean* AUC_0^{180} *(pmol·min/mL ± SD) of perfusate metabolites following 180 min perfusions of 0.1 µM and 1.2 µM NNK with and without 20 µM PEITC (n=3).*

	Keto Acid	NNAL-*N*-oxide	Diol	NNK-*N*-oxide	Keto Alcohol	NNAL	NNK
0.1 µM	700 ± 120	270 ± 40	150 ± 20	4050 ± 200	1960 ± 90	720 ± 50	4550 ± 320
0.1 µM + PEITC	370 ± 10[a]	130 ± 20[a]	70 ± 10[a]	1550 ± 170[a]	950 ± 80[a]	1260 ± 80[a]	8970 ± 350[a]
1.2 µM	6060 ± 840	2490 ± 750	1380 ± 410	36700 ± 7400	19400 ± 3500	10700 ± 1300	78000 ± 7100
1.2 µM + PEITC	3400 ± 240[a]	660 ± 320[a]	450 ± 220[a]	11000 ± 1800[a]	7700 ± 1500[a]	12900 ± 1100	96700 ± 5000[a]

[a] *p-value < 0.05, compared to the same concentration without PEITC.*

The major tissue metabolites were hydroxy acid (6.4 ± 1.9 pmol/mg protein) and NNAL-*N*-oxide (4.2 ± 1.2 pmol/mg protein), which accounted for approximately 32% and 21% of the total tissue metabolites (Figure 3.4). With the higher dose of NNK, more individual DNA adducts were detected in the tissue (Table 3.3). O^2-POB-dThd (362 ± 11 fmol/mg DNA) and O^6-methyl-Gua (284 ± 14 fmol/mg DNA) were formed to a greater extent than O^6-POB-dGuo (43.7 ± 2.4 fmol/mg DNA) and 7-POB-Gua (32.1 ± 3.2 fmol/mg DNA) in the tissue. None of the individual PHB-DNA adducts were present at detectable levels in the lung.

The ratio of *(S)*-NNAL to *(R)*-NNAL in the perfusate was 2.16 ± 0.06 (Table 3.4). The tissue data were near the limit of detection and inconsistent. One sample had a ratio of 1.59, while in the second only *(S)*-NNAL was detected, and neither enantiomer was detected in the third tissue sample.

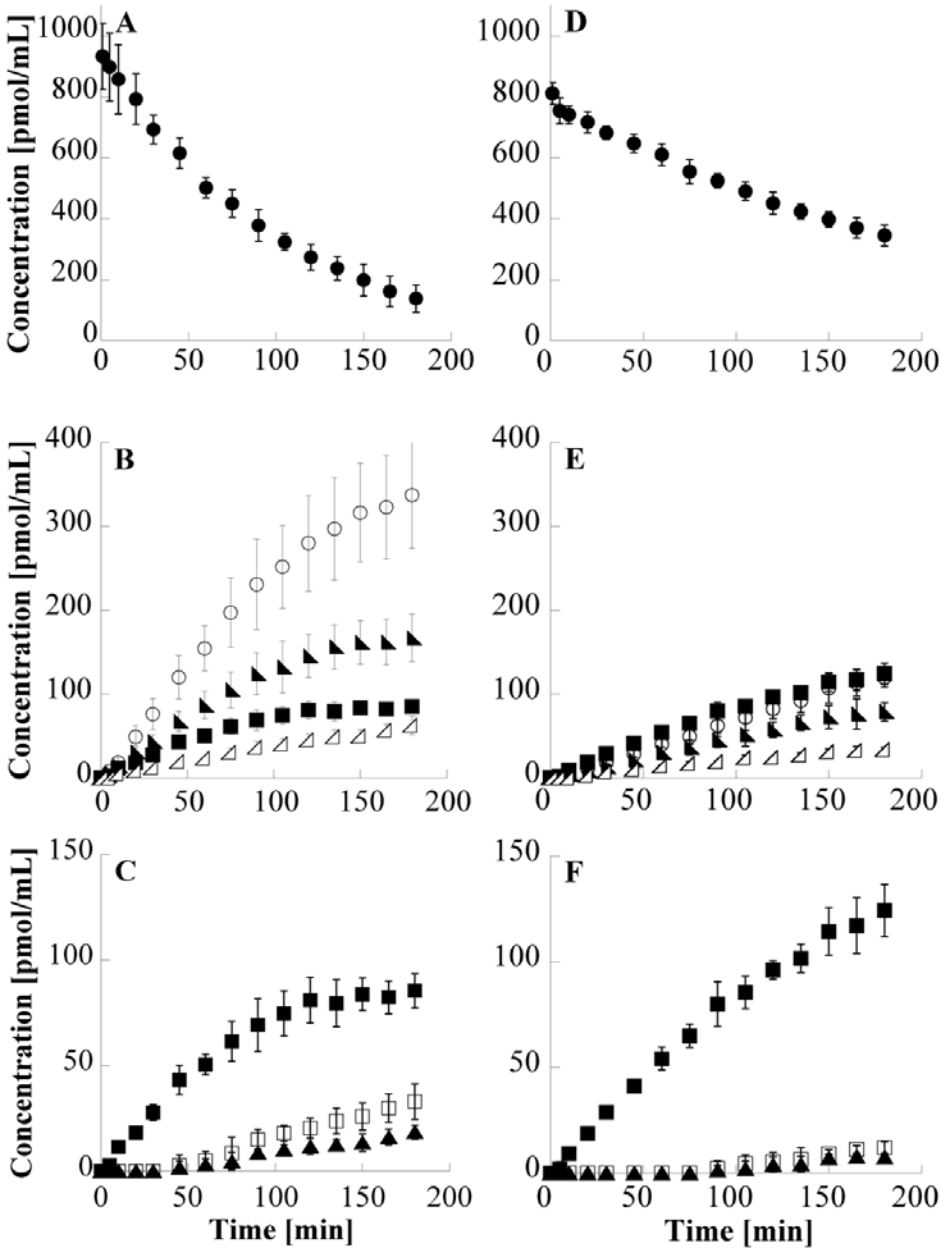

Figure 3.3 – *Average concentration (pmol/mL ± SD) vs time (min) profiles of NNK and metabolites in the perfusate of 1.2 µM NNK (A, B, C) and 1.2 µM NNK + PEITC (D, E, F), (n=3). Symbol designations are as follows: NNK, ●; NNK-N-oxide, ❍; NNAL, ■; NNAL- N-oxide, ❑; keto alchol, ◣; keto acid, ◅ ; diol, ▲. The profile of NNAL is replotted in figures E and F for comparison purposes. Where error bars are not apparent, they are smaller than the symbol.*

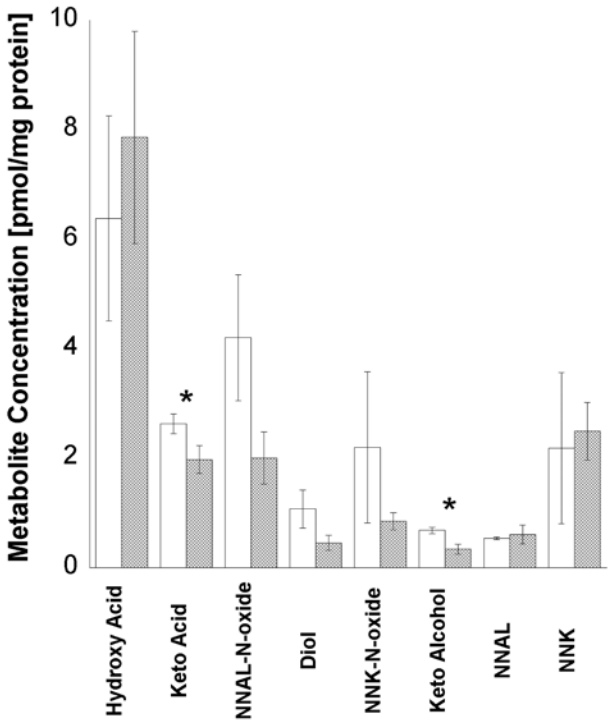

Figure 3.4 – *Average concentration of metabolites (pmol/mg tissue ± SD) in the tissue following a 180 min perfusion with 1.2 μM NNK (open bars) or 1.2 μM NNK + PEITC (shaded bars), (n=3). * p-value < 0.05.*

3.C.iv - 1.2 μM NNK + 20 μM PEITC Perfusions

The presence of PEITC inhibited the metabolism of NNK (Figure 3.3B). Approximately 48% of the final perfusate compounds was attributable to NNK (345 ± 34 pmol/mL), which was significantly greater than the 16% associated with NNK (138 ± 45 pmol/mL) when 1.2 μM NNK was dosed alone. The formation of all metabolites, except NNAL, was inhibited by PEITC (Figure 3.3D & F). The major perfusate metabolites were NNAL and NNK-*N*-oxide, which had comparable concentrations. The concentration of NNAL increased from 85.4 ± 8.1 pmol/mL when NNK was perfused

alone, to 124 ± 12 pmol/mL with the co-administration of PEITC. Meanwhile, the concentration of NNK-*N*-oxide decreased from 337 ± 64 pmol/mL to 120 ± 11 pmol/mL. The concentration of all other oxidative metabolites decreased as well. The presence of PEITC was associated with a significant decrease in AUC from 0 to 180 min for all oxidative metabolites and a significant increase in the AUC of NNK (Table 3.5). A significant change in NNAL AUC was not observed. The addition of PEITC resulted in a decrease in CL_{app} from 0.66 ± 0.09 mL/min to 0.36 ± 0.03 mL/min. A decrease in ER_{app} from 0.083 ± 0.011 to 0.044 ± 0.004 was also observed, while $t_{1/2,app}$ increased from 64 ± 16 min to 149 ± 11 min (Table 3.2).

The major tissue metabolites were hydroxy acid (7.9 ± 1.9 pmol/mg protein) and NNK (2.5 ± 0.5 pmol/mg protein). Overall there did not appear to be a consistent change in the tissue concentrations of metabolites with the addition of PEITC (Figure 3.4). The reduction in NNK metabolism led to a decrease in covalent binding in the tissue. The estimated total covalent binding significantly decreased from 2.28 ± 0.02 pmol/mg protein to 1.38 ± 0.29 pmol/mg protein. The formation of individual DNA adducts also decreased significantly with the administration of PEITC (Table 3.3). The major DNA adduct in the tissue was O^6-methyl-Gua (163 ± 3 fmol/mg DNA), followed by O^2-POB-dThd (89.2 ± 2.2 fmol/mg DNA), 7-POB-Gua (18.0 ± 10.0 fmol/mg DNA), and O^6-POB-dGuo (11.4 ± 2.1 fmol/mg DNA).

The ratio of the NNAL enantiomers in the perfusate decreased significantly from 2.16 ± 0.06 to 1.86 ± 0.05 with the co-administration of PEITC. The ratio of NNAL in the tissue was determined by two samples to be approximately 3.32.

3.D - Discussion

3.D.i - Comparison to Previous IPRL Study

This study examined the effects of NNK concentration and the co-administration of PEITC on metabolism, metabolite distribution, and DNA adduct formation in the perfused rat lung. The final metabolite composition in the perfusate of the 0.1 μM NNK perfusions was similar to the 0.035 μM NNK perfusion previously reported, despite a number of differences in the experimental designs [98]. Both studies found that a majority of the metabolites formed were from detoxification pathways (55%), while bioactivation pathways accounted for approximately 30% of metabolism. The extent of formation of most metabolites was in agreement between the two studies, with the exception of minor differences in the formation of diol and keto alcohol.

While the extent of metabolite formation was comparable between the two studies, the estimated apparent clearance (CL_{app}) was lower in the present study (1.07 ± 0.9 mL/min) than in the previous study (2.1 ± 0.5 mL/min). The difference in CL_{app} may be attributable to the concentration difference of NNK between the two experiments, since clearance was shown to decrease with increased concentration in the present study. Since the CL_{app} is much lower than perfusate flow, NNK is a low extraction ratio compound with respect to the lung.

The present study examined the metabolites in the lung tissue. Less than 4% of the radioactivity was recovered in the lung tissue, and the metabolite profile of the tissue was different than that of the perfusate. Hydroxy acid was not detected in the perfusate in

any of the treatment groups, but it was the major metabolite in the tissue for all groups. This may be due to diffusional barriers within the lung. Hydroxy acid is the most hydrophilic of the metabolites and thus may not transverse the membranes as easily as the other more lipophilic metabolites, resulting in its accumulation in the lung tissue. In both studies the estimated apparent volumes of distribution were approximately equal to the volume of the reservoir, indicating that the partitioning of NNK and its metabolites into the lung tissue was not extensive.

It is important to note that the pharmacokinetic parameters that are reported here are apparent values. The equations that were used to estimate these parameters were derived based on the assumption that no reversible metabolism takes place in the system. Reconversion of NNAL to NNK is possible [29], but the extent of the reconversion in this system is unknown. If the reoxidation of NNAL to NNK is minor in the lung, then the estimates provided here should be fairly accurate. However, if the reconversion of NNAL to NNK is extensive, then the clearance of NNK from the lung reported here would be underestimated. Studies investigating the reconversion of NNAL to NNK in the IPRL are reported in Chapter 4.

3.D.ii - Effects of NNK Concentration

NNK at a concentration of 0.1 μM was effectively metabolized in the lung. When the NNK concentration was increased twelve-fold to 1.2 μM the efficiency of the lung metabolism appeared to decrease, as is evident by the decrease in apparent clearance. The increase in dose did result in a moderate decrease in the extent of formation of NNK-*N*-

oxide, a modest increase in NNAL, and an increase in unmetabolized NNK at the end of the 180 min perfusion. NNK-*N*-oxide remained the major metabolite at 40% of the perfusate metabolites, as opposed to 50% at the lower dose. At the end of the 1.2 μM perfusion there was more unmetabolized NNK in the perfusate than after the 0.1 μM perfusion. These results are supported by *in vitro* metabolism studies of NNK in alveolar type II cells. Those studies showed that higher doses of NNK reduce the formation of NNK-*N*-oxide and the other oxidative metabolites, while increasing the formation of NNAL and the level of unmetabolized NNK [110]. Another *in vitro* study by Richter *et al.*, showed that NNK concentration did not greatly affect metabolite formation in the lung tissue of rats [111]. However, they did observe that an increased NNK concentration was accompanied by an increase in NNAL at the "expense" of NNK-*N*-oxide. It is possible that higher doses of NNK saturated certain critical cytochrome P450 metabolic pathways, resulting in shunting through the NNAL pathway. However, the enzymes responsible for NNAL formation were apparently not efficient enough to compensate for the decrease in P450 activity, so overall less NNK was metabolized. The saturation of metabolism with increased NNK is also supported by the work of Devereux *et al.*, which showed a decrease in the efficiency of O^6-methyl-Gua formation with an increase in NNK [40].

O^2-POB-dThd was the only DNA adduct detected in the tissue at the low concentration of NNK, and was the major POB-DNA adduct detected in the lung of rats that were chronically treated with NNK in the drinking water [59,62]. No other DNA adducts were detected in the lung tissue of the 0.1 μM perfusions. The metabolite profiles indicate that the intermediates for methyl and PHB-DNA adducts were formed, so it is possible

that those adducts are present in the tissue below the limit of detection of the assay. In the 1.2 μM perfusions all three POB-DNA adducts and O^6-methyl-Gua were detected, but none of the PHB-DNA adducts were observed in the lung tissue. O^2-POB-dThd remained the major POB-DNA adduct. There was slightly more O^6-POB-dGuo than 7-POB-Gua in the lung, which was in contrast to the *in vivo* results that showed 7-POB-Gua at a significantly greater level than O^6-POB-dGuo throughout the entire 20 week bioassay [62]. It is possible that there is an efficient DNA repair mechanism for O^6-POB-dGuo that reduces its level in the rat lung *in vivo*, but would not be present in the lung perfusion system. The formation of DNA adducts in the IPRL system further supports the idea that bioactivation in the lung, and not the liver, is responsible for the development of pulmonary tumors[112].

The concentration of NNK did not have a noticeable effect on the ratio of *(S)*-NNAL to *(R)*-NNAL in the perfusate. In all four groups *(S)*-NNAL was formed to a greater extent than *(R)*-NNAL, which is consistent with previously reported *in vitro* data[29]. For both NNK concentrations, the level of NNAL in the tissue was low. At the 0.1 μM concentration NNAL was below the limit of detection, and thus the ratio of the enantiomers could not be determined. In the 1.2 μM concentration perfusions the NNAL tissue levels were higher, but still near the limit of detection of the assay. As a result, the ratio could only be determined in some tissue samples, depending on how much sample was available for analysis after the quantitation of metabolites.

3.D.iii - Effects of PEITC

PEITC inhibits the formation of NNK-induced lung tumors in rats [53,84]. The chemopreventive nature of PEITC has been attributed to its ability to inhibit P450 metabolism, resulting in a decrease in the bioactivation of NNK, thus decreasing the formation of potentially carcinogenic DNA adducts [89,91,105,113]. The addition of PEITC to the perfusion system resulted in a significant decrease in the formation of all perfusate oxidative metabolites and an increase in NNAL formation, regardless of the NNK dose. The carbonyl reduction of NNK to NNAL is considered to be primarily catalyzed through non-P450 pathways, for example by 11-β-hydroxysteroid, aldo-keto reductase (AKR), and carbonyl reductase (CR) [31,114], which could explain the apparent lack of inhibition of NNAL formation. In fact, the increase in NNAL formation could be due to shunting through the carbonyl reduction pathway as a result of the decrease in P450 oxidative metabolism. Previous *in vitro* studies also showed a decrease in the formation of oxidative metabolites with the treatment of PEITC [87-89,91]. While the *in vitro* studies did not show a significant increase in NNAL formation, *in vivo* studies showed a significant increase in NNAL and NNAL-glucuronide in the urine of rats that were co-administered PEITC with NNK, as well as a significant decrease in hemoglobin adducts resulting from α-hydroxylation [84].

The decrease in oxidative metabolism consequently led to a decrease in DNA adduct formation and total covalent binding in the tissue via α-hydroxylation pathways. The addition of PEITC inhibited the formation of O^2-POB-dThd and O^6-POB-dGuo by 70 – 75%, and decreased the formation of O^6-methyl-Gua and 7-POB-Gua by 40 – 45 %.

These results are consistent with previous *in vivo* and *in vitro* studies that showed a decrease in DNA adduct formation with the addition of PEITC [52,53,105].

In the 1.2 µM perfusions, the addition of PEITC significantly reduced the ratio of *(S)*-NNAL to *(R)*-NNAL in the perfusate. This could be a result of increased formation of *(R)*-NNAL or a decrease in the formation of *(S)*-NNAL. Either way, a decrease in the amount of *(S)*-NNAL, the more carcinogenic enantiomer, could be an additional mechanism in the chemopreventive nature of PEITC.

3.E – Conclusions

In summary, the current study shows that increased NNK concentration results in a significant decrease in the apparent pulmonary clearance, with only minor shifts in the metabolite profiles. The detection of DNA adducts indicate that metabolic activation in the lung leads to DNA damage, and that bioactivation via the liver is not required. PEITC inhibits the formation of oxidative metabolites, which subsequently results in a decrease in DNA adduct formation. *(S)*-NNAL, the more carcinogenic enantiomer, was formed to a greater extent than *(R)*-NNAL in the lung, which could be an important mechanism for the lung selective carcinogenicity of NNK. This study is the first to assess the pulmonary metabolism of NNK in the IPRL system that examined the time course of metabolite formation in the perfusate, quantitated the metabolites in the tissue, and measured the formation of individual DNA adducts. It is also the first study to examine the effect of PEITC on the pulmonary metabolism of NNK in the IPRL system. The results show the utility of the IPRL system in examining metabolism and DNA adduct formation in the lung.

CHAPTER 4: METABOLISM OF NNAL ENANTIOMERS IN THE IPRL SYSTEM

4.A – Introduction

The carbonyl reduction of NNK to NNAL is an important metabolic pathway in rodents and humans. NNAL, like NNK, is a carcinogen in rats and mice[15]. Unlike NNK however, NNAL is a chiral compound that exists as two enantiomers, *(S)*-NNAL and *(R)*-NNAL. The enantiomers have similar physical characteristics, but have different biological effects. *(S)*-NNAL is as potent a pulmonary carcinogen as NNK in A/J mice, whereas *(R)*-NNAL is significantly less carcinogenic[21]. The difference in carcinogenicity between the two enantiomers may be due to metabolic and distributional differences.

In vitro and *in vivo* data have shown *(S)*-NNAL to undergo oxidative metabolism and reoxidation to NNK to a greater extent than *(R)*-NNAL[21,29,77]. *(R)*-NNAL, on the other hand, is extensively glucuronidated, a detoxification pathway that *(S)*-NNAL seems to lack[77]. *In vivo* data have also reported that *(S)*-NNAL has a significantly larger steady-state volume of distribution than *(R)*-NNAL, and appeared to persist in the lung tissue longer than NNK and *(R)*-NNAL[77,78]. Furthermore, NNK and *(S)*-NNAL produced similar levels of POB and PHB-DNA adducts in the lung, while *(R)*-NNAL exposure resulted in lower POB-DNA adduct levels and more PHB-DNA adducts than NNK and *(S)*-NNAL[62,63]. Based on the data available, it has been hypothesized that the persistence of *(S)*-NNAL in the lung tissue coupled with its apparent ability to reoxidize to NNK, may be important to the lung-specific carcinogenicity of NNK. The objective of this study was to examine the pulmonary metabolism, distribution, and DNA adduct

formation of *(S)*-NNAL and *(R)*-NNAL in the IPRL system to gain more insight into the interactions of these enantiomers with the lung.

4.B – Materials and Methods

All materials and methods were the same as those reported in Chapter 3, except where indicated otherwise.

4.B.i – Chemicals

[5-^{3}H]*(S)*-NNAL (21.2 Ci/mmol) and [5-^{3}H]*(R)*-NNAL (25.8 Ci/mmol) were purchased from Moravek Biochemicals (Brea, CA). All other chemicals were the same as those previously reported.

4.B.ii – Isolated Lung Perfusion

4.B.ii.a – Metabolism Studies

The pulmonary metabolism of the NNAL enantiomers was examined using an initial reservoir concentration of 1.2 μM *(S)*-NNAL or *(R)*-NNAL. Once the lungs were rinsed of blood and a recirculating perfusion was established, a bolus was injected into the perfusate reservoir. To achieve the 1.2 μM *(S)*-NNAL concentration, 200 μL of unlabeled *(S)*-NNAL solution (0.29 nmol/μL in EtOH:H_2O (50:50)) was administered simultaneously with 50 μL (~50 μCi) of [5-^{3}H]*(S)*-NNAL. In the *(R)*-NNAL perfusions,

180 µL of unlabeled (*R*)-NNAL (0.32 nmol/µL in EtOH:H_2O (50:50)) was administered with 50 µL (~50 µCi) of [5-^{3}H](*R*)-NNAL.

Perfusate samples of 250 µL were taken from the reservoir at 0, 1, 30, 60, 90, 120, 150, 180, 210, 240, 270, 300, 330, and 360 min post-dose. The duration of the perfusion was increased from the 180 min used with NNK to 360 min because of the limited metabolism observed with *(S)*-NNAL and *(R)*-NNAL. Immediately following the collection of the 360 min perfuate sample, an additional 5 mL perfusate sample was collected and stored at -4 °C, and was used to determine the percent of *(S)*-NNAL and *(R)*-NNAL in the final perfusate. The lungs were then perfused with 50 mL of blank perfusate. The tissue was minced, weighed, flash-frozen in liquid nitrogen, and stored at -80 °C until further analysis. The quantification of metabolites in the perfusate and tissue was carried out via the extraction and HPLC methods described in Chapter 3.

4.B.ii.b – DNA Adduct Studies

The DNA adduct perfusions were carried out in the same manner as those conducted for the metabolism studies, except that only unlabeled *(S)*-NNAL and *(R)*-NNAL were used and perfusate samples were not collected. For the 1.2 µM *(S)*-NNAL perfusions 210 µL of the unlabeled *(S)*-NNAL solution (0.29 nmol/µL in EtOH:H_2O (50:50)) was administered to the reservoir. In the 1.2 µM *(R)*-NNAL perfusions 185 µL of the unlabeled *(R)*-NNAL solution (0.32 nmol/µL in EtOH:H_2O (50:50)) was added. After the 360 min perfusion, the lungs were perfused with 50 mL of blank perfusate. The tissue was then minced, weighed, flash-frozen in liquid nitrogen, and stored at -80 °C

until analysis for individual DNA adduct formation was performed using the methods described in Chapter 3.

4.B.iii – Metabolism in S9 Fractions

4.B.iii.a – Preparation of S9 Fraction

Rats were euthanized with carbon dioxide, and the liver and lung were quickly excised from the body and rinsed in 0.9% saline. The tissue was flash-frozen in liquid nitrogen and kept on dry ice. The frozen tissue was placed between sheets of aluminum foil and crushed with a rubber mallet. Small aliquots of fragmented tissue were homogenized in a 10 mL glass homogenizer with 2-4 mL of 50mM Tris buffer + 1 mM EDTA + 1.15% KCl (w/v), pH 7.4. The homogenized tissue samples were centrifuged at 9,000 x g (10,000 rpm) in a Beckman Optima L-90K ultracentrifuge (Beckman Coulter, Schaumburg, IL) for 60 min at 4 °C. The resulting supernatant was the S9 fraction, and was isolated from the tissue pellet and aliquoted into microcentrifuge tubes. Incubations were carried out immediately and the remaining S9 fractions were stored at -80 °C.

4.B.iii.b – S9 Fraction Incubations

All S9 incubations were carried out in 50 mM Tris-HCl (pH 7.0) containing 1 mM EDTA and 1.15% KCl (w/v) with a total volume of 200 µL. Each incubation contained 20 µL of NADPH regenerating system (4 mM NADPH, 100 mM glucose-6-phosphate, and 4 U/mL glucose-6-phosphate dehydrogenase). The lung S9 incubations

contained approximately 1.5 mg protein/mL and the liver incubations contained roughly 1.0 mg protein/mL. The metabolism of [5-^{3}H]*(S)*-NNAL was investigated at 0.1 µM and 1.6 µM. [5-^{3}H]*(R)*-NNAL incubations were carried out with concentrations of 0.1 µM and 1.7 µM, and the concentration of the [5-^{3}H]NNK incubations was 0.2 µM. All incubations were carried out at 37 °C in an orbital shaker (80 rpm) for 60 min. The reactions were terminated by adding 20 µL each of 0.3 M zinc sulfate and 0.3 M barium hydroxide. Samples were centrifuged at 13,000 x g for 10 min to pellet the precipitated protein, and the metabolites were analyzed by injecting 100 µL of the final supernatant onto HPLC with UV and radioflow detectors as previously reported (Chapter 3). The incubations were performed solely for the purpose of measuring the relative extent of NNK formation for the enantiomers and were not optimized to be linear with time, drug concentration, or protein concentration.

4.B.iv – Albumin Binding

Albumin binding was tested using Centrifree® centrifugal filtration devices with a molecular weight cut off of 30,000 (Millipore Corporation, Billerica, MA). Solutions of [5-^{3}H]NNK, [5-^{3}H]*(S)*-NNAL, and [5-^{3}H]*(R)*-NNAL at concentrations of 0.1 µM and 1.2 µM were made in perfusate (as described in Chapter 3) with and without albumin. Solutions were allowed to mix at 37 ºC for 30 min before 650 µL of each solution was transferred to Centrifree® devices and sealed with Parafilm™. All solutions were tested in triplicate. Samples were centrifuged at 1500 x g and 37 ºC for 1.5 hrs. The resulting filtrate was analyzed from duplicate aliquots of 200 µL by LSC and was compared to the

initial activity of each solution as determined by analyzing 300 µL in duplicate by LSC. Nonspecific binding to the Centrifree® device was measured by the solutions that did not contain albumin, while albumin binding was determined by solutions that contained albumin.

4.C – Results

4.C.i - 1.2 µM (S)-NNAL 360 min Perfusion

Figure 4.1A shows the perfusate concentration-time data for the 1.2 µM *(S)*-NNAL perfusions. The concentration-time data were used to estimate the apparent pharmacokinetic parameters for the pulmonary metabolism of *(S)*-NNAL (Table 4.1). At the end of the 360 min perfusion, NNAL-*N*-oxide (400 ± 30 pmol/mL) was the major perfusate metabolite and accounted for approximately 49% of the final perfusate concentration, while unmetabolized NNAL (250 ± 26 pmol/mL) made up about 31% of the final concentration. Hydroxy acid (77.2 ± 12.6 pmol/mL) and diol (86.2 ± 8.8 pmol/mL) were also detected in the perfusate, but at lower concentrations than NNAL and NNAL-*N*-oxide (Figure 4.1B). In some perfusate samples it appeared that NNK-*N*-oxide and keto alcohol may have been present *(data not shown)*, but the signal-to-noise ratio was not great enough for them to be quantified. Neither NNK-*N*-oxide nor keto alcohol were present in the tissue at detectable levels, thus it seems unlikely that NNK-*N*-oxide or keto alcohol was present in the perfusate. NNK was not detected in any of the perfusate samples.

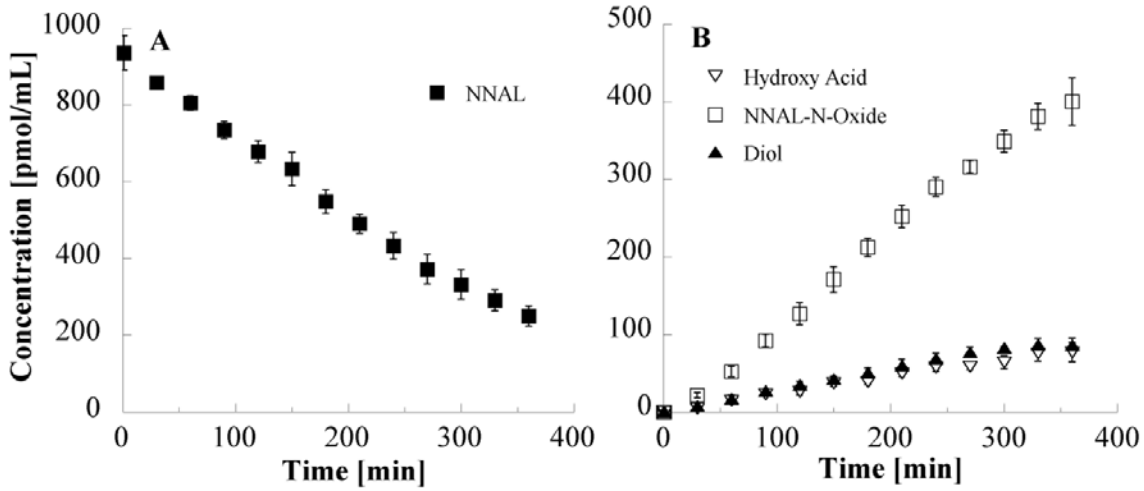

Figure 4.1 *– Average concentration (pmol/mL ± SD) vs time (min) profiles of NNAL (A) and metabolites (B) in the perfusate of 1.2 µM (S)-NNAL during a 360 min perfusion, (n=3). Where error bars are not visible, they are smaller than the symbol.*

Table 4.1 – *Apparent pharmacokinetic parameters (mean ± SD, n=3) for the pulmonary metabolism of 1.2 µM (S)-NNAL, 1.2 µM (R)-NNAL, and 0.1 µM (R)-NNAL.*

	1.2 µM *(S)*-NNAL	**1.2 µM *(R)*-NNAL**	**0.1 µM *(R)*-NNAL**
$t_{1/2,\,app}$ **[min]**	145 ± 26	128 ± 15	127 ± 32
V_z **[mL]**	49 ± 7	47 ± 6	58 ± 9
CL_{app} **[mL/min]**	0.23 ± 0.02	0.26 ± 0.04	0.32 ± 0.03
ER_{app}	0.029 ± 0.002	0.032 ± 0.005	0.040 ± 0.004

A 1-way ANOVA with Holm-Sidak was used for determining significant differences compared to the 1.2 µM (R)-NNAL perfusion group. No significant differences were observed.

The NNAL in the final perfusate samples was analyzed to determine the composition of the two enantiomers (Table 4.2). In two of the perfusate samples *(R)*-NNAL was detected, but at less than 1% of the total NNAL. When the standard solutions for [5-^{3}H]*(S)*-NNAL, *(S)*-NNAL, [5-^{3}H]*(R)*-NNAL, *(R)*-NNAL were analyzed both of the *(R)*-NNAL solutions and *(S)*-NNAL appeared to be pure, but the [5-^{3}H]*(S)*-NNAL contained approximately 1.3% of *(R)*-NNAL as an impurity. Thus the *(R)*-NNAL that was present in the perfusate samples may have been due to impurities in the stock solution.

Table 4.2 – *The percent (mean ± SD, n=3) of (S)-NNAL and (R)-NNAL in the perfusate and tissue following perfusions with each enantiomer.*

	1.2 µM *(S)*-NNAL	**1.2 µM *(R)*-NNAL**	**0.1 µM *(R)*-NNAL**
Perfusate	99.6 ± 0.5 % *(S)*-NNAL 0.40 ± 0.46 % *(R)*-NNAL	0.33 ± 0.29 % *(S)*-NNAL 99.7 ± 0.3% *(R)*-NNAL	4.2 ± 5.8 % *(S)*-NNAL 95.8 ± 5.8 % *(R)*-NNAL
Tissue	only *(S)*-NNAL detected, but close to limit of detection	only *(R)*-NNAL detected, but close to limit of detection	37 ± 10 % *(S)*-NNAL 51 ± 19 % *(R)*-NNAL

In the tissue NNAL-*N*-oxide was the major metabolite (Figure 4.2). However, the concentration reported here overestimates its actual formation because the diol peak was not separated from the NNAL-*N*-oxide peak. Diol typically elutes at the tail end of NNAL-*N*-oxide, but in the tissue samples it appeared to be present as a shoulder on the oxide peak. The contribution of diol is believed to be less than 10% based on the results of the 0.1 µM *(R)*-NNAL perfusions. The relatively small size of the diol peak compared

to the NNAL-*N*-oxide peak may account for the lack of separation of these two metabolites. Hydroxy acid and NNAL were also detected in the tissue, along with a metabolite that eluted at the same time as the keto acid standard. NNAL contributed to less than 3% of the final tissue concentration, with *(S)*-NNAL being the only enantiomer detected (Table 4.2). However, since the NNAL concentration was close to the limit of detection, it would have been unlikely to see low concentrations of *(R)*-NNAL even if it were present in the tissue. NNK was not detected in any of the tissue samples.

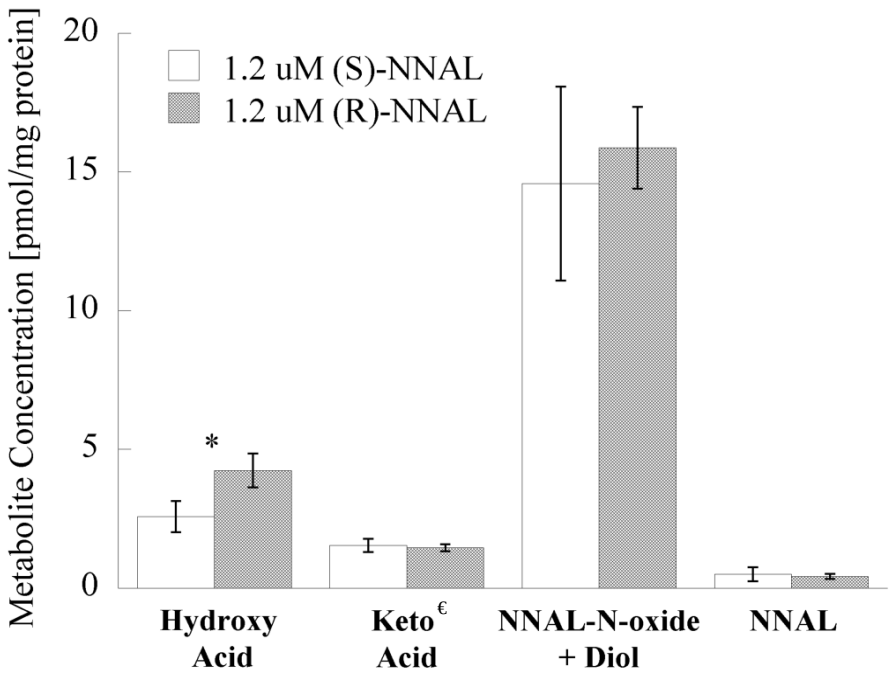

Figure 4.2 *– Average concentration (pmol/mg protein ± SD) of each metabolite in the tissue following a 360 min perfusion with 1.2 µM (S)-NNAL (open bars) or 1.2 µM (R)-NNAL (shaded bars), (n=3). * p-value < 0.05.* $^{€}$ *could be keto acid or a metabolite eluting at the same time as the keto acid standard.*

The major DNA adduct detected in the tissue of the 1.2 µM *(S)*-NNAL perfusions was O^2-PHB-dThd (252 ± 36 fmol/mg DNA), followed by O^6-PHB-dGuo (25 ± 7 fmol/mg DNA) (Table 4.3). Low levels of O^2-POB-dThd (2.7 ± 0.5 fmol/mg DNA) were also detected, indicating that some reoxidation to NNK had occurred. 7-PHB-Gua, 7-POB-Gua, O^6-POB-dGuo, and O^6-methyl-Gua DNA adducts were not detected in any of the lung tissue samples.

Table 4.3 – *Levels of individual DNA adducts (fmol/mg DNA) (mean ± SD, n=3) in the lung tissue after 360 min perfusions with 1.2 µM (S)-NNAL or 1.2 µM (R)-NNAL.*

	O^6-PHB-dGuo	O^2-PHB-dThd	O^2-POB-dThd
1.2 µM *(S)*-NNAL	25 ± 7	252 ± 36	2.7 ± 0.5
1.2 µM *(R)*-NNAL	20 ± 2	247 ± 30	-

7-PHB-Gua, 7-POB-Gua, O^6-POB-dGuo, and O^6-methyl-Gua DNA adducts were not detected in any of the lung tissue samples.

4.C.ii – 1.2 µM (R)-NNAL 360 min Perfusion

The perfusate concentration-time data for the 1.2 µM *(R)*-NNAL perfusions are shown in Figure 4.3. NNAL-*N*-oxide (400 ± 17 pmol/mL) was the major perfusate metabolite, accounting for approximately 50% of the final perfusate concentration (Figure 4.3B). Hydroxy acid (95 ± 7 pmol/mL) and diol (82 ± 3 pmol/mL) were also detected in the perfusate, while neither NNK nor any of its metabolites were. NNAL (225 ± 56 pmol/mL) contributed to 28% of the final concentration, and was primarily

composed of the *(R)* enantiomer. In two of the perfusate samples *(S)*-NNAL accounted for approximately 0.5% of the total NNAL, but was not detected in the third sample. However, in the third perfusate sample the area of the NNAL peak was less than half of the area in the other two samples, so the low concentration of the sample might explain the absence of *(S)*-NNAL. The estimated apparent pharmacokinetic parameters for the pulmonary metabolism of 1.2 µM *(R)*-NNAL were not significantly different from those of 1.2 µM *(S)*-NNAL (Table 4.1).

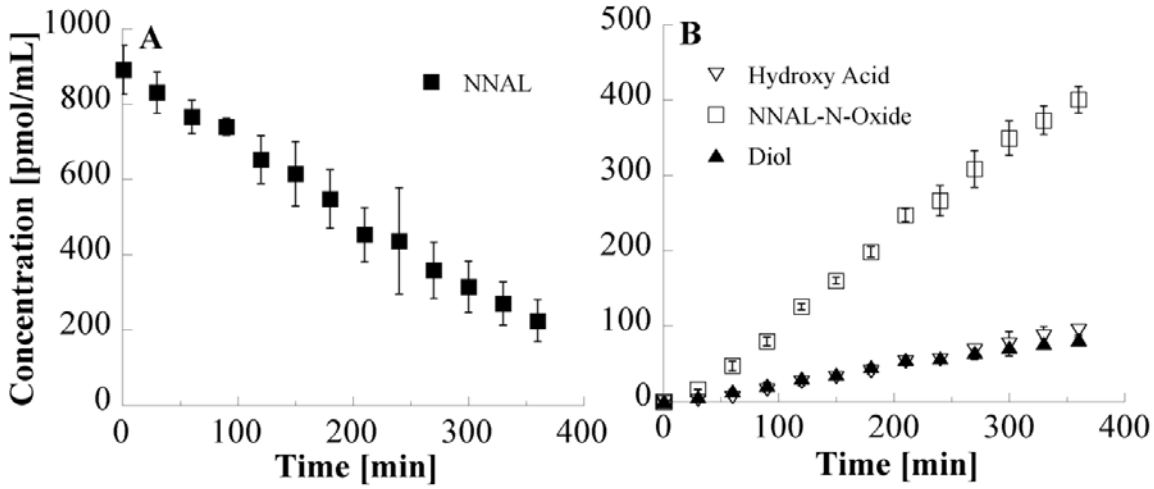

Figure 4.3 *– Average concentration (pmol/mL ± SD) vs time (min) profiles of NNAL (A) and metabolites (B) in the perfusate of 1.2 µM (R)-NNAL during a 360 min perfusion, (n=3). Where error bars are not visible, they are smaller than the symbol.*

NNAL-*N*-oxide, hydroxy acid, NNAL, and a metabolite that eluted at the same time as keto acid were all detected in the tissue (Figure 4.2). Diol was most likely present, but was not distinguishable from NNAL-*N*-oxide. The percent of hydroxy acid in the tissue was significantly greater in the *(R)*-NNAL perfusions than in the *(S)*-NNAL

perfusions, while the percent of NNAL-*N*-oxide/diol was significantly greater in the *(S)*-NNAL perfusions than for the *(R)*-NNAL. In all three tissue samples only *(R)*-NNAL was detected in the tissue, but the levels of NNAL for chiral analysis were also close to the limit of detection in all of the samples.

Both O^2-PHB-dThd (247 ± 30 fmol/mg DNA) and O^6-PHB-dGuo (20 ± 2 fmol/mg DNA) were detected in the tissue of the 1.2 µM *(R)*-NNAL perfusions (Table 4.3). However, neither the level of O^2-PHB-dThd nor O^6-PHB-dGuo were significantly different between the *(S)*-NNAL and *(R)*-NNAL perfusions. No other DNA adducts were detected in the tissue.

4.C.iii – 0.1 µM (R)-NNAL 360 min Perfusion

The metabolism of *(R)*-NNAL at a concentration of 0.1 µM was also checked to determine if its metabolism was dose-dependent. Only metabolism perfusions were performed since limited DNA adduct formation was expected based on the DNA adduct results of NNK. The concentration of NNAL and its metabolites versus time are shown in Figure 4.4. The major perfusate metabolite was NNAL-*N*-oxide (31.2 ± 2.1 pmol/mL), which accounted for roughly 53% of the final perfusate concentration. Both hydroxy acid (7.1 ± 0.2 pmol/mL) and diol (7.2 ± 1.7 pmol/mL) were detected in the perfusate, but NNK and its subsequent metabolites were not. NNAL (13.2 ± 2.1 pmol/mL) constituted approximately 23% of the final concentration, and was composed of both enantiomers in two of the three perfusate samples (Table 4.2). *(S)*-NNAL accounted for 2 and 10% in the two samples in which it was detected. The NNAL level in the third sample was close to

the limit of detection, which may account for the absence of *(S)*-NNAL. The estimated pharmacokinetic parameters for the metabolism of *(R)*-NNAL were not significantly different between the 1.2 µM and the 0.1 µM perfusions (Table 4.1).

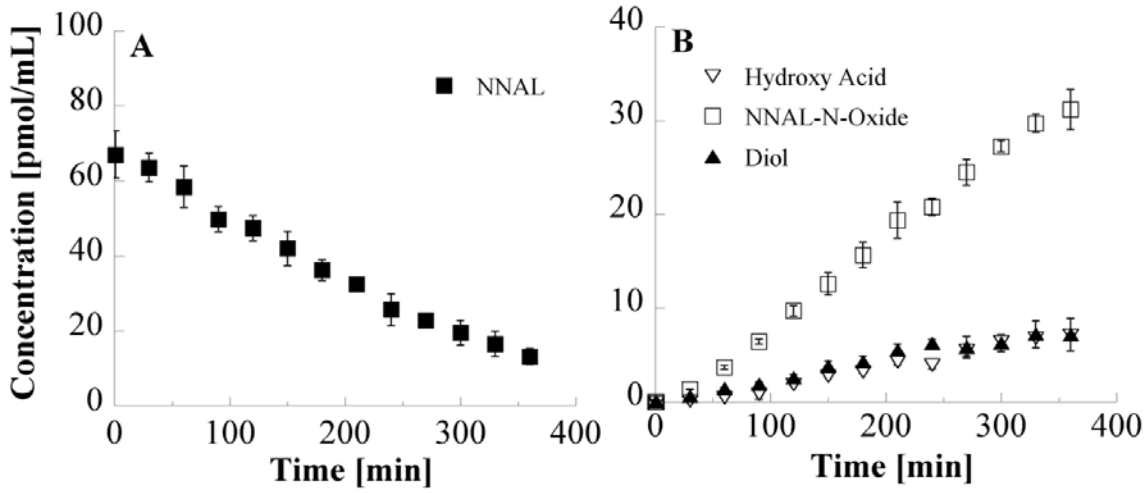

Figure 4.4 *– Average concentration (pmol/mL ± SD) vs time (min) profiles of NNAL (A) and metabolites (B) in the perfusate of 0.1 µM (R)-NNAL during a 360 min perfusion, (n=3). Where error bars are not visible, they are smaller than the symbol.*

NNAL-*N*-Oxide was also the major metabolite in the tissue, accounting for roughly 55% of the total radioactivity (Figure 4.5). In these samples it was possible to distinguish diol from NNAL-*N*-oxide. Diol accounted for approximately 8% of the total radioactivity in the tissue, but the two metabolites were expressed together for comparison to the 1.2 µM *(R)*-NNAL perfusions. Hydroxy acid, NNAL, and a metabolite that eluted at the same time as keto acid were also detected in the tissue. The fraction of NNAL in the tissue was significantly greater in the 0.1 µM perfusion than in the 1.2 µM perfusions. The composition of the NNAL in the tissue was comprised of both enantiomers (Table 4.2). In two samples, *(S)*-NNAL accounted for roughly 30% of the

NNAL, and 48% in the third sample. It should be noted that the levels of NNAL in the tissue samples were close to the limit of detection.

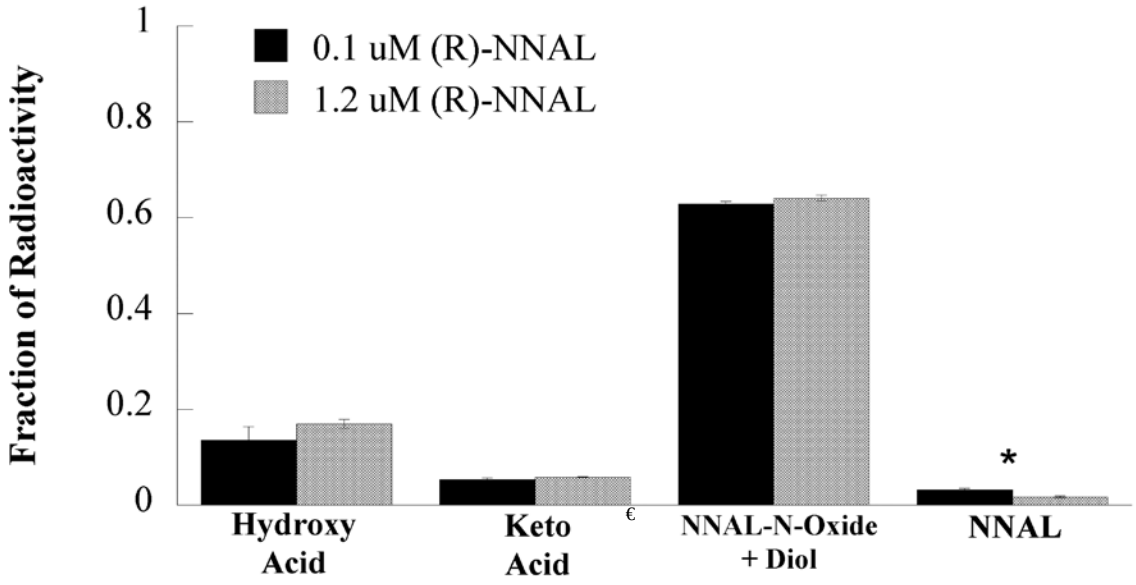

Figure 4.5 *– Average fraction of radioactivity ± SD of each metabolite in the tissue following a 360 min perfusion with 0.1 µM (R)-NNAL (dark bars) or 1.2 µM (R)-NNAL (shaded bars), (n=3). * p-value < 0.05.* [€] *may be keto acid or a metabolite eluting at the same time as the keto acid standard.*

4.C.iv – S9 Fraction with (S)-NNAL, (R)-NNAL, and NNK

A difference in the metabolism of *(S)*-NNAL and *(R)*-NNAL was expected in the IPRL system. Since no noticeable differences were observed and the metabolism of the enantiomers was not as efficient as the metabolism of NNK, it was hypothesized that the preformed NNAL enantiomers may have encountered diffusional barriers in the lung tissue preventing them from readily gaining access to the enzymatic sites. Therefore, the metabolism of *(S)*-NNAL, *(R)*-NNAL, and NNK were examined in lung and liver S9 fractions to eliminate any potential barriers.

The rates of formation for the metabolites are listed in Table 4.4. It should be noted that the S9 experiments were not optimized for linearity with protein concentration or time. Instead the goal was to measure the extent of metabolite formation, and to ensure that the incubations were carried out in a manner that would allow for the detection of NNK formation. The only consistent significant difference between the metabolism of *(S)*-NNAL and *(R)*-NNAL in the lung at both concentrations was the formation rate of NNK. In both the lung and liver the rate of reoxidation to NNK was significantly greater for *(S)*-NNAL than *(R)*-NNAL. The large standard deviations reported for the rate of NNK formation from *(R)*-NNAL are due to the fact that NNK was only detected in some of the *(R)*-NNAL samples, whereas it was detected in all of the *(S)*-NNAL incubations. The liver was more efficient at the reconversion of NNAL to NNK than the lung, but the lung S9 fraction was able to catalyze the reaction. It should be noted that the composition of the enantiomers of NNAL at the end of each incubation was not determined. Since only a small fraction of the dosed enantiomer was metabolized during the incubations, it would be highly unlikely that the formation of the other enantiomer would be detected.

4.C.v – Albumin Binding

Neither NNK, *(S)*-NNAL, nor *(R)*-NNAL showed appreciable non-specific binding to the Centrifree® devices or specific binding to the albumin present in the perfusate.

Table 4.4 *– Rate of metabolite formation (fmol/min/mg protein) in lung (1.5 mg protein) and liver (1.0 mg protein) S9 incubations with 0.1 and 1.6 µM (S)-NNAL, 0.1 and 1.7 µM (R)-NNAL, and 0.2 µM NNK. Values are expressed as means ± standard deviation, (n=3).*

	Hydroxy Acid	Keto Acid	NNAL-*N*-Oxide + Diol	NNK-*N*-Oxide	Keto Alcohol	NNAL	NNK
0.1 µM - Lung							
(S)-NNAL	2.7 ± 1.2	1.2 ± 0.5	18.4 ± 7.8		0.9 ± 0.5		1.2 ± 0.4
(R)-NNAL	2.7 ± 1.4	1.1 ± 0.4	10.4 ± 5.5*		0.7 ± 0.2		0.2 ± 0.2*
1.6 µM - Lung							
(S)-NNAL	21.3 ± 9.6	13.9 ± 4.1	108.5 ± 57.3		5.2 ± 5.4		10.9 ± 4.4
(R)-NNAL+	27.8 ± 12.3	21.1 ± 5.8*	71.3 ± 40.8		6.2 ± 5.3		1.3 ± 2.6*
0.1 µM - Liver							
(S)-NNAL	3.5 ± 0.9		4.4 ± 1.2		1.1 ± 0.5		7.4 ± 2.4
(R)-NNAL	2.6 ± 0.4*		3.8 ± 0.9		0.4 ± 0.3*		1.0 ± 0.2*
1.6 µM - Liver							
(S)-NNAL	28.2 ± 10.6		32.6 ± 8.5		14.4 ± 4.3		84.8 ± 19.1
(R)-NNAL+	28.7 ± 9.8		36.0 ± 9.6		6.0 ± 6.1*		11.0 ± 6.3*
0.2 µM - NNK							
Lung		5.9 ± 2.2	3.9 ± 1.0	79.0 ± 25.1	59.2 ± 19.3	28.8 ± 2.8	
Liver	4.0 ± 3.6	7.8 ± 1.7	5.4 ± 1.0†	6.4 ± 1.8†	15.6 ± 3.9†	398 ± 73†	

** p-value < 0.05, (R)-NNAL was compared to (S)-NNAL of same group*

+ Actual incubation concentration was 1.7 µM (R)-NNAL

† p-value < 0.05, Comparison of NNK metabolites in lung versus liver

4.D – Discussion

(S)-NNAL has been shown to be a more potent pulmonary carcinogen than *(R)*-NNAL[21]. Research suggests that the difference in carcinogenicity is due to metabolic and pharmacokinetic differences between the two enantiomers. The metabolism of *(S)*-NNAL and *(R)*-NNAL has been studied, but not as extensively as the metabolism of NNK. In this study the pulmonary metabolism, the distribution of *(S)*-NNAL and *(R)*-NNAL metabolites in the perfusate and tissue, and the formation of DNA adducts were examined in the IPRL system in an effort to better understand the difference in their pulmonary carcinogenicity and their potential role in the lung-specific carcinogenicity of NNK.

Originally, the objective was to repeat the same perfusions performed with NNK *(Chapter 3)*, with *(S)*-NNAL and *(R)*-NNAL, and compare the pulmonary metabolism among the three compounds. However, when 0.1 µM *(S)*-NNAL was perfused for 180 min, NNAL accounted for approximately 58% of the final perfusate concentration, reoxidation to NNK was not observed, and DNA adducts were not detected in the tissue *(results shown in Chapter 2)*. In contrast, when NNK was perfused at 0.1 µM for 180 min, less than 4% of the final perfusate concentration consisted of NNK *(results shown in Chapter 3)*, indicating that *(S)*-NNAL was not metabolized as efficiently by the lung as NNK. In an effort to measure the reoxidation of each enantiomer back to NNK the perfusions were lengthened to 360 min to allow more NNAL to be metabolized.

When the metabolism of *(S)*-NNAL and *(R)*-NNAL was examined in the IPRL system at an initial perfusate concentration of 1.2 µM, there was no noticeable difference

in the formation of perfusate metabolites, nor was NNK detected in any of the perfusate or tissue samples. These results were unexpected because all of the previously reported *in vitro* and *in vivo* work showed a significant difference in the metabolism of the two enantiomers and in their reconversion to NNK[21,29,77,78]. Minor differences in the tissue metabolites were observed, but they were not the substantial differences that were expected. A metabolite that eluted at a similar time to the keto acid standard was present in the tissue of both enantiomers. If the metabolite was keto acid, it would indicate that both enantiomers were reoxidized to NNK. However, its concentration in the tissue was similar for both enantiomers, suggesting that the reoxidation to NNK was similar for *(S)*-NNAL and *(R)*-NNAL, which is inconsistent with previous reports. Furthermore, the major pulmonary metabolites of NNK were NNK-*N*-oxide and keto alcohol, so it seems unlikely that keto acid would form in the tissue before these other two metabolites. It is possible that the metabolite was actually NNAL(ADP^+) and not keto acid. Previous reports have shown the two metabolites to elute at similar times[115].

The levels of PHB-DNA adducts in the lung tissue were also similar for the two enantiomers. However, O^2-POB-dThd was detected at low levels only in the tissue of the *(S)*-NNAL perfusions. The formation of the POB-DNA adduct indicates that *(S)*-NNAL was reconverted to NNK, since POB-DNA adducts can only form from NNK[81]. This appeared to be one of the only indicators of metabolic difference between the enantiomers. This suggests that the measurement of DNA adducts may be a more sensitive and direct method of measuring the bioactivation of NNK and NNAL than measuring metabolite formation. *In vivo* data have shown that the chronic administration

of *(S)*-NNAL produces similar levels of POB-DNA adducts as chronically administered NNK in the lung[62,63]. However, in the IPRL system 1.2 µM NNK produced approximately 362 ± 11 fmol/mg DNA of O^2-POB-dThd, while 1.2 µM *(S)*-NNAL only produced roughly 2.7 ± 0.5 fmol/mg DNA of O^2-POB-dThd. These results indicate that the DNA adduct formation from NNAL metabolism in the IRPL system is not representative of *in vivo* DNA adduct formation in the lung.

The effect of concentration on metabolism was examined with *(R)*-NNAL, but could not be tested with *(S)*-NNAL because there was not enough remaining tritiated stock to perform the experiments. The perfusate metabolic profiles and the estimated apparent pharmacokinetic parameters were similar for the 0.1 µM and 1.2 µM *(R)*-NNAL perfusions. The percent of each metabolite in the tissue was also similar. However, the percent of NNAL in the tissue from the 0.1 µM perfusions was significantly greater than the 1.2 µM perfusions. Also at the lower concentration, *(S)*-NNAL contributed to a larger percent of the NNAL composition in the perfusate and tissue. It may be possible that at the higher concentration of NNAL the metabolic pathway responsible for the reoxidation to NNK was saturated and because the reoxidation to NNK was a minor pathway, a significant effect on the total metabolic clearance and metabolite formation was not observed.

The concentration-time profiles for the two enantiomers showed that their concentrations did not decline in a monoexponential manner, which indicated that the system was nonlinear. Since the perfusate concentrations of NNAL in the *(S)*-NNAL and *(R)*-NNAL perfusions were approximately 10 times greater than the concentrations of

NNAL achieved when NNK was dosed, it is possible that the metabolic pathways responsible for the metabolism of NNAL were being saturated. It should also be noted that if an influx transporter contributed to the distribution of NNAL into the pulmonary tissue, then it may be possible that the nonlinearity of the system could be in part due to saturation of the influx transporter. The saturation of an influx transporter may explain the higher percent of NNAL in the tissue in the 0.1 µM perfusions than in the 1.2 µM perfusions, but more work would have to be done to confirm this.

Perhaps one of the most surprising results was the estimated volume of distribution of *(S)*-NNAL, which was approximately the same as the reservoir volume. This indicated that there was not extensive partitioning of *(S)*-NNAL into the pulmonary tissue. This lack of partitioning was also observed with *(R)*-NNAL and NNK. Based on *in vivo* data, *(S)*-NNAL was expected to have a significantly larger volume of distribution than either *(R)*-NNAL or NNK[77]. In fact, both enantiomers had a larger steady-state volume of distribution than NNK *in vivo,* but in the IPRL system their volumes of distribution were similar to that of NNK. The combination of limited metabolism, low volumes of distribution, and low levels of NNAL in the tissue, suggested that *(S)*-NNAL and *(R)*-NNAL may be unable to efficiently penetrate into the lung tissue due to the presence of diffusional barriers.

One of the original objectives of this work was to examine the stereospecific and stereoselective binding of NNAL in the tissue. The goal was to perfuse the lung with [^{3}H]*(S)*-NNAL followed by a bolus dose of excess unlabeled *(S)*-NNAL or *(R)*-NNAL to compete for binding sites. However, the apparent inability of either *(S)*-NNAL or *(R)*-

NNAL to partition into the tissue indicated that meaningful binding interaction experiments with *(S)*-NNAL and *(R)*-NNAL in the IPRL system would not be possible.

It was hypothesized that the poor pulmonary metabolism and lack of difference in the metabolic profiles of the two enantiomers was a result of the preformed NNAL enantiomers interacting differently with the lung tissue than the NNAL generated from NNK. Typically, metabolism results in metabolites that are more polar than their parent compound, making it easier to eliminate them from the body. Therefore, when the more polar NNAL was dosed it may have encountered diffusional barriers in the tissue that NNK did not. This problem of preformed versus generated metabolites has been previously observed[116]. It is possible that if the rate process by which the preformed NNAL enantiomers obtained access to the enzyme sites was slower than all the metabolic processes, that a difference in the metabolism of *(S)*-NNAL and *(R)*-NNAL may not be observed.

The metabolism of the enantiomers was examined using lung and liver S9 fractions to see if eliminating potential diffusional barriers would alter the metabolic profiles of the enantiomers. The results of the S9 incubations showed that *(S)*-NNAL was reoxidized to NNK to a significantly greater extent than *(R)*-NNAL in both the lung and the liver. The metabolism of NNK in the lung S9 fraction yielded a metabolic profile that was similar to the profile observed in the NNK perfusions. The similarity in the profiles between the two systems indicates that NNK most likely does not encounter difficulties diffusing through the intact lung to gain access to the metabolic sites. For *(S)*-NNAL and *(R)*-NNAL though, the formation of NNK and keto alcohol were observed in the S9

fractions, but not in the IRPL perfusions. These results lend support to the idea that diffusional barriers may impede the metabolism of the NNAL enantiomers in the IRPL system. Although there was a significant difference in the formation of NNK between the two enantiomers, the rates of the metabolites were not significantly different between the enantiomers at both doses. When the metabolism of the enantiomers was examined in lung and liver microsomes, *(S)*-NNAL showed significantly higher oxidative metabolic rates than *(R)*-NNAL in the lung[29]. It is unclear why metabolic differences were observed between the enantiomers in previous microsomal incubations, but not in the current S9 incubations.

4.E – Conclusions

In the IPRL system, perfusate and tissue metabolites were similar for *(S)*-NNAL and *(R)*-NNAL, along with the levels of PHB-DNA adducts that formed in the tissue. The only major difference observed between the pulmonary metabolism of the two enantiomers was that *(S)*-NNAL metabolism resulted in the formation of low levels of POB-DNA adducts, indicating its reoxidation to NNK. As a result, it may be concluded that measuring the formation of DNA adducts, instead of metabolite formation, may be a more sensitive and direct method for quantifying the bioactivation of NNK and NNAL. The similar metabolic profiles of *(S)*-NNAL and *(R)*-NNAL in the IPRL system could be a result of differences between the treatment of preformed versus generated metabolites in the lung. There may be diffusional barriers that prevent the preformed NNAL enantiomers from readily gaining access to the enzymatic sites required for metabolism.

The potential diffusional barriers could be a result of slower passive diffusion due to the more polar nature of NNAL than NNK, or perhaps the saturation of an influx transporter responsible for the distribution of NNAL into the lung tissue.

CHAPTER 5: PULMONARY METABOLISM MODEL

5.A – Introduction

The objective of modeling the data was to attempt to answer some of the unresolved questions concerning the metabolism of NNK, *(S)*-NNAL, and *(R)*-NNAL in the IPRL system. It was observed that the pulmonary clearance of NNK decreased with an increase in NNK concentration, indicating that one or more of its metabolic pathways were nonlinear. It was unclear, based on the concentration-time data alone, which pathways were being saturated. Furthermore, the metabolic profiles of *(S)*-NNAL and *(R)*-NNAL were similar in the IPRL system, which was in contrast to previously published data[29,64,77,78]. It was hypothesized that the preformed NNAL may encounter a diffusional barrier that is not encountered by NNAL formed from NNK. Thus, a comparison between the formation clearances of the NNAL metabolites when NNAL was dosed and NNK was dosed may provide some insight.

5.B – Methods and Results

5.B.i – Formation Clearance Estimates by Differential Equations

In order to estimate formation clearances for each of the metabolites using differential equations, a simple metabolic model describing the metabolism of NNK and NNAL was constructed (Figure 5.1). The model was non-physiologically based, so it did not take into consideration the convective flow of NNK in the perfusate or the distribution of NNK to and from the tissue.

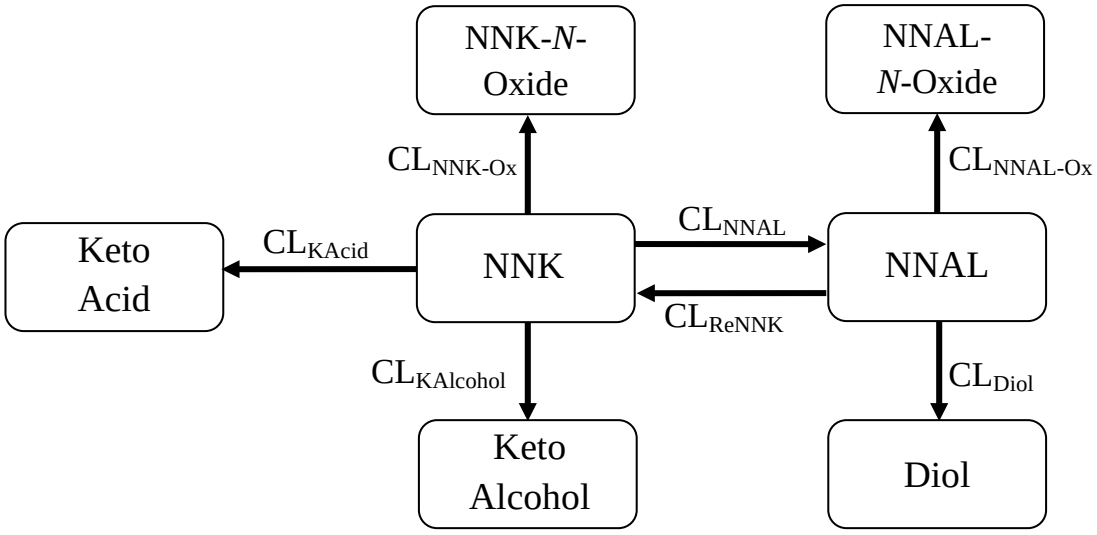

Figure 5.1 *– Model for the pulmonary metabolism of NNK and NNAL.*

From the model, differential equations 1 – 6 were derived to describe the formation clearances of the individual metabolites.

(1) $V_{res}\frac{dC_{NNK}}{dt} = \mathrm{CL_{ReNNK}}\, C_{NNAL} - (CL_{NNK-Ox} + CL_{KAcid} + CL_{KAlcohol} +$

$CLNNALCNNK$

(2) $$V_{res}\frac{dC_{NNK-Ox}}{dt} = CL_{NNK-Ox}C_{NNK}$$

(3) $$V_{res}\frac{dC_{KAcid}}{dt} = CL_{KAcid}\,C_{NNK}$$

(4) $$V_{res}\frac{dC_{KAlcohol}}{dt} = CL_{KAlcohol}C_{NNK}$$

(5) $$V_{res}\frac{dC_{NNAL-Ox}}{dt} = CL_{NNAL-Ox}C_{NNAL}$$

(6) $$V_{res}\frac{dC_{Diol}}{dt} = CL_{Diol}\,C_{NNAL}$$

where V_{res} represents the volume of the reservoir; C_{NNK} and C_{NNAL} are the concentrations of NNK and NNAL in the reservoir; CL_{ReNNK} is the formation clearance for the reoxidation of NNAL to NNK; $CL_{NNK\text{-}Ox}$, $CL_{NNAL\text{-}Ox}$, CL_{KAcid} , $CL_{KAlcohol}$, CL_{NNAL} , CL_{Diol} are the formation clearances of NNK-*N*-oxide, NNAL-*N*-oxide, keto acid, keto alcohol, NNAL, and diol, respectively. The differential equations were then integrated from 0 to 180 min. It was assumed that all of the metabolic pathways were linear, so the formation clearances were constant with respect to time and NNK concentration. Equations 7 – 11 represent the relationships for the formation clearances of the NNK and NNAL metabolites. Rearrangement of equation 12 represents a means to determine the formation clearance of NNAL (CL_{NNAL}).

(7) $$CL_{NNK-Ox} = \frac{V_{res}\, C_{NNK\ -Ox}^{180}}{AUC_{NNK}^{0-180}}$$

(8) $$CL_{KAcid} = \frac{V_{res}\, C_{KAcid}^{180}}{AUC_{NNK}^{0-180}}$$

(9) $$CL_{KAlcohol} = \frac{V_{res}\, C_{KAlco\ hol}^{180}}{AUC_{NNK}^{0-180}}$$

(10) $$CL_{Diol} = \frac{V_{res}\, C_{Diol}^{180}}{AUC_{NNAL}^{0-180}}$$

(11) $$CL_{NNAL-Ox} = \frac{V_{res}\, C_{NNAL\ -Ox}^{180}}{AUC_{NNAL}^{0-180}}$$

(12) $$AUC_{NNK}^{0-180} = \frac{V_{res}\left(C_{NNK}^{0} - C_{NNK}^{180}\right) - CL_{ReNNK}\ AUC_{NNAL}^{0-180}}{\left(CL_{NNK\ -Ox} + CL_{KAcid}\ + CL_{KAlco\ hol} + CL_{NNAL}\right)}$$

where C_{NNK-Ox}^{180}, $C_{NNAL-Ox}^{180}$, C_{KAcid}^{180}, $C_{KAlcohol}^{180}$, C_{Diol}^{180}, C_{NNK}^{180} represent the concentrations of the metabolites in the perfusate at 180 min; C_{NNK}^{0} is the concentration of NNK in the perfusate at 0 min; AUC_{NNK}^{0-180} and AUC_{NNAL}^{0-180} represent the area under the curve for NNK and NNAL from 0 to 180 min in the perfusate.

To obtain an estimate of CL_{NNAL}, equation 12 was further simplified since it contained an additional unknown quantity, CL_{ReNNK}. It was assumed that $CL_{ReNNK}\,AUC_{NNAL}^{0-180}$ was much smaller than $V_{res}\,(C_{NNK}^{0} - C_{NNK}^{180})$, and thus the term could be ignored. This was a fairly reasonable assumption because the value of CL_{ReNNK} would have had to have been around 5 mL/min in order for $CL_{ReNNK}\,AUC_{NNAL}^{0-180}$ to be equal to $V_{res}\,(C_{NNK}^{0} - C_{NNK}^{180})$. This would have been more than 10 times greater than any of the calculated values for the other formation clearances (Table 5.1). As a result, the formation clearance of NNAL was described by equation 13.

(13) $$CL_{NNAL} = \frac{V_{res}\,(C_{NNK}^{0} - C_{NNK}^{180})}{AUC_{NNK}^{0-180}} - (CL_{NNK-Ox} + CL_{KAcid} + CL_{KAlcohol})$$

The calculated formation clearance of every metabolite, except NNAL, was significantly different between the 0.1 μM and 1.2 μM NNK perfusions. This indicated that the formation clearances of the individual metabolites were not constant with NNK concentration, and that the assumption of linear metabolism did not accurately describe the system. Since the integration of differential equations with nonlinear clearances was far more complex than those with linear clearances, SAAM II was used for modeling nonlinear metabolism.

Table 5.1 – *Estimated formation clearances (mL/min ± SD) of NNK metabolites. Statistical differences were determined by unpaired t-tests.* * *p-value < 0.05.*

	0.1 μM NNK	1.2 μM NNK
$CL_{NNK\text{-}Ox}$	0.38 ± 0.04	$0.22 \pm 0.04^{*}$
$CL_{KAlcohol}$	0.16 ± 0.01	$0.11 \pm 0.02^{*}$
CL_{KAcid}	0.09 ± 0.02	$0.04 \pm 0.01^{*}$
CL_{NNAL}	0.19 ± 0.02	0.15 ± 0.01
$CL_{NNAL\text{-}Ox}$	0.25 ± 0.02	$0.15 \pm 0.03^{*}$
CL_{Diol}	0.14 ± 0.01	$0.09 \pm 0.01^{*}$

5.B.ii – SAAM II Modeling

SAAM II (version 1.2, SAAM Institute Inc, University of Washington) uses numerical methods to estimate parameters used in the models constructed based on experimental data. It was used here to create models for the pulmonary metabolism of NNK, *(S)*-NNAL, and *(R)*-NNAL to determine which metabolic pathways were linear and which were nonlinear. It was also used to determine if the pulmonary metabolism of NNAL varied depending on if it was formed from NNK or dosed directly.

5.B.ii.a – Simple NNK Model

In order to develop a detailed model for the metabolism of NNK and the formation of its individual metabolites, first a series of simple models looking at only the

disappearance of NNK were created. The goal of the simple models was to determine if linear or nonlinear metabolism, or a combination of both, best explained the disappearance of NNK from the perfusate. Figures 5.2, 5.4, and 5.6 illustrate the three SAAM models that were developed to examine the best fit for the NNK perfusate data.

All three of the simple NNK models consisted of two compartments. The amount of NNK in the perfusate was represented by compartment "1", and the amount of NNK in the tissue was designated by compartment "2". The rate constants k(2,1) and k(1,2) represented the convective flow of NNK between the perfusate and the tissue. In the two models that examined linear metabolism, k(0,2) denoted the rate constant for all linear pathways. In the models that examined nonlinear metabolism a third compartment, "3", was added to signify nonlinear metabolites, and k(3,2) represented the rate constant for nonlinear metabolism. Each model was used to simultaneously fit the average NNK concentration-time data from the 0.1 μM and 1.2 μM perfusions.

The first model (Figure 5.2) used to fit the data assumed only linear metabolism. The resulting fits of this model are shown in Figure 5.3. It can be seen that the linear metabolism model appeared to fit the 1.2 μM NNK perfusions well, but overestimates the NNK perfusate concentration a later time points in the 0.1 μM NNK perfusions. These results indicate that the model is under-predicting the metabolism of NNK at the lower perfusion concentration. The Akaike information criterion (AIC), a parameter used to compare the goodness of fit between various models, was 3.83 for the linear metabolism model.

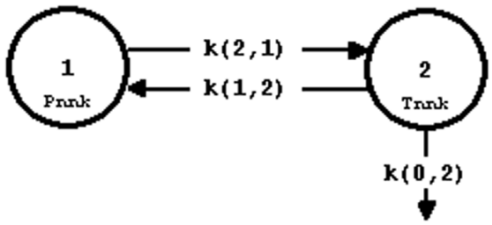

Figure 5.2 *– Linear metabolism model for the pulmonary metabolism of NNK.*

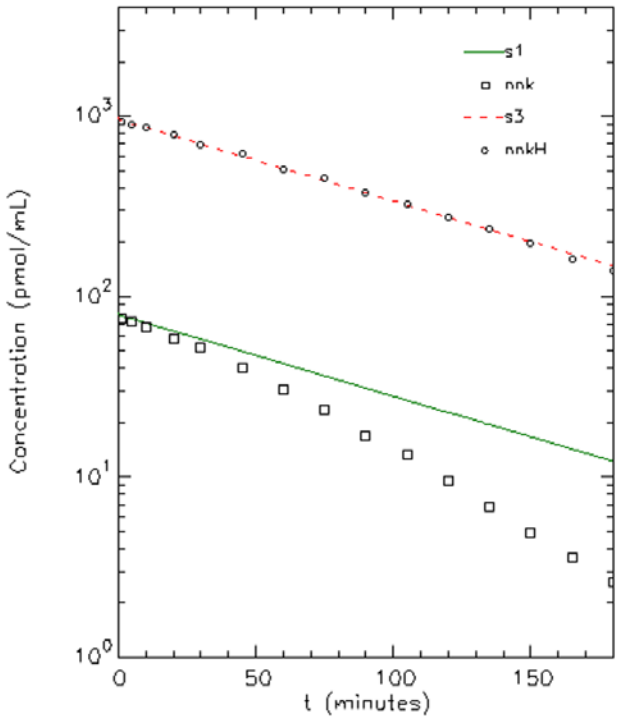

Figure 5.3 *– Fits of the linear metabolism model to the average NNK concentration-time profiles for 0.1 µM (nnk) and 1.2 µM NNK perfusions (nnkH).*

The second model (Figure 5.4) used to fit the data assumed both linear and nonlinear metabolism. Figure 5.5 shows that this model appeared to fit both the 0.1 µM and the 1.2 µM perfusions well. The AIC was 2.54 for this model.

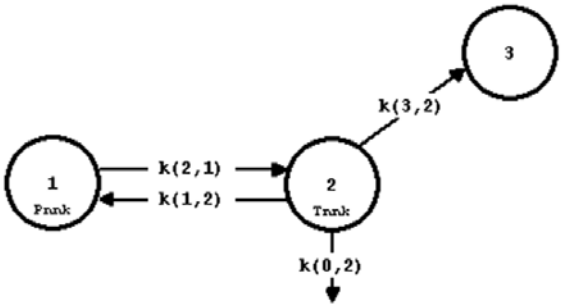

Figure 5.4 *– Linear and nonlinear metabolism model for the pulmonary metabolism of NNK.*

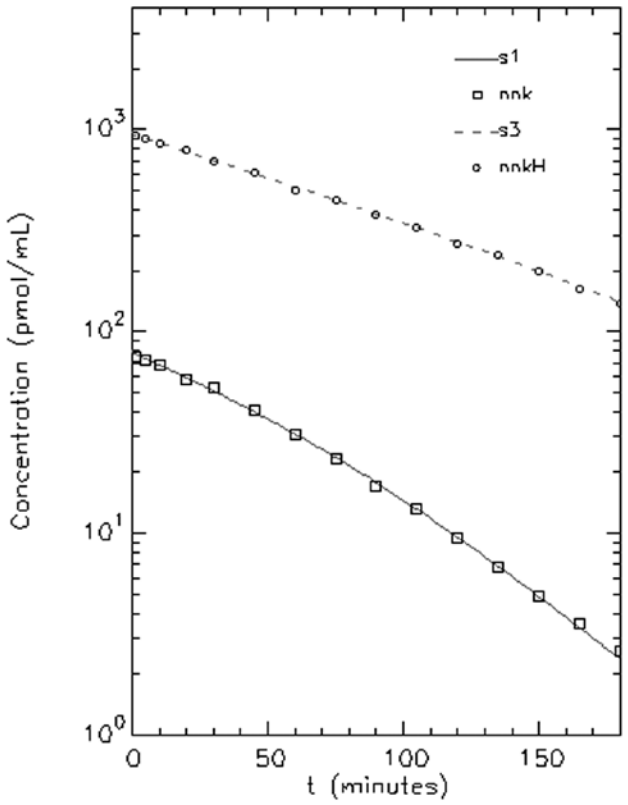

Figure 5.5 *– Fits of the linear and nonlinear metabolism model to the average NNK concentration-time profiles for 0.1 µM (nnk) and 1.2 µM NNK perfusions (nnkH).*

The third model (Figure 5.6) used to fit the data assumed only nonlinear metabolism. Figure 5.7 shows the resulting fits of this model. The nonlinear model

appeared to slightly under-predict the NNK perfusate concentration at the later points in the 1.2 µM NNK perfusion, and over-predicted the concentration at the later time points in the 0.1 µM NNK perfusions. Overall the fit appeared to be better than the linear model, but not as good as the model that assumed both linear and nonlinear metabolism. The AIC value for this nonlinear model was 3.24.

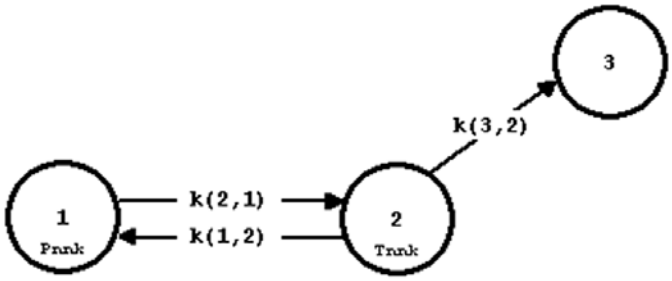

Figure 5.6 *– Nonlinear metabolism model for the pulmonary metabolism of NNK.*

Based on the fits of the three models, their AIC values, and their weighted residual plots, it appeared that a model containing both linear and nonlinear metabolic pathways fit the data better than either linear or nonlinear metabolism alone.

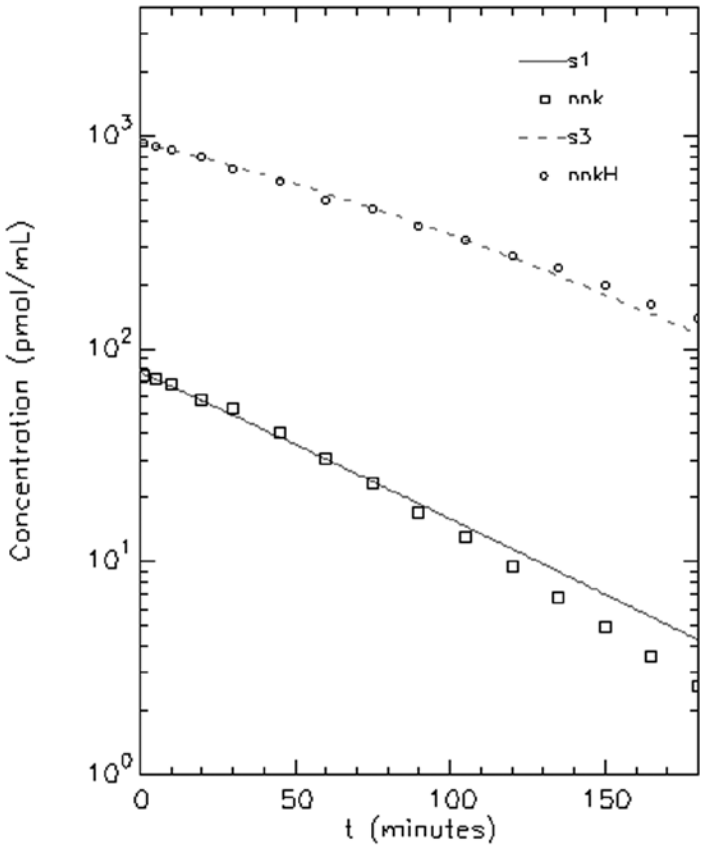

Figure 5.7 *– Fits of the nonlinear metabolism model to the average NNK concentration-time profiles for 0.1 µM (nnk) and 1.2 µM NNK perfusions (nnkH).*

5.B.ii.b – Complete NNK Model

Based on the results obtained from the simple NNK models, it seemed that both linear and nonlinear metabolism needed to be incorporated into a model that would represent the complete metabolism of NNK. In building the complete model each metabolic pathway was systematically checked as to whether linear or nonlinear kinetics

best characterized the formation of that particular metabolite. The final model is illustrated in Figure 5.8.

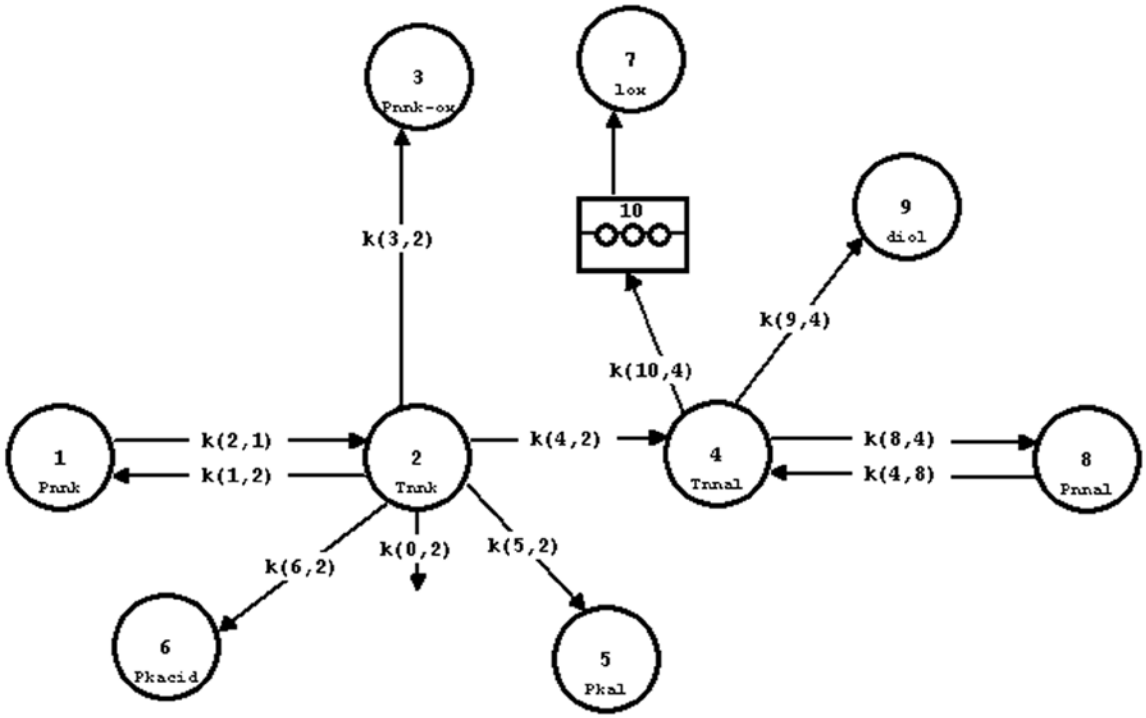

Figure 5.8 *– Complete metabolism model for the pulmonary metabolism of NNK.*

Table 5.2 lists all the compartments and metabolic rate constants used in the model. The rate constants k(2,1) and k(1,2) represent the convective flow of NNK between the perfusate and the tissue, and k(8,4) and k(4,8) represented the convective flow of NNAL between the perfusate and the tissue.

Table 5.2 *– List of all the compartments and metabolic rate constants in the complete NNK metabolism model.*

Model Compartments		
1	NNK perfusate	Measured
2	NNK tissue	Calculated
3	NNK-*N*-oxide perfusate	Measured
4	NNAL tissue	Calculated
5	Keto alcohol perfusate	Measured
6	Keto acid perfusate	Measured
7	NNAL-*N*-oxide perfusate	Measured
8	NNK perfusate	Measured
9	Diol perfusate	Measured
10	NNAL-*N*-oxide delay	Calculated
Metabolic Rate Constants		
k(3,2)	NNK-*N*-oxide metabolism	Nonlinear
k(5,2)	Keto alcohol metabolism	Nonlinear
k(6,2)	Keto acid metabolism	Nonlinear
k(4,2)	NNAL metabolism	Linear
k(0,2)	Non-specified NNK metabolism	Linear
k(10,4)	NNAL-*N*-oxide metabolism	Nonlinear
k(9,4)	Diol metabolism	Nonlinear

The fits for the perfusate concentrations of NNK in the 0.1 µM and 1.2 µM perfusion are shown in Figure 5.9.

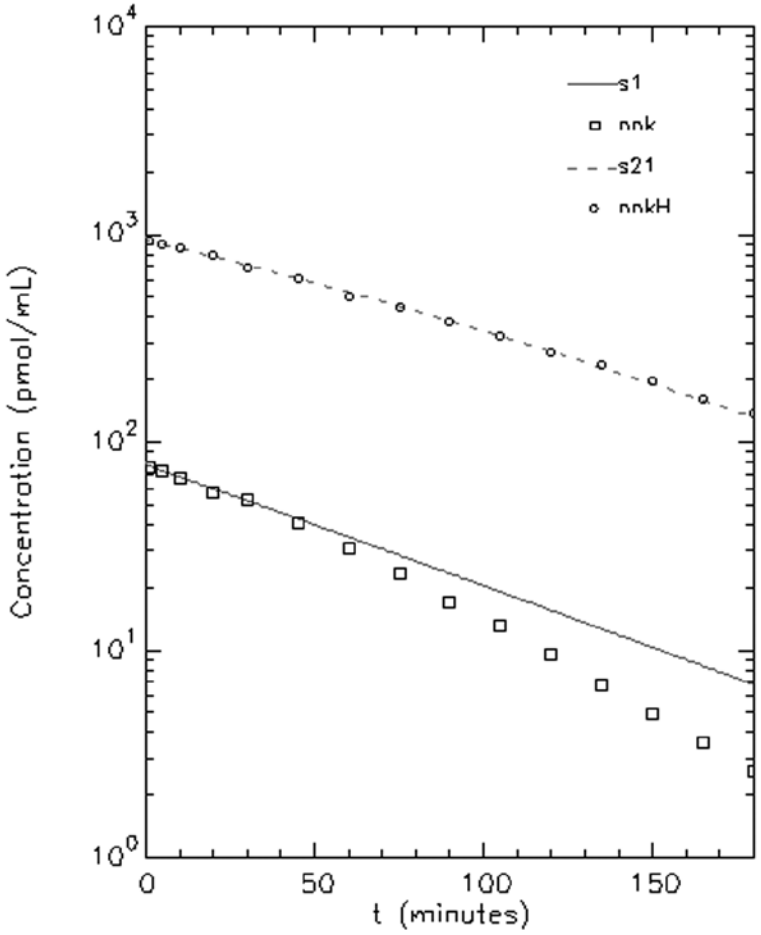

Figure 5.9 *– Fits of the complete NNK metabolism model to the average NNK concentration-time profiles for 0.1 µM (nnk) and 1.2 µM NNK perfusions (nnkH).*

The model was able to characterize the disappearance of NNK from the perfusate in the 1.2 µM perfusion fairly well, but it overestimated the NNK perfusate concentration at the later time points in the 0.1 µM perfusion.

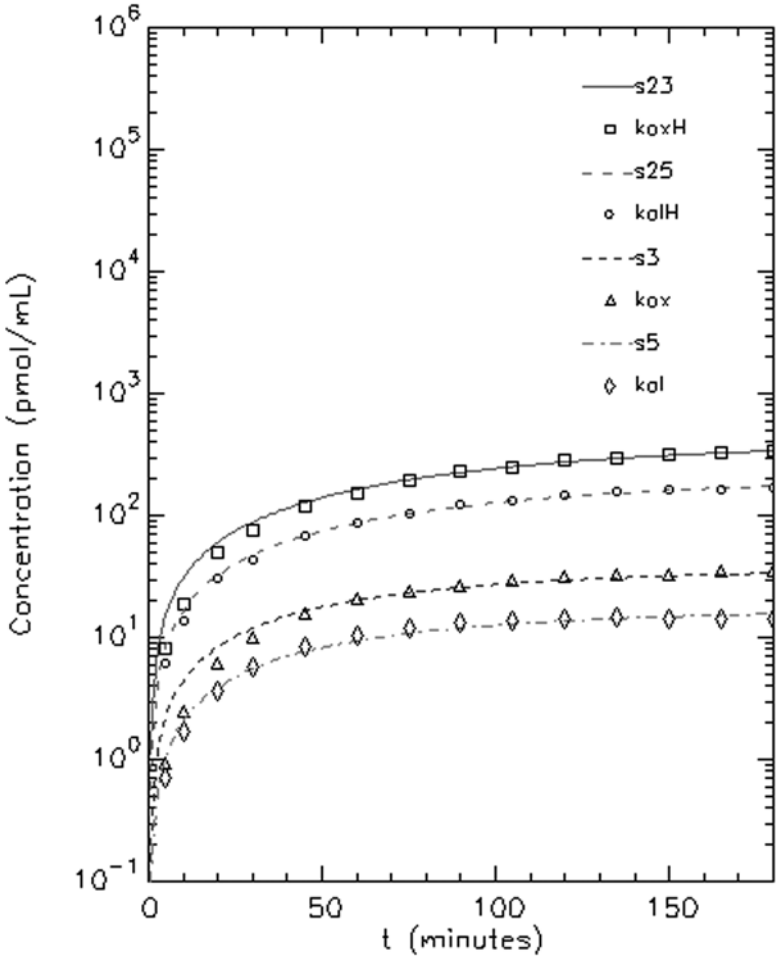

Figure 5.10 *– Fits of the complete NNK metabolism model to the average concentration-time profiles of NNK-N-oxide and keto alcohol for the 0.1 µM (kox, kal) and 1.2 µM NNK perfusions (koxH, kalH).*

While it appeared that the initial concentration of NNK-*N*-oxide in the perfusate may be slightly overestimated by the model, the overall fits for NNK-*N*-oxide and keto alcohol matched the data well at both perfusion concentrations (Figure 5.10).

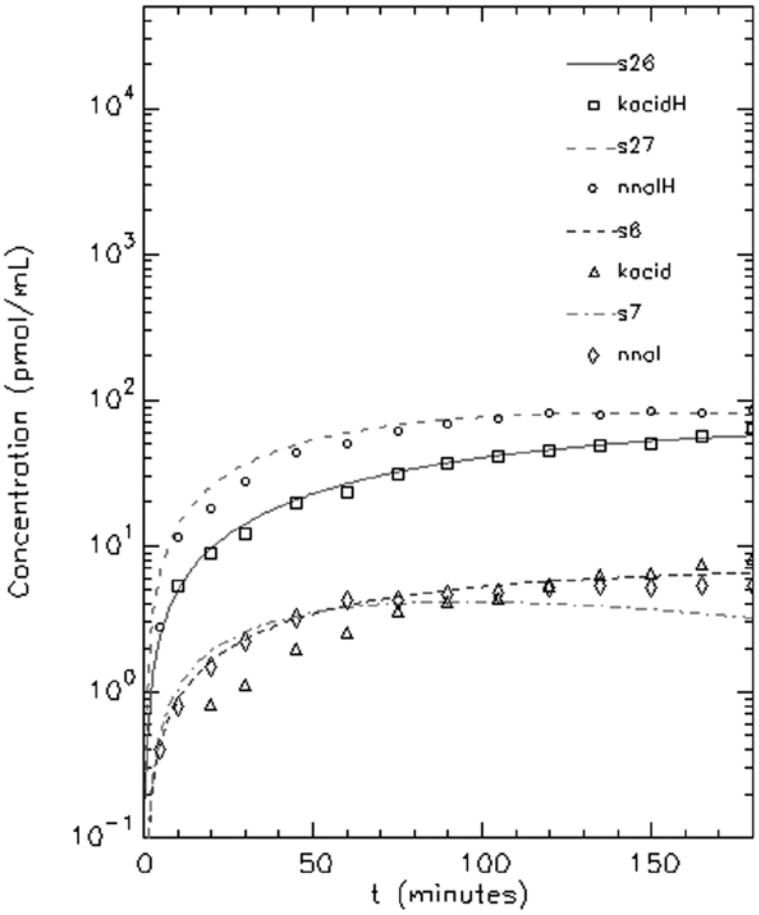

Figure 5.11 *– Fits of the complete NNK metabolism model to the average concentration-time profiles of NNAL and keto acid for the 0.1 µM (nnal, kacid) and 1.2 µM NNK perfusions (NNALH, kacidH).*

Keto alcohol and NNAL were fit fairly well at the higher perfusion concentration (Figure 5.11). For the 0.1 µM perfusion, initial concentrations of NNAL were fit fairly well, but the concentrations at the later time points were underestimated. Keto acid on the other hand, was fit better at later times and overestimated at initial time points.

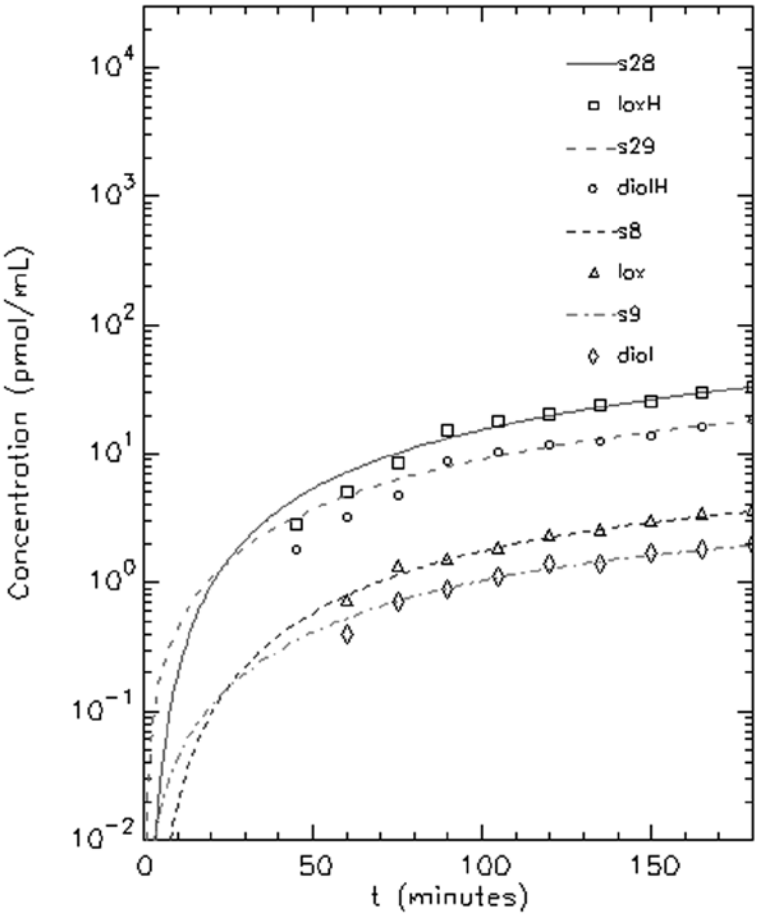

Figure 5.12 *– Fits of the complete NNK metabolism model to the average concentration-time profiles of NNAL-N-oxide and diol for the 0.1 µM (lox, diol) and 1.2 µM NNK perfusions (loxH, diolH).*

Both the diol and NNAL-*N*-oxide concentrations were fit well for the 0.1 µM perfusions, but their concentrations at early time points were slightly overestimated for the 1.2 µM perfusions.

Table 5.3 *– Parameter and variable estimates for the complete NNK metabolism model.*

Parameter/Variable	Value	Coefficient of Variation	95% Confidence Interval
$Delay_{NNALox}$	10.2 min	28.2	4.5 – 15.8
$K_{m\text{-}ketoacid}$	560 pmol/mL	15.2	390 - 720
$K_{m\text{-}NNKox}$	830 pmol/mL	7.1	710 - 950
$K_{m\text{-}ketoalcohol}$	1210 pmol/mL	10.2	967 - 1460
$K_{m\text{-}NNALox/diol}$	62 pmol/mL	7.5	52 - 71
$V_{max\text{-}ketoacid}$	51 pmol/min	8.4	43 - 60
$V_{max\text{-}NNKox}$	390 pmol/min	4.8	350 - 420
$V_{max\text{-}ketoalcohol}$	260 pmol/min	7.4	220 - 300
$V_{max\text{-}NNALox}$	25 pmol/min	5.1	22 – 27
$V_{max\text{-}diol}$	13 pmol/min	4.9	11 – 14
$V_{reservoir}$	62.3 mL	0.6	61.7 – 63.1
k(0,2)	0.050 min^{-1}	7.2	0.043 – 0.057
k(4,2)	0.057 min^{-1}	1.8	0.055 – 0.059

The estimated values for the parameters and variables of the model are listed in Table 5.3, along with the coefficient of variation and the 95% confidence interval for each estimate. Table 5.4 reports the maximum intrinsic clearances for the nonlinear metabolic pathways, which were calculated by dividing the V_{max} by the K_m for each pathway. By using a single K_m parameter to fit both diol and NNAL-*N*-oxide, a better fit was obtained than when estimates for each were factored into the model.

Table 5.4 *– Estimated maximum intrinsic clearance (mL/min) values for the nonlinear metabolic pathways of NNK, (S)-NNAL, and (R)-NNAL.*

Intrinsic Clearance	NNK	*(S)*-NNAL	*(R)*-NNAL
$CL_{Int\text{-}ketoacid}$	0.091	-	-
$CL_{Int\text{-}NNKox}$	0.47	-	-
$CL_{Int\text{-}ketoalcohol}$	0.21	-	-
$CL_{Int\text{-}Hacid}$	-	0.016	0.040
$CL_{Int\text{-}NNALox}$	0.40	0.087	0.16
$CL_{Int\text{-}diol}$	0.21	0.019	0.031

5.B.ii.c – NNAL Model

The model developed to describe the pulmonary metabolism of *(S)*-NNAL and *(R)*-NNAL in the IPRL system is illustrated in Figure 5.13. The designations for the compartments and metabolic rate constants are listed in Table 5.5. The convective flows of NNAL between the tissue and the perfusate are represented by k(2,1) and k(1,2).

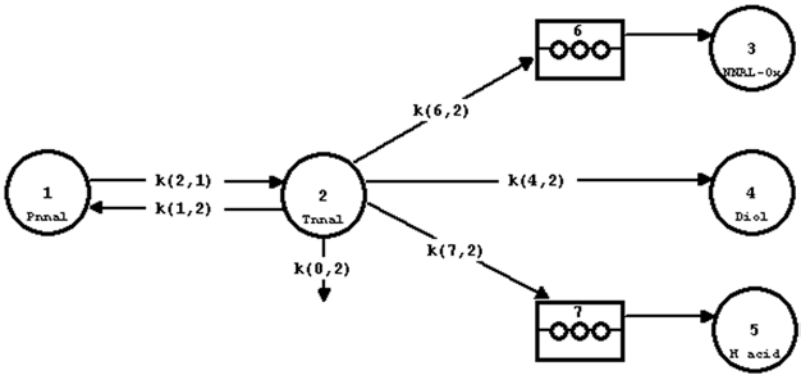

Figure 5.13 *–Pulmonary metabolism model for (S)-NNAL and (R)-NNAL.*

Table 5.5 *– List of all the compartments and metabolic rate constants in the NNAL metabolism model.*

Model Compartments		
1	NNAL perfusate	Measured
2	NNAL tissue	Calculated
3	NNAL-*N*-oxide perfusate	Measured
4	Diol perfusate	Measured
5	Hydroxy acid perfusate	Measured
6	NNAL-*N*-oxide delay	Calculated
7	Hydroxy acid delay	Calculated
Metabolic Rate Constants		
k(6,2)	NNAL-*N*-oxide metabolism	Nonlinear
k(4,2)	Diol metabolism	Nonlinear
k(7,2)	Hydroxy acid metabolism	Nonlinear
k(0,2)	Non-specified metabolism	Linear

Figures 5.14 and 5.15 show the fits of the NNAL, NNAL-*N*-oxide, diol, and keto acid concentration-time data for the 1.2 µM *(R)*-NNAL and 1.2 µM *(S)*-NNAL perfusions.

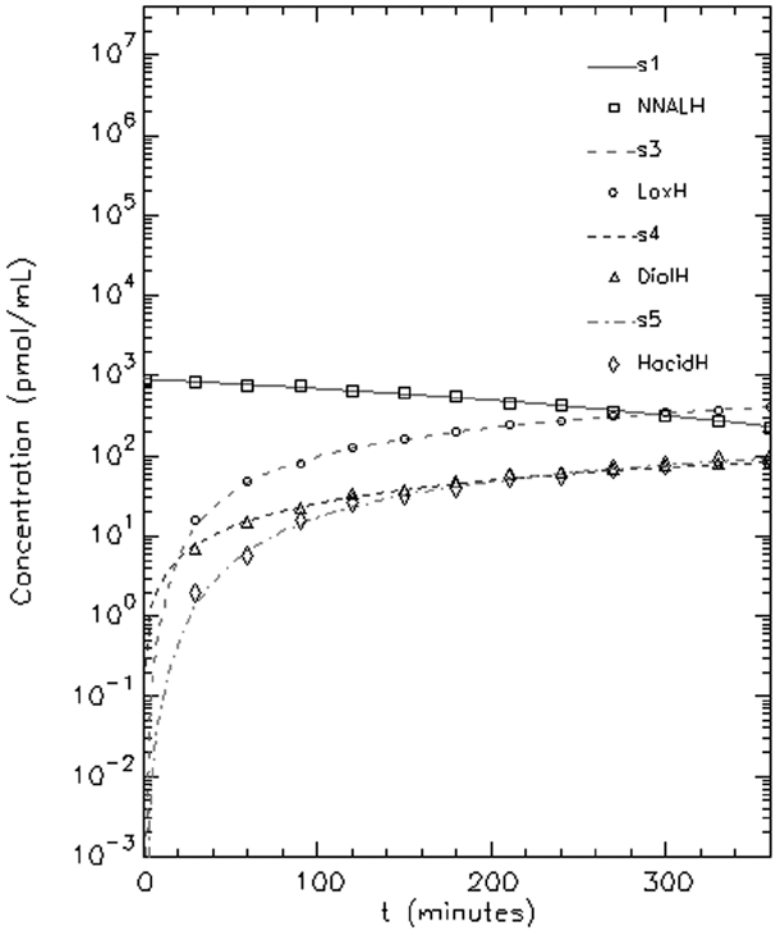

Figure 5.14 *– Fits for the perfusate concentrations of NNAL (NNALH), NNAL-N-oxide (LoxH), diol (DiolH), and hydroxy acid (HacidH) in the 1.2 µM (R)-NNAL perfusions using the NNAL metabolism model.*

From Figures 5.14 and 5.15 it appears that the NNAL model fit the data well for both enantiomers at all time points. The weighted residual plots showed a random scatter about zero, indicating that the data were not constantly overestimated or underestimated at any point. The model selected also gave the lowest AIC value for both enantiomers of all the models that were examined. Tables 5.6 and 5.7 list the estimates of each of the parameters and variables used to construct the model.

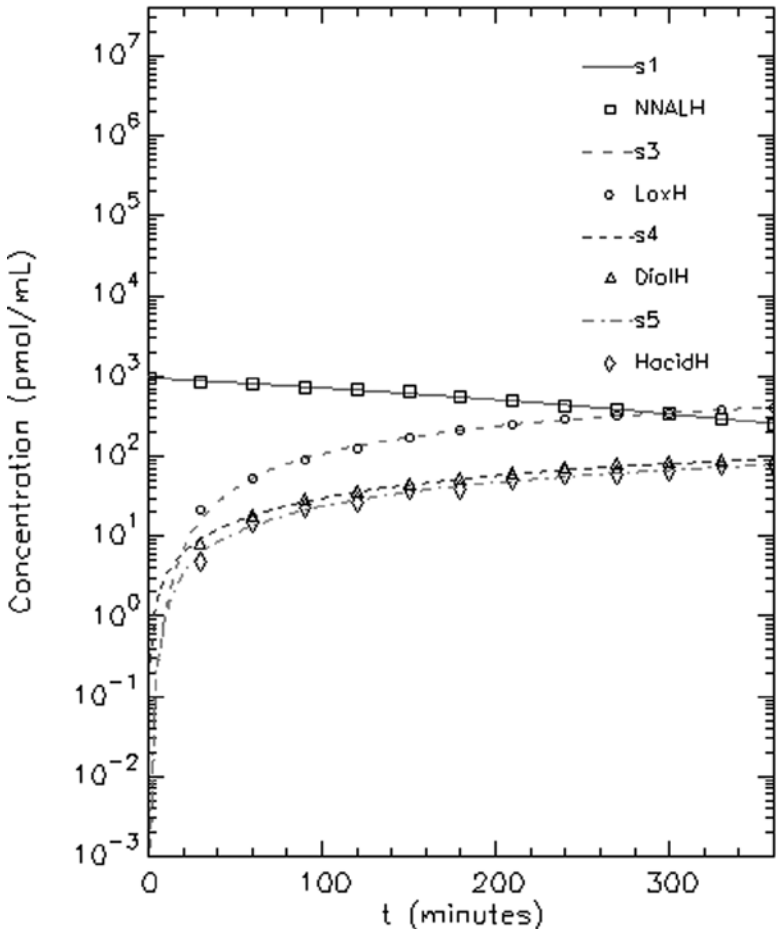

Figure 5.15 *– Fits for the perfusate concentrations of NNAL (NNALH), NNAL-N-oxide (LoxH), diol (DiolH), and hydroxy acid (HacidH) in the 1.2 μM (S)-NNAL perfusions using the NNAL metabolism model.*

Table 5.6 *– Parameter estimates for the (R)-NNAL model.*

Parameter/Variable	Value	Coefficient of Variation	95% Confidence Interval
$Delay_{Hacid}$	50 min	11.6	38 – 62
$Delay_{NNALox}$	26 min	13.1	19 - 33
K_m	140 pmol/mL	32.4	49 - 230
$V_{max\text{-}NNALox}$	23 pmol/min	7.1	19 – 26
$V_{max\text{-}Diol}$	4.4 pmol/min	6.4	3.8 – 4.9
$V_{max\text{-}Hacid}$	5.6 pmol/min	7.5	4.7 – 6.4
$V_{reservoir}$	64 mL	1.2	63 - 66
k(0,2)	0.012 min^{-1}	20.4	0.007 – 0.017

Table 5.7 *– Parameter estimates for the (S)-NNAL model.*

Parameter/Variable	Value	Coefficient of Variation	95% Confidence Interval
$Delay_{Hacid}$	7.3 min	78.0	-4.2 – 19
$Delay_{NNALox}$	23 min	12.4	17 - 29
K_m	300 pmol/mL	23.4	160 - 440
$V_{max\text{-}NNALox}$	26 pmol/min	8.2	22 – 31
$V_{max\text{-}Diol}$	5.7 pmol/min	7.6	4.8 – 6.5
$V_{max\text{-}Hacid}$	4.8 pmol/min	8.5	4.0 – 5.6
$V_{reservoir}$	61 mL	0.8	60 - 62
k(0,2)	0.017 min^{-1}	9.0	0.014 – 0.020

5.D – Discussion

The results from the metabolite formation clearance estimates indicated that the metabolism of NNK in the lung could not be explained by linear metabolism alone. The formation clearances were not constant with NNK concentration, which suggested that at least some of the metabolic pathways responsible for the metabolism of NNK were governed by Michaelis-Menten kinetics. Since solving differential equations using a clearance term that is not constant with concentration can be extremely complex, SAAM II was used to develop models for the metabolism of NNK, *(S)*-NNAL, and *(R)*-NNAL that incorporated both linear and nonlinear metabolic pathways. Initial models examining only the disappearance of NNK from the perfusate confirmed that linear metabolism alone did not accurately describe the metabolism of NNK. Instead, a model that contained both linear and nonlinear metabolic pathways appeared to better characterize its pulmonary metabolism.

The final model presented for the metabolism of NNK included both linear and nonlinear metabolism. All of the metabolites, except NNAL, were best fit using Michaelis-Menten kinetics. The addition of a non-specified linear metabolic pathway improved the fit, and may account for other metabolic pathways that were not directly measured in the perfusions. A delay compartment was added for the formation of NNAL-*N*-oxide because of its delayed appearance in the perfusate. The addition of the delay allowed the concentration of NNAL-*N*-oxide at the early time points to be fit better. The presence of the delay could either explain the delayed formation of NNAL-*N*-oxide because NNAL has to be formed first, or it could represent a delay in the metabolite

distributing into the perfusate due to diffusional barriers that might exist in the lung tissue for the polar metabolite. The addition of a delay for the diol pathway did not improve the fit, and thus it was omitted from the final model. The final model appeared to fit the concentration-time profiles of NNK and its metabolites fairly well. However, it overestimated the concentration of NNK at later time points in the 0.1 μM perfusion and did not accurately fit the formation of all of the metabolites, indicating that other mechanisms not considered in the model may be contributing to the system.

The model developed for the metabolism of NNAL was able to fit both the *(S)*-NNAL and *(R)*-NNAL concentration-time data, but the fits were not identical. The confidence intervals for $V_{max\text{-}NNALox}$, reservoir volume, and the delay for NNAL-*N*-oxide were similar for the two enantiomers. The intervals for the K_m and $V_{max\text{-}Diol}$ values however, showed less overlap. The delay for hydroxy acid seemed to fit the *(R)*-NNAL data better than the *(S)*-NNAL. The inclusion of zero in the confidence interval of *(S)*-NNAL for the delay indicated that it may not be important to the model, but when it was removed the AIC increased slightly and the model no longer fit the initial hydroxy acid concentrations as well. It also appeared that the addition of a non-specified linear pathway fit *(S)*-NNAL better than the *(R)*-NNAL. These differences in the fit of the NNAL enantiomers may indicate that there are differences in their metabolism that cannot be readily observed in the concentration-time data alone.

One of the main objectives of modeling the data was to determine if the formation of NNAL-*N*-oxide and diol differed depending on which carcinogen was dosed to the lung. If the formation of these metabolites from the NNAL enantiomers were less than

their formation when NNK was dosed, it could indicate that the metabolism observed in the *(S)*-NNAL and *(R)*-NNAL perfusions may not be representative of the metabolism of the NNAL formed during the NNK perfusions. A difference in metabolite formation may indicate the existence of diffusional barriers that impede the metabolism of the preformed enantiomers.

Based on the maximum intrinsic clearance estimates for the metabolites reported in Table 5.4, it appeared that the metabolism of the NNAL formed from NNK was greater than the metabolism of the preformed NNAL enantiomers. Since the average concentration-time data of NNK, NNAL, and their metabolites were used, it was not possible to carry out statistical analysis. Therefore, the confidence intervals for each of the K_m and V_{max} estimates used to determine the maximum intrinsic clearance were examined. The combined K_m for NNAL-*N*-oxide and diol formed from NNK had a lower and tighter confidence interval than that for *(S)*-NNAL or *(R)*-NNAL. The larger K_m confidence intervals for the enantiomers may be because hydroxy acid metabolism was included in their estimates. Since the confidence interval for $K_{m\text{-}NNALox/diol}$ falls completely within the *(R)*-NNAL confidence interval, it is not possible to say that there is a difference in their estimates. The $V_{max\text{-}NNALox}$ confidence intervals were similar for all three compounds, while the $V_{max\text{-}Diol}$ confidence interval for NNK did not overlap with the intervals of *(S)*-NNAL or *(R)*-NNAL. Based on the overlap in most of the confidence intervals for the parameter estimates it is not possible to conclude with any degree of certainty that they are significantly difference between the metabolism of formed and

preformed NNAL. Further analysis of the individual perfusion experiments may yield additional insight.

5.E - Conclusions

Models for the pulmonary metabolism of NNK, *(S)*-NNAL, and *(R)*-NNAL were reported here. While the models appeared to fit a majority of the data fairly well, they did not accurately fit all of the concentration-time data. It is likely that other mechanisms not considered in the models are contributing to the dynamics of these systems. One thing that seemed clear from the models was that both linear and nonlinear metabolic pathways contribute to the metabolism of these carcinogens. Due to the overlap in the confidence intervals for the parameters governing the metabolism of NNAL-*N*-oxide and diol, it was not possible to draw any firm conclusions about differences in the formation of the NNAL metabolites when the individual preformed enatiomers were administered versus when NNAL was formed from NNK.

CHAPTER 6: SUMMARY

The pulmonary metabolism of the lung-specific tobacco carcinogen, 4-(methylnitrosamino)-1-(3-pyridyl)-1-butanone (NNK), and its chiral metabolite 4-(methylnitrosamino)-1-(3-pyridyl)-1-butanol (NNAL) was the focus of this research project. It has been hypothesized that the lung-specific carcinogenicity of NNK may be due in part to the retention of *(S)*-NNAL in the lung tissue and its ability to reoxidize to NNK, which would prolong the exposure of the lung to NNK as compared to other tissues. As a result, the objective of this research was to examine the metabolism, distribution of metabolites, and DNA adduct formation of NNK, *(S)*-NNAL, and *(R)*-NNAL in the lung using the isolated perfused rat lung (IPRL) system.

One of the initial challenges of this work was developing the skills and knowledge to establish and maintain a successful lung perfusion system. The difficulties of developing the IPRL system are discussed in Chapter 2. A key finding was that failure to adequately cut the heart to allow for unrestricted flow of perfusate out of the lungs would lead to the formation of edema in the lungs and a failed perfusion.

The results of the NNK perfusions are reported in Chapter 3 and examine the effects of NNK concentration and PEITC co-administration on the formation and distribution of metabolites, and DNA adduct formation. It was observed that increased NNK concentration (1.2 μM) resulted in a significant decrease in the apparent pulmonary clearance, with only minor shifts in the metabolite profiles. The detection of DNA adducts indicated that metabolic activation in the lung leads to DNA damage, and that

bioactivation via the liver is not required. The formation of DNA adducts in the IPRL system showed that adducts formed rapidly and that chronic dosing was not required for their formation. The co-administration of PEITC (20 μM) inhibited the formation of oxidative metabolites, which subsequently resulted in a decrease in DNA adduct formation. However, the preliminary PEITC results reported in Chapter 2 indicated that low concentrations of PEITC (0.1 μM and 0.2 μM) did not appear to affect the oxidative metabolism of NNK, and that higher concentrations (10 μM and 20 μM) were required. However, more extensive work needs to be done to accurately determine the effective concentration of PEITC needed to inhibit the bioactivation of NNK.

The preliminary perfusions with *(S)*-NNAL and *(R)*-NNAL indicated that the enantiomers were not metabolized as efficiently in the lung as NNK. As a result, the duration of the NNAL perfusions had to be increased from 180 min to 360 min to allow more time for metabolism to occur. In contrast to previously published data, the perfusate and tissue metabolites in the IPRL system were similar for *(S)*-NNAL and *(R)*-NNAL, along with the levels of PHB-DNA adducts that formed in the tissue. The only major difference observed between the two enantiomers was the formation of low levels of POB-DNA adducts in the *(S)*-NNAL perfusions, which indicated reoxidation to NNK. The lack of stereoselective metabolism could possibly be due to diffusional barriers, which impeded the preformed NNAL enantiomers from gaining access to the metabolic sites. When the metabolism of *(S)*-NNAL and *(R)*-NNAL was examined using lung S9 fractions, it was observed that the rate of *(S)*-NNAL reoxidization to NNK was significantly greater than that of *(R)*-NNAL. The formation of NNK and keto alcohol was

observed in the lung S9 incubations, but not in the IRPL perfusions, indicating that diffusional barriers may by impairing the metabolism of the NNAL enantiomers in the IRPL system. It was observed that neither the perfusate concentration of *(S)*-NNAL nor *(R)*-NNAL declined in a monoexponential manner, indicating nonlinear kinetics. The nonlinearity could be a result of saturation at the distributional and/or metabolic phases. As a result, the potential contribution of a pulmonary influx transporter to the distribution of the NNAL enantiomers into the lung tissue should be examined. Furthermore, the initial perfusate concentrations of the NNAL perfusion were approximately 10 times higher than the NNAL concentrations achieved when NNK was dosed, so the effects of NNAL concentration on metabolism also need to be investigated.

Although the mechanism of the stereoselective retention of *(S)*-NNAL remains an open issue, the present work has shown the utility of the IPRL system in examining pulmonary metabolism and DNA adduct formation. In this research the IPRL system was used to assess the pulmonary metabolism of NNK and the enantiomers of NNAL by examining the time course of metabolite formation in the perfusate, quantifying the metabolites in the tissue, and measuring the formation of individual DNA adducts. The results suggest that measuring the formation of DNA adducts, instead of metabolite formation, may be a more sensitive and direct method for quantifying the bioactivation of NNK and NNAL. While the IPRL system has been shown to be useful in examining pulmonary metabolism, it may not be the best system for elucidating the role of *(S)*-NNAL in the carcinogenicity of NNK.

REFERENCES

1. American Cancer Society. Cancer Facts and Figures 2009. Atlanta: American cancer Society, Inc.

2. IARC. IARC Monographs on the Evaluation of the Carcinogenic Risks of Chemicals to Humans. Vol. 38, Tobacco Smoking. Lyon, France: IARC; 1986.

3. IARC. IARC Monographs on the Evaluation of the Carcinogenic Risks of Chemicals to Humans. Vol. 83, Tobacco Smoke and Involuntary Smoking. Lyon, France: IARC; 2004.

4. Sasco AJ, Secretan MB, Straif K 2004. Tobacco smoking and cancer: a brief review of recent epidemiological evidence. Lung Cancer 45 Suppl 2:S3-9.

5. American Cancer Society. Cancer Prevention & Early Detection Facts & Figures 2003. Atlanta: American Cancer Society, Inc.

6. Hecht SS 2003. Tobacco carcinogens, their biomarkers and tobacco-induced cancer. Nat Rev Cancer 3(10):733-744.

7. Hecht SS 1999. Tobacco smoke carcinogens and lung cancer. J Natl Cancer Inst 91(14):1194-1210.

8. Hecht SS, Hoffmann D 1989. The relevance of tobacco-specific nitrosamines to human cancer. Cancer Surv 8(2):273-294.

9. Hecht SS, Hoffmann D 1988. Tobacco-specific nitrosamines, an important group of carcinogens in tobacco and tobacco smoke. Carcinogenesis 9(6):875-884.

10. Hoffmann D, Adams JD, Brunnemann KD, Hecht SS 1979. Assessment of tobacco-specific *N*-nitrosamines in tobacco products. Cancer Res 39(7 Pt 1):2505-2509.

11. Hoffmann D, Lavoie EJ, Hecht SS 1985. Nicotine: a precursor for carcinogens. Cancer Lett 26(1):67-75.

12. Hecht SS, Chen CB, Hirota N, Ornaf RM, Tso TC, Hoffmann D 1978. Tobacco-specific nitrosamines: formation from nicotine in vitro and during tobacco curing and carcinogenicity in strain A/J mice. J Natl Cancer Inst 60(4):819-824.

13. Hoffmann D, Hecht SS 1985. Nicotine-derived *N*-nitrosamines and tobacco-related cancer: current status and future directions. Cancer Res 45(3):935-944.

14. Hecht SS, Chen CB, Ornaf RM, Jacobs E, Adams JD, Hoffmann D 1978. Reaction of nicotine and sodium nitrite: formation of nitrosamines and fragmentation of the pyrrolidine ring. J Org Chem 43(1):72-76.

15. Hecht SS 1998. Biochemistry, biology, and carcinogenicity of tobacco-specific *N*-nitrosamines. Chem Res Toxicol 11(6):559-603.

16. IARC. IARC Monographs on the Evaluation of the Carcinogenic Risks of Chemicals to Humans. Vol. 89, Smokeless tobacco and some tobacco-specific *N*-nitrosamines. Lyon, France: IARC; 2007.

17. Yuan JM, Koh WP, Murphy SE, Fan Y, Wang R, Carmella SG, Han S, Wickham K, Gao YT, Yu MC, Hecht SS 2009. Urinary levels of tobacco-specific nitrosamine metabolites in relation to lung cancer development in two prospective cohorts of cigarette smokers. Cancer Res 69(7):2990-2995.

18. Castonguay A, Lin D, Stoner GD, Radok P, Furuya K, Hecht SS, Schut HA, Klaunig JE 1983. Comparative carcinogenicity in A/J mice and metabolism by cultured mouse peripheral lung of *N'*-nitrosonornicotine, 4-(methylnitrosamino)-1-(3-pyridyl)-1-butanone, and their analogues. Cancer Res 43(3):1223-1229.

19. Hecht SS, Chen CB, Ohmori T, Hoffmann D 1980. Comparative carcinogenicity in F344 rats of the tobacco-specific nitrosamines, N'-nitrosonornicotine and 4-(*N*-methyl-*N*-nitrosamino)-1-(3-pyridyl)-1-butanone. Cancer Res 40(2):298-302.

20. Hoffmann D, Rivenson A, Amin S, Hecht SS 1984. Dose-response study of the carcinogenicity of tobacco-specific *N*-nitrosamines in F344 rats. J Cancer Res Clin Oncol 108(1):81-86.

21. Upadhyaya P, Kenney PM, Hochalter JB, Wang M, Hecht SS 1999. Tumorigenicity and metabolism of 4-(methylnitrosamino)-1-(3-pyridyl)-1-butanol enantiomers and metabolites in the A/J mouse. Carcinogenesis 20(8):1577-1582.

22. Belinsky SA, Foley JF, White CM, Anderson MW, Maronpot RR 1990. Dose-response relationship between O^6-methylguanine formation in Clara cells and induction of pulmonary neoplasia in the rat by 4-(methylnitrosamino)-1-(3-pyridyl)-1-butanone. Cancer Res 50(12):3772-3780.

23. Hecht SS, Adams JD, Numoto S, Hoffmann D 1983. Induction of respiratory tract tumors in Syrian golden hamsters by a single dose of 4-(methylnitrosamino)-1-(3-pyridyl)-1-butanone (NNK) and the effect of smoke inhalation. Carcinogenesis 4(10):1287-1290.

24. Wiener D, Doerge DR, Fang JL, Upadhyaya P, Lazarus P 2004. Characterization of *N*-glucuronidation of the lung carcinogen 4-(methylnitrosamino)-1-(3-pyridyl)-1-butanol (NNAL) in human liver: importance of UDP-glucuronosyltransferase 1A4. Drug Metab Dispos 32(1):72-79.

25. Jalas JR, Hecht SS 2003. Synthesis of stereospecifically deuterated 4-(methylnitrosamino)-1-(3-pyridyl)-1-butanol (NNAL) iastereomers and metabolism by A/J mouse lung microsomes and cytochrome P450 2A5. Chem Res Toxicol 16(6):782-793.

26. Lamoureux J, Castonguay A 1997. Absence of metabolism of 4-(methylnitrosamino)-1-(3-pyridyl)-1-butanone (NNK) by flavin-containing monooxygenase (FMO). Carcinogenesis 18(10):1979-1984.

27. Maser E 1998. 11-*Beta*-hydroxysteroid dehydrogenase responsible for carbonyl reduction of the tobacco-specific nitrosamine 4-(methylnitrosamino)-1-(3-pyridyl)-1-butanone in mouse lung microsomes. Cancer Res 58(14):2996-3003.

28. Maser E, Richter E, Friebertshauser J 1996. The identification of 11-*beta*-hydroxysteroid dehydrogenase as carbonyl reductase of the tobacco-specific nitrosamine 4-(methylnitrosamino)-1-(3-pyridyl)-1-butanone. Eur J Biochem 238(2):484-489.

29. Upadhyaya P, Carmella SG, Guengerich FP, Hecht SS 2000. Formation and metabolism of 4-(methylnitrosamino)-1-(3-pyridyl)-1-butanol enantiomers *in vitro* in mouse, rat and human tissues. Carcinogenesis 21(6):1233-1238.

30. Maser E, Stinner B, Atalla A 2000. Carbonyl reduction of 4-(methylnitrosamino)-1-(3-pyridyl)-1-butanone (NNK) by cytosolic enzymes in human liver and lung. Cancer Lett 148(2):135-144.

31. Breyer-Pfaff U, Martin HJ, Ernst M, Maser E 2004. Enantioselectivity of carbonyl reduction of 4-methylnitrosamino-1-(3-pyridyl)-1-butanone by tissue fractions from human and rat and by enzymes isolated from human liver. Drug Metab Dispos 32(9):915-922.

32. Finckh C, Atalla A, Nagel G, Stinner B, Maser E 2001. Expression and NNK reducing activities of carbonyl reductase and 11-*beta*-hydroxysteroid dehydrogenase type 1 in human lung. Chem Biol Interact 130-132(1-3):761-773.

33. Atalla A, Maser E 2001. Characterization of enzymes participating in carbonyl reduction of 4-methylnitrosamino-1-(3-pyridyl)-1-butanone (NNK) in human placenta. Chem Biol Interact 130-132(1-3):737-748.

34. Atalla A, Breyer-Pfaff U, Maser E 2000. Purification and characterization of oxidoreductases-catalyzing carbonyl reduction of the tobacco-specific nitrosamine 4-methylnitrosamino-1-(3-pyridyl)-1-butanone (NNK) in human liver cytosol. Xenobiotica 30(8):755-769.

35. Chen G, Dellinger RW, Sun D, Spratt TE, Lazarus P 2008. Glucuronidation of tobacco-specific nitrosamines by UGT2B10. Drug Metab Dispos 36(5):824-830.

36. Lazarus P, Zheng Y, Aaron Runkle E, Muscat JE, Wiener D 2005. Genotype-phenotype correlation between the polymorphic UGT2B17 gene deletion and NNAL glucuronidation activities in human liver microsomes. Pharmacogenet Genomics 15(11):769-778.

37. Ren Q, Murphy SE, Zheng Z, Lazarus P 2000. *O*-Glucuronidation of the lung carcinogen 4-(methylnitrosamino)-1- (3-pyridyl)-1-butanol (NNAL) by human UDP-glucuronosyltransferases 2B7 and 1A9. Drug Metab Dispos 28(11):1352-1360.

38. Ren Q, Murphy SE, Dannenberg AJ, Park JY, Tephly TR, Lazarus P 1999. Glucuronidation of the lung carcinogen 4-(methylnitrosamino)-1-(3-pyridyl)-1-butanol (NNAL) by rat UDP-glucuronosyltransferase 2B1. Drug Metab Dispos 27(9):1010-1016.

39. Shelby MK, Cherrington NJ, Vansell NR, Klaassen CD 2003. Tissue mRNA expression of the rat UDP-glucuronosyltransferase gene family. Drug Metab Dispos 31(3):326-333.

40. Devereux TR, Anderson MW, Belinsky SA 1988. Factors regulating activation and DNA alkylation by 4-(*N*-methyl-*N*-nitrosamino)-1-(3-pyridyl)-1-butanone and nitrosodimethylamine in rat lung and isolated lung cells, and the relationship to carcinogenicity. Cancer Res 48(15):4215-4221.

41. Hecht SS 1999. DNA adduct formation from tobacco-specific *N*-nitrosamines. Mutat Res 424(1-2):127-142.

42. Belinsky SA, White CM, Boucheron JA, Richardson FC, Swenberg JA, Anderson M 1986. Accumulation and persistence of DNA adducts in respiratory tissue of rats following multiple administrations of the tobacco specific carcinogen 4-(*N*-methyl-*N*-nitrosamino)-1-(3-pyridyl)-1-butanone. Cancer Res 46(3):1280-1284.

43. Belinsky SA, White CM, Devereux TR, Swenberg JA, Anderson MW 1987. Cell selective alkylation of DNA in rat lung following low dose exposure to the tobacco specific carcinogen 4-(*N*-methyl-*N*-nitrosamino)-1-(3-pyridyl)-1-butanone. Cancer Res 47(4):1143-1148.

44. Hecht SS, Trushin N, Castonguay A, Rivenson A 1986. Comparative tumorigenicity and DNA methylation in F344 rats by 4-(methylnitrosamino)-1-(3-pyridyl)-1-butanone and *N*-nitrosodimethylamine. Cancer Res 46(2):498-502.

45. Maertens LA, Upadhyaya P, Hecht SS, Zimmerman CL Formation and distribution of NNK metabolites in an isolated perfused rat lung. Drug Metab Dispos 38(5):752-760.

46. Abbott PJ, Saffhill R 1979. DNA synthesis with methylated poly(dC-dG) templates. Evidence for a competitive nature to miscoding by O^6-methylguanine. Biochim Biophys Acta 562(1):51-61.

47. Eadie JS, Conrad M, Toorchen D, Topal MD 1984. Mechanism of mutagenesis by O^6-methylguanine. Nature 308(5955):201-203.

48. Loechler EL, Green CL, Essigmann JM 1984. In vivo mutagenesis by O^6-methylguanine built into a unique site in a viral genome. Proc Natl Acad Sci U S A 81(20):6271-6275.

49. Ziegel R, Shallop A, Jones R, Tretyakova N 2003. K-ras gene sequence effects on the formation of 4-(methylnitrosamino)-1-(3-pyridyl)-1-butanone (NNK)-DNA adducts. Chem Res Toxicol 16(4):541-550.

50. Belinsky SA, Devereux TR, Anderson MW 1990. Role of DNA methylation in the activation of proto-oncogenes and the induction of pulmonary neoplasia by nitrosamines. Mutat Res 233(1-2):105-116.

51. Peterson LA, Mathew R, SE BPM, Trushin N, Hecht SS 1991. *In vivo* and *in vitro* persistence of pyridyloxobutyl DNA adducts from 4-(methylnitrosamino)-1-(3-pyridyl)-1-butanone. Carcinogenesis 12(11):2069-2072.

52. Staretz ME, Foiles PG, Miglietta LM, Hecht SS 1997. Evidence for an important role of DNA pyridyloxobutylation in rat lung carcinogenesis by 4-(methylnitrosamino)-1-(3-pyridyl)-1-butanone: effects of dose and phenethyl isothiocyanate. Cancer Res 57(2):259-266.

53. Morse MA, Wang CX, Stoner GD, Mandal S, Conran PB, Amin SG, Hecht SS, Chung FL 1989. Inhibition of 4-(methylnitrosamino)-1-(3-pyridyl)-1-butanone-induced DNA adduct formation and tumorigenicity in the lung of F344 rats by dietary phenethyl isothiocyanate. Cancer Res 49(3):549-553.

54. Pauly GT, Peterson LA, Moschel RC 2002. Mutagenesis by O^6-[4-oxo-4-(3-pyridyl)butyl]guanine in Escherichia coli and human cells. Chem Res Toxicol 15(2):165-169.

55. Mijal RS, Loktionova NA, Vu CC, Pegg AE, Peterson LA 2005. O^6-pyridyloxobutylguanine adducts contribute to the mutagenic properties of pyridyloxobutylating agents. Chem Res Toxicol 18(10):1619-1625.

56. Ronai ZA, Gradia S, Peterson LA, Hecht SS 1993. G to A transitions and G to T transversions in codon 12 of the Ki-ras oncogene isolated from mouse lung tumors induced by 4-(methylnitrosamino)-1-(3-pyridyl)-1-butanone (NNK) and related DNA methylating and pyridyloxobutylating agents. Carcinogenesis 14(11):2419-2422.

57. Hecht SS, Spratt TE, Trushin N 1988. Evidence for 4-(3-pyridyl)-4-oxobutylation of DNA in F344 rats treated with the tobacco-specific nitrosamines 4-(methylnitrosamino)-1-(3-pyridyl)-1-butanone and *N'*-nitrosonornicotine. Carcinogenesis 9(1):161-165.

58. Peterson LA, Liu XK, Hecht SS 1993. Pyridyloxobutyl DNA adducts inhibit the repair of O^6-methylguanine. Cancer Res 53(12):2780-2785.

59. Lao Y, Villalta PW, Sturla SJ, Wang M, Hecht SS 2006. Quantitation of pyridyloxobutyl DNA adducts of tobacco-specific nitrosamines in rat tissue DNA by

high-performance liquid chromatography-electrospray ionization-tandem mass spectrometry. Chem Res Toxicol 19(5):674-682.

60. Hecht SS, Villalta PW, Sturla SJ, Cheng G, Yu N, Upadhyaya P, Wang M 2004. Identification of O^2-substituted pyrimidine adducts formed in reactions of 4-(acetoxymethylnitrosamino)- 1-(3-pyridyl)-1-butanone and 4-(acetoxymethylnitrosamino)-1-(3-pyridyl)-1-butanol with DNA. Chem Res Toxicol 17(5):588-597.

61. Upadhyaya P, Sturla SJ, Tretyakova N, Ziegel R, Villalta PW, Wang M, Hecht SS 2003. Identification of adducts produced by the reaction of 4-(acetoxymethylnitrosamino)-1-(3-pyridyl)-1-butanol with deoxyguanosine and DNA. Chem Res Toxicol 16(2):180-190.

62. Lao Y, Yu N, Kassie F, Villalta PW, Hecht SS 2007. Formation and accumulation of pyridyloxobutyl DNA adducts in F344 rats chronically treated with 4-(methylnitrosamino)-1-(3-pyridyl)-1-butanone and enantiomers of its metabolite, 4-(methylnitrosamino)-1-(3-pyridyl)-1-butanol. Chem Res Toxicol 20(2):235-245.

63. Upadhyaya P, Kalscheuer S, Hochalter JB, Villalta PW, Hecht SS 2008. Quantitation of pyridylhydroxybutyl-DNA adducts in liver and lung of F-344 rats treated with 4-(methylnitrosamino)-1-(3-pyridyl)-1-butanone and enantiomers of its metabolite 4-(methylnitrosamino)-1-(3-pyridyl)-1-butanol. Chem Res Toxicol 21(7):1468-1476.

64. Upadhyaya P, Lindgren BR, Hecht SS 2009. Comparative levels of O^6-methylguanine, pyridyloxobutyl-, and pyridylhydroxybutyl-DNA adducts in lung and liver of rats treated chronically with the tobacco-specific carcinogen 4-(methylnitrosamino)-1-(3-pyridyl)-1-butanone. Drug Metab Dispos 37(6):1147-1151.

65. Smith SW 2009. Chiral toxicology: it's the same thing...only different. Toxicol Sci 110(1):4-30.

66. 1992. FDA's Policy Statement on the Development of New Stereoisomeric Drugs. Fed Regist, ed.: U.S. Food and Drug Administration. p 22249.

67. Au N, Rettie AE 2008. Pharmacogenomics of 4-hydroxycoumarin anticoagulants. Drug Metab Rev 40(2):355-375.

68. Fitos I, Visy J, Kardos J 2002. Stereoselective kinetics of warfarin binding to human serum albumin: effect of an allosteric interaction. Chirality 14(5):442-448.

69. Nordberg A 1993. A Comparison of the *(S)(-)* and *(R)(+)* Enantiomers of Nicotine with Respect to Pharmacological and Behavorial Effects and Receptor Binding Properties in Experimental Animal and Man. Med Chem Res 2:522-529.

70. Pictet AR, A 1904. Synthese des Nicotins. Ber Dtsch Chem Ges 37:1225-1235.

71. Hicks CS, Sinclair DA 1947. Toxicities of the optical isomers of nicotine and nornicotine. Aust J Exp Biol Med Sci 25:83-86.

72. Cundy KC, Sato M, Crooks PA 1985. Stereospecific *in vivo N*-methylation of nicotine in the guinea pig. Drug Metab Dispos 13(2):175-185.

73. Cundy KC, Godin CS, Crooks PA 1985. Stereospecific *in vitro N*-methylation of nicotine in guinea pig tissues by an S-adenosylmethionine-dependent *N*-methyltransferase. Biochem Pharmacol 34(2):281-284.

74. Nwosu CG, Crooks PA 1988. Species variation and stereoselectivity in the metabolism of nicotine enantiomers. Xenobiotica 18(12):1361-1372.

75. Nwosu CG, Godin CS, Houdi AA, Damani LA, Crooks PA 1988. Enantioselective metabolism during continuous administration of *S-(-)*- and *R-(+)*-nicotine isomers to guinea-pigs. J Pharm Pharmacol 40(12):862-869.

76. Thuerauf N, Kaegler M, Dietz R, Barocka A, Kobal G 1999. Dose-dependent stereoselective activation of the trigeminal sensory system by nicotine in man. Psychopharmacology (Berl) 142(3):236-243.

77. Zimmerman CL, Wu Z, Upadhyaya P, Hecht SS 2004. Stereoselective metabolism and tissue retention in rats of the individual enantiomers of 4-(methylnitrosamino)-1-(3-

pyridyl)-1-butanol (NNAL), metabolites of the tobacco-specific nitrosamine, 4-(methylnitrosamino)-1-(3-pyridyl)-1-butanone (NNK). Carcinogenesis 25(7):1237-1242.

78. Wu Z, Upadhyaya P, Carmella SG, Hecht SS, Zimmerman CL 2002. Disposition of 4-(methylnitrosamino)-1-(3-pyridyl)-1-butanone (NNK) and 4-(methylnitrosamino)-1-(3-pyridyl)-1-butanol (NNAL) in bile duct-cannulated rats: stereoselective metabolism and tissue distribution. Carcinogenesis 23(1):171-179.

79. Rivenson A, Hoffmann D, Prokopczyk B, Amin S, Hecht SS 1988. Induction of lung and exocrine pancreas tumors in F344 rats by tobacco-specific and Areca-derived *N*-nitrosamines. Cancer Res 48(23):6912-6917.

80. Pritchard M, Fournel-Gigleux S, Siest G, Mackenzie P, Magdalou J 1994. A recombinant phenobarbital-inducible rat liver UDP-glucuronosyltransferase (UDP-glucuronosyltransferase 2B1) stably expressed in V79 cells catalyzes the glucuronidation of morphine, phenols, and carboxylic acids. Mol Pharmacol 45(1):42-50.

81. Zhang S, Wang M, Villalta PW, Lindgren BR, Upadhyaya P, Lao Y, Hecht SS 2009. Analysis of Pyridyloxobutyl and Pyridylhydroxybutyl DNA Adducts in Extrahepatic Tissues of F344 Rats Treated Chronically with 4-(Methylnitrosamino)-1-(3-pyridyl)-1-butanone and Enantiomers of 4-(Methylnitrosamino)-1-(3-pyridyl)-1-butanol. Chem Res Toxicol.

82. Chung FL, Kelloff G, Steele V, Pittman B, Zang E, Jiao D, Rigotty J, Choi CI, Rivenson A 1996. Chemopreventive efficacy of arylalkyl isothiocyanates and *N*-acetylcysteine for lung tumorigenesis in Fischer rats. Cancer Res 56(4):772-778.

83. Morse MA, Amin SG, Hecht SS, Chung FL 1989. Effects of aromatic isothiocyanates on tumorigenicity, O^6-methylguanine formation, and metabolism of the tobacco-specific nitrosamine 4-(methylnitrosamino)-1-(3-pyridyl)-1-butanone in A/J mouse lung. Cancer Res 49(11):2894-2897.

84. Hecht SS, Trushin N, Rigotty J, Carmella SG, Borukhova A, Akerkar S, Rivenson A 1996. Complete inhibition of 4-(methylnitrosamino)-1-(3-pyridyl)-1-butanone-induced rat lung tumorigenesis and favorable modification of biomarkers by phenethyl isothiocyanate. Cancer Epidemiol Biomarkers Prev 5(8):645-652.

85. Morse MA, Reinhardt JC, Amin SG, Hecht SS, Stoner GD, Chung FL 1990. Effect of dietary aromatic isothiocyanates fed subsequent to the administration of 4-(methylnitrosamino)-1-(3-pyridyl)-1-butanone on lung tumorigenicity in mice. Cancer Lett 49(3):225-230.

86. Smith TJ, Guo Z, Li C, Ning SM, Thomas PE, Yang CS 1993. Mechanisms of inhibition of 4-(methylnitrosamino)-1-(3-pyridyl)-1-butanone bioactivation in mouse by dietary phenethyl isothiocyanate. Cancer Res 53(14):3276-3282.

87. Staretz ME, Hecht SS 1995. Effects of phenethyl isothiocyanate on the tissue distribution of 4-(methylnitrosamino)-1-(3-pyridyl)-1-butanone and metabolites in F344 rats. Cancer Res 55(23):5580-5588.

88. Staretz ME, Koenig LA, Hecht SS 1997. Effects of long term dietary phenethyl isothiocyanate on the microsomal metabolism of 4-(methylnitrosamino)-1-(3-pyridyl)-1-butanone and 4-(methylnitrosamino)-1-(3-pyridyl)-1-butanol in F344 rats. Carcinogenesis 18(9):1715-1722.

89. Guo Z, Smith TJ, Wang E, Sadrieh N, Ma Q, Thomas PE, Yang CS 1992. Effects of phenethyl isothiocyanate, a carcinogenesis inhibitor, on xenobiotic-metabolizing enzymes and nitrosamine metabolism in rats. Carcinogenesis 13(12):2205-2210.

90. Nakajima M, Yoshida R, Shimada N, Yamazaki H, Yokoi T 2001. Inhibition and inactivation of human cytochrome P450 isoforms by phenethyl isothiocyanate. Drug Metab Dispos 29(8):1110-1113.

91. Smith TJ, Guo ZY, Thomas PE, Chung FL, Morse MA, Elkind K, Yang CS 1990. Metabolism of 4-(methylnitrosamino)-1-(3-pyridyl)-1-butanone in mouse lung microsomes and its inhibition by isothiocyanates. Cancer Res 50(21):6817-6822.

92. Guo Z, Smith TJ, Wang E, Eklind KI, Chung FL, Yang CS 1993. Structure-activity relationships of arylalkyl isothiocyanates for the inhibition of 4-(methylnitrosamino)-1-(3-pyridyl)-1-butanone metabolism and the modulation of xenobiotic-metabolizing enzymes in rats and mice. Carcinogenesis 14(6):1167-1173.

93. Niemeier RW 1984. The isolated perfused lung. Environ Health Perspect 56:35-41.

94. Rhoades RA 1984. Isolated perfused lung preparation for studying altered gaseous environments. Environ Health Perspect 56:43-50.

95. Wen Y, Remmel RP, Zimmerman CL 1999. First-pass disposition of *(-)-6*-aminocarbovir in rats. I. Prodrug activation may be limited by access to enzyme. Drug Metab Dispos 27(1):113-121.

96. Soria I, Zimmerman CL 1993. Disposition of *(-)*carbovir in the in situ perfused rat liver and intestinal vasculature preparations. Drug Metab Dispos 21(4):724-729.

97. Maertens LH, S; Zimmerman, C 2004. Optimization of an Isolated Perfused Rat Lung System for Study of the metabolism of NNK. The AAPS Journal 6(4):Abstract W5324.

98. Schrader E, Hirsch-Ernst KI, Richter E, Foth H 1998. Metabolism of 4-(methylnitrosamino)-1-(3-pyridyl)-1-butanone (NNK) in isolated rat lung and liver. Naunyn Schmiedebergs Arch Pharmacol 357(3):336-343.

99. Wangensteen D, Piper R, Johnson JA, Sinha AA, Niewoehner D 1986. Solute conductance of blood-gas barrier in hamsters exposed to hyperoxia. J Appl Physiol 60(6):1908-1916.

100. Wangensteen OD, Bartlett MM, James JK, Yang ZF, Low PS 1996. Riboflavin-enhanced transport of serum albumin across the distal pulmonary epithelium. Pharm Res 13(12):1861-1864.

101. Godinez RI, Longmore WJ 1973. Use of the isolated perfused rat lung in studies on lung lipid metabolism. J Lipid Res 14(2):138-144.

102. Byron PR, Niven RW 1988. A novel dosing method for drug administration to the airways of the isolated perfused rat lung. J Pharm Sci 77(8):693-695.

103. Palazzo RM, Wangensteen OD, Niewoehner DE 1992. Time course of functional repair of the alveolar epithelium after hyperoxic injury. J Appl Physiol 73(5):1881-1887.

104. Wiley J, Chien D, Nungesser N, Lin D, Hecht SS 1988. Synthesis of 4-(Methlnitrosamino)-1-(3-pyridyl)-1-butone, 4-(carbethoxynitrosamino)-1-(3-pyridyl)-1-butanone, and *N'*-nitrosonornicotine labelled with tritium in the pyridine ring. Journal of Labelled Compounds and Radiopharmaceuticals XXV(7):707-716.

105. Guo Z, Smith TJ, Thomas PE, Yang CS 1991. Metabolic activation of 4-(methylnitrosamino)-1-(3-pyridyl)-1-butanone as measured by DNA alkylation *in vitro* and its inhibition by isothiocyanates. Cancer Res 51(18):4798-4803.

106. Hecht SS, Spratt TE, Trushin N 2000. Absolute configuration of 4-(methylnitrosamino)-1-(3-pyridyl)-1-butanol formed metabolically from 4-(methylnitrosamino)-1-(3-pyridyl)-1-butanone. Carcinogenesis 21(4):850.

107. Hecht SS, Spratt TE, Trushin N 1997. Absolute configuration of 4-(methylnitrosamino)-1-(3-pyridyl)-1-butanol formed metabolically from 4-(methylnitrosamino)-1-(3-pyridyl)-1-butanone. Carcinogenesis 18(9):1851-1854.

108. McKennis H, Jr., Schwartz SL, Turnbull LB, Tamaki E, Bowman ER 1964. The Metabolic Formation of Gamma-(3-Pyridyl)-Gamma-Hydroxybutyric Acid and Its Possible Intermediary Role in the Mammalian Metabolism of Nicotine. J Biol Chem 239:3981-3989.

109. Jalas JR, Ding X, Murphy SE 2003. Comparative metabolism of the tobacco-specific nitrosamines 4-(methylnitrosamino)-1-(3-pyridyl)-1-butanone and 4-(methylnitrosamino)-1-(3-pyridyl)-1-butanol by rat cytochrome P450 2A3 and human cytochrome P450 2A13. Drug Metab Dispos 31(10):1199-1202.

110. Schrader E, Hirsch-Ernst KI, Scholz E, Kahl GF, Foth H 2000. Metabolism of 4-(Methylnitrosamino)-1-(3-pyridyl)-1-butanone (NNK) in primary cultures of rat alveolar type II cells. Drug Metab Dispos 28(2):180-185.

111. Richter E, Engl J, Friesenegger S, Tricker AR 2009. Biotransformation of 4-(methylnitrosamino)-1-(3-pyridyl)-1-butanone in lung tissue from mouse, rat, hamster, and man. Chem Res Toxicol 22(6):1008-1017.

112. Weng Y, Fang C, Turesky RJ, Behr M, Kaminsky LS, Ding X 2007. Determination of the role of target tissue metabolism in lung carcinogenesis using conditional cytochrome P450 reductase-null mice. Cancer Res 67(16):7825-7832.

113. von Weymarn LB, Chun JA, Hollenberg PF 2006. Effects of benzyl and phenethyl isothiocyanate on P450s 2A6 and 2A13: potential for chemoprevention in smokers. Carcinogenesis 27(4):782-790.

114. Atalla A, Maser E 1999. Carbonyl reduction of the tobacco-specific nitrosamine 4-(methylnitrosamino)-1-(3-pyridyl)-1-butanone (NNK) in cytosol of mouse liver and lung. Toxicology 139(1-2):155-166.

115. Peterson LA, Ng DK, Stearns RA, Hecht SS 1994. Formation of NADP(H) analogs of tobacco-specific nitrosamines in rat liver and pancreatic microsomes. Chem Res Toxicol 7(5):599-608.

116. Pang KS 2009. Safety testing of metabolites: Expectations and outcomes. Chem Biol Interact 179(1):45-59.